

Strong optical coupling between 3D confined resonant modes in microtube cavities

Dissertation

Vorgelegt der Fakultät Mathematik und Naturwissenschaften
der Technische Universität Dresden

Zur Erlangung des akademischen Grades

Doctor rerum naturalium (Dr. rer. nat.)

Von: **Xiaoyu Wang**

geboren am: **03. 06. 1992 in China**

eingereicht am: **27. 07. 2022**

verteidigt am: **24. 11. 2022**

Gutachter: **Prof. Dr. Oliver G. Schmidt**
Prof. Dr. Vladimir Fomin

Bibliografische Beschreibung

Xiaoyu Wang

Strong optical coupling between 3D confined resonant modes in microtube cavities

Dissertation; 124 Seiten; 45 Abbildungen, 1 Tabellen, 167 Referenzen

Fakultät Mathematik und Naturwissenschaften

Technische Universität Dresden (2022)

Abstract

Coupled whispering-gallery-mode (WGM) optical microcavities have been extensively explored to tune the resonant eigenfrequencies and spatial distributions of the optical modes, finding many unique photonic applications in a variety of fields, such as nonlinear optics, laser physics, and non-Hermitian photonics. As one type of WGM microcavities, microtube cavities with axial potential wells support 3D confined resonances by circulating light along the microtube cross-section and axis simultaneously, which offers a promising possibility to explore multidimensional and multichannel optical coupling.

In this thesis, the optical coupling of 3D confined resonant modes is investigated in coupled microtube cavities fabricated by self-rolling of prestrained nanomembranes. In the first coupling system, multiple sets of 3D optical modes are generated in a single microtube cavity owing to nanogap induced resonant trajectory splitting. The large overlap of optical fields in the split resonant trajectories triggers strong optical coupling of the 3D confined resonant modes. The spectra anticrossing feature and changing-over of one group of coupled fundamental modes are demonstrated as direct evidence of strong coupling. The spatial optical field distribution of 3D coupling modes was experimentally mapped upon the strong coupling regime, which allows direct observation of the energy transfer process between two hybrid states. Numerical calculations based on a quasi-potential model and the mode detuning process are in excellent agreement with the experimental results. On this basis, monolithically integrated twin microtube cavities are proposed to achieve the collective coupling of two sets of 3D optical modes. Owing to the aligned twin geometries, two sets of 3D optical modes in twin microtubes are spectrally and spatially matched, by which both the fundamental and higher-order axial modes are respectively coupled with each other. Multiple groups of the coupling modes provide multiple effective channels for energy exchange between coupled microcavities, which are illustrated by the measured spatial optical field distributions. The spectral anticrossing and

changing-over features of each group of coupled modes are revealed in experiments and calculations, indicating the occurrence of strong coupling. In addition, the simulated 3D mode profiles of twin microcavities confirm the collective strong coupling behavior, which is in good agreement with the experimental results. Our work provides a compact and robust scheme for realizing 3D optical coupling, which is of high interest for promising applications such as 3D non-Hermitian systems and multi-channel optical signal processing.

Keywords: microtube cavities, coupled microtube systems, 3D confined resonant modes, 3D optical coupling, energy exchange

Zusammenfassung

Optische Mikrokavitäten mit gekoppeltem Whispering-Gallery-Mode (WGM) wurden ausgiebig erforscht, um die resonanten Eigenfrequenzen und räumlichen Verteilungen der optischen Moden abzustimmen, wobei viele einzigartige photonische Anwendungen in einer Vielzahl von Bereichen gefunden wurden, wie z. Hermitesche Photonik. Als eine Art von WGM-Mikrokavitäten unterstützen Mikroröhrenkavitäten mit axialen Potentialmulden 3D-begrenzte Resonanzen, indem sie Licht gleichzeitig entlang des Mikroröhrenquerschnitts und der Mikroröhrenachse zirkulieren lassen, was eine vielversprechende Möglichkeit bietet, mehrdimensionale und mehrkanalige optische Kopplung zu erforschen.

In dieser Dissertation wird die optische Kopplung von begrenzten 3D-Resonanzmoden in gekoppelten Mikroröhrenkavitäten untersucht, die durch Selbstrollen von vorgespannten Nanomembranen hergestellt werden. Im ersten Kopplungssystem werden mehrere Sätze optischer 3D-Moden in einem einzigen Mikroröhren-Hohlraum aufgrund einer Nanolücken-induzierten resonanten Trajektorien Aufspaltung erzeugt. Die große Überlappung optischer Felder in den geteilten Resonanzbahnen löst eine starke optische Kopplung der 3D-eingeschränkten Resonanzmoden aus. Als direkter Beweis für eine starke Kopplung wird die Spektren-Antikreuzungseigenschaft und das Umschalten einer Gruppe gekoppelter Grundmoden demonstriert. Die räumliche optische Feldverteilung von 3D-Kopplungsmoden wurde experimentell auf das starke Kopplungsregime abgebildet, was eine direkte Beobachtung des Energietransferprozesses zwischen zwei Hybridzuständen ermöglicht. Numerische Berechnungen basierend auf einem Quasi-Potential-Modell und dem Prozess der Modenverstimmung stimmen hervorragend mit den experimentellen Ergebnissen überein. Auf dieser Grundlage werden monolithisch integrierte Zwillingsmikroröhrenhöhlräume vorgeschlagen, um die kollektive Kopplung von zwei Sätzen optischer 3D-Moden zu erreichen. Aufgrund der ausgerichteten Zwillings Geometrien werden zwei Sätze optischer 3D-Moden in

Zwillingsmikroröhren spektral und räumlich angepasst, wodurch sowohl die fundamentalen als auch die axialen Moden höherer Ordnung jeweils miteinander gekoppelt sind. Mehrere Gruppen der Kopplungsmoden stellen mehrere effektive Kanäle für den Energieaustausch zwischen gekoppelten Mikrokavitäten bereit, die durch die gemessenen räumlichen optischen Feldverteilungen veranschaulicht werden. Die spektralen Antikreuzungs- und Umschaltmerkmale jeder Gruppe von gekoppelten Moden werden in Experimenten und Berechnungen offenbart, was auf das Auftreten einer starken Kopplung hinweist. Darüber hinaus bestätigen die simulierten 3D-Modusprofile von Zwillingsmikrokavitäten das kollektive starke Kopplungsverhalten, das in guter Übereinstimmung mit den experimentellen Ergebnissen steht. Unsere Arbeit liefert ein kompaktes und robustes Schema zur Realisierung der optischen 3D-Kopplung, das für vielversprechende Anwendungen wie 3D-Nicht-Hermitian-Systeme und optische Mehrkanal-Signalverarbeitung von großem Interesse ist.

Schlüsselwörter: Mikroröhrchen-Hohlräume, Gekoppelte Mikroröhrchen-Systeme, Begrenzte 3D-Resonanzmoden, Optische 3D-Kopplung, Energieaustausch

Contents

Chapter 1 Introduction	1
1.1 Motivation.....	1
1.2 Dissertation structure	3
Chapter 2 Background	7
2.1 Whispering-gallery-mode optical microcavities.....	7
2.2 Optical microtube cavities	9
2.2.1 General fabrication methods	9
2.2.2 Material sciences and engineering	14
2.2.3 Construction of functional microtube cavities.....	18
2.3 Coupled microtube cavities.....	28
Chapter 3 Experimental methods	31
3.1 Sample preparation.....	31
3.1.1 Nanomembranes deposition.....	31
3.1.2 Photolithography	32
3.2 Characterization methods.....	33
3.2.1 Scanning electron microscopy	33
3.2.2 Optical measurement setup	33
Chapter 4 Nanogap Enabled Trajectory Splitting and 3D Optical Coupling in Self-Assembled Microtubular Cavities	35
4.1 Introduction	36
4.2 Experimental section.....	37
4.3 Results and discussion.....	38
4.4 Conclusion.....	52

Chapter 5 Collective Coupling of 3D Confined Optical Modes in Monolithic Twin Microtube Cavities Formed by Nanomembrane Origami	55
5.1 Introduction	57
5.2 Experimental section	58
5.3 Results and discussion.....	60
5.4 Conclusion.....	78
Chapter 6 Summary and Outlook	81
6.1 Summary	81
6.2 Outlook.....	84
Bibliography.....	87
Publications	105
Presentations	107
Acknowledgements	109
Erklärung	111
Curriculum Vitae	113

Chapter 1 Introduction

1.1 Motivation

Light–matter interactions are intrinsically weak due to low density of states (DOS) of photon in vacuum and the size mismatch between light wavelength and the size of matter. With the development of advanced micro-/nano-fabrication techniques, optical microcavities have been exploited to enhance the interactions by increasing the DOS of photon in cavities.¹ The confinement of photons in microcavities have triggered high research interests in both fundamental and application-oriented studies, such as cavity quantum electrodynamics and low threshold lasers.²⁻⁶ According to the different light confinement methods, optical microcavities can be categorized as Fabry–Pérot microcavities, photonic crystal microcavities, as well as whispering gallery mode (WGM) microcavities. Fabry–Pérot microcavities confine light between two planar or curved high reflective mirrors. For photonic crystal cavities, periodic dielectric materials with desired defects are designed to form an energy band structure and trap a certain frequency range of light inside. In WGM microcavities, analogous to the propagation of sound in the gallery spaces of St. Paul's Cathedral, resonant light is confined by continuous total internal reflection which occurs at the interface of an optical dense matter with the ambient surrounding.

To further explore the manipulation of resonant light, coupled optical cavities were formed by artificial coupled photonics structures, which provides an excellent platform to tune the eigenfrequencies and spatial distributions of the resonant modes.⁷ In recent studies, the coherent coupling of resonant modes has been widely investigated to explore a variety of novel physical phenomena and practical applications, ranging from non-Hermitian photonics to nonlinear optics.⁸⁻¹⁰ Among various optical cavities, the WGM microcavities have been identified as

versatile photonic structures for building optical coupling systems. The coupled microcavity geometries play an important role to ensure a good spectral and spatial match of resonant modes for efficient optical coupling. In general, the coupling systems can be realized by putting two or more planar WGM cavities (i.e., microtoroids,^{11, 12} microdisks,¹³⁻¹⁷ microrings,¹⁸⁻²⁰ microspheres^{21, 22}) into close proximity. In such a coupling system, the energy exchange happens at a tangent site between the adjacent resonant trajectories. The corresponding optical coupling is fixed at one 2D plane, which limits the degree of freedom for the manipulation of coupled modes. The efficient 3D optical coupling of resonant light has not been reported, in which the wavevector can exist in more than one direction (i.e., azimuthal and axial directions). Therefore, it is of high interest to explore the 3D optical coupling for both fundamental and applied studies such as non-trivial evolution of wavevector and direction-selective coupling.^{23, 24}

As a special type of WGM microcavities, microtube cavities with axial potential wells can support 3D optical resonances.²⁵⁻²⁷ In addition to the resonance in an azimuthal plane, the resonant light can simultaneously oscillate along the tube axis serving as a new degree of freedom for tuning the optical coupling.^{24, 27-29} Specifically, the axial optical potential well in a microtube cavity splits the original azimuthal mode into fundamental and multiple higher-order axial modes with different spatial distributions,²⁷ which promises to achieve multichannel optical coupling in coupled microtube cavities. In this thesis, the optical coupling of 3D confined resonant modes is investigated based on microtube cavities fabricated by self-rolling of prestrained nanomembranes. In the first kind of optical coupling systems, the interlayer nanogap in the tube wall enables a single resonant trajectory partially splitting into two or three ones while sharing the same axial confinement. The split trajectories support multiple sets of 3D confined resonant modes in individual microtube cavities. The optical field largely overlaps in the split resonant trajectories, enabling strong optical coupling of 3D confined resonant light. The spectra anticrossing feature and changing-over of one group of coupled fundamental modes

are demonstrated as direct evidence of strong coupling. The spatial optical field distribution of 3D coupling modes was experimentally mapped upon the strong coupling regime, which shows the corresponding energy transfer process between the two hybrid states. Numerical calculations based on the quasi-potential model and the mode detuning process are in excellent agreement with the experimental results. In the second work, a collective coupling of two sets of 3D optical modes is demonstrated in monolithically integrated twin microtube cavities formed by nanomembranes origami. With almost the same geometries, the twin microtube cavities allow good spectral matching of multiple axial modes. As a result, both the fundamental and higher-order axial modes supported by the twin microcavities are simultaneously coupled with each other. Through mode detuning, spectral anticrossing and changing-over features of multiple groups of coupling modes are observed in both experimental and simulations, revealing the occurrence of strong coupling. The well-aligned collective strong coupling offers multiple coupling channels for efficient energy exchange between coupled microcavities, which is illustrated by the spatial optical field distributions. The simulated 3D mode profiles in the twin microtubes agree well with the experimental results. Our work provides a compact and robust scheme for realizing 3D confined optical coupling, which promises broad applications for 3D non-Hermitian systems, nonlinear optics, and multichannel optical signal processing.

1.2 Dissertation structure

This dissertation is organized in the following way:

Chapter 1 describes the motivation of this work.

Chapter 2 gives the research background including the introduction to optical WGM microcavities, microtube cavities, and research progress of optical coupling systems based on microtube cavities.

Chapter 3 presents the overall experimental methods. Detailed information is given about sample fabrications including the nanomembrane deposition, patterning, and releasing. The optical and structural properties are characterized by photoluminescence laser confocal setup and scanning electron microscopy (SEM), respectively.

In **chapter 4**, microtube cavities with interlayer nanogaps in the tube wall are fabricated by well-controlled nanomembrane release. The interlayer nanogap partially splits the resonant trajectory into two or three ones while sharing the axial confinement induced by the same lobe structure. The split trajectories support multiple sets of 3D confined resonant modes in individual microtube cavities. The large overlapping of optical fields in the split resonant trajectories enables strong optical coupling of 3D confined resonant modes. The anticrossing feature and modes changing-over are demonstrated as direct evidence of strong coupling. In particular, the spatial optical field distribution of 3D coupling modes is experimentally mapped under the strong coupling regime, which shows the corresponding energy transfer process between the two hybrid states. Numerical calculations based on a quasipotential model and the mode detuning process are in excellent agreement with the experimental results. Our work offers a compact and robust scheme for realizing multiple sets of 3D confined resonant modes and their coupling in a single microtube cavity, which is of high interest for promising applications such as optical modulations, lasing, sensing, and on-chip 3D integration.

In **chapter 5**, collective strong coupling between two sets of 3D confined resonant modes is realized in monolithically integrated twin microtube cavities via a nanomembrane origami method. This unique parallel configuration enables optical coupling to occur at the tangent line of twin microtubes along the tube axis increasing the coupling region. Owing to the aligned twin geometries of the double microtube cavities, two sets of 3D confined resonant modes are spectrally and spatially matched. Both the fundamental and higher-order axial modes are strongly coupled with each other, namely as collective strong coupling. During the detuning

process, the spectral anticrossing feature and the modes changing-over of each group coupling system as direct evidence of strong coupling are revealed in experiments and calculations. The measured evolution of spatial optical field distributions allows the direct observation of the energy exchange between each group of coupling modes in the collective strong coupling regime. Each group of coupling modes can be treated as an independent strong coupling system providing an effective path for energy exchange between coupled microcavities. Moreover, 3D mode profiles of twin microcavities simulated via the FDTD method are in excellent agreement with the experimental results. Our work offers a compact design of monolithic twin microcavities for realizing collective strong coupling of 3D optical modes, which could be exploited for manipulating higher-order optical coupling, multichannel optical signal processing, and 3D non-Hermitian systems.

Chapter 6 summarizes all the results in this dissertation and presents an outlook for the future work.

Chapter 2 Background

In this chapter, the research background of optical coupling supported by microtube cavities are given. A brief introduction to optical WGM microcavities is firstly given. Then, the rolled-up microtube cavities are described in terms of fabrication, materials, integration, and functionalization (*i.e.*, manual micromanipulation, on-chip integration, and postmodification). Moreover, the latest research progress of optical coupling systems based on microtube cavities is highlighted.

2.1 Whispering-gallery-mode optical microcavities

WGM microcavities support light propagation along the resonator-surrounding interface via total internal reflection, where the resonant condition is expressed as $n\pi D = m\lambda$.³⁰ n is the effective refractive index of the resonator, D is the resonator diameter, m is the mode number, and λ is the light wavelength in vacuum. An ideal WGM cavity with a high quality (Q) factor and a small mode volume (V) confine light to small volumes by resonant recirculation. The Q factor indicates the ability of energy storage of a microcavity determining the photon lifetime. Q is defined as the ratio of the energy stored in the oscillating cavity to the energy dissipated per cycle by damping processes:³¹

$$Q = 2\pi \frac{\text{energy stored}}{\text{energy dissipated per cycle}} = \omega_0 \frac{\text{stored energy}}{\text{power loss}} = \omega_0 \tau = \frac{\omega_0}{\Delta\omega} \quad (2.1)$$

where ω_0 is the angular frequency of a resonance, τ is the decay time for the stored energy, $\Delta\omega$ denotes the linewidth of the Lorentzian peak. In terms of the microtube cavities, the Q factor mainly comprises five components as follows:³²

$$\frac{1}{Q} = \frac{1}{Q_{abs.}} + \frac{1}{Q_{rough}} + \frac{1}{Q_{rad.}} + \frac{1}{Q_{notch}} + \frac{1}{Q_{void}} \quad (2.2)$$

Each term in this equation is connected with a specific loss, which comes from absorption of the material, scattering because of surface roughness, radiative emission, scattering from notches formed by the edges of the rolled-up microtubes, voids in the tube wall, respectively.

Microscale volume could enhance the electromagnetic field strength for interactions. V is defined as the ratio of stored energy of light and maximum energy density:³³

$$V = \frac{\text{energy stored}}{\text{maximum energy density}} = \frac{\int \epsilon(r)|E(r)|^2 d^3r}{\max[\epsilon(r)|E(r)|^2]} \quad (2.3)$$

where $\epsilon(r)$ is the optical permittivity of the cavity material and $E(r)$ is the electric field. In addition, the WGM resonances can be characterized by integer mode numbers including the polar (l), the radial (r), and the azimuthal mode numbers (m) which are related to the electromagnetic field distribution in the polar, the radial, and the azimuthal directions, respectively.²²

The WGM resonance phenomenon was first demonstrated in a spherical sample in 1961.³⁴ Since then, a variety of WGM microcavities have been demonstrated for the study of light–matter interactions and related sensing and lasing applications.^{3, 35, 36} As illustrated in Figure 2.1,³⁷ WGM microcavities in carefully designed geometries can be classified into several types including microspheres,³⁸ microrings,³⁹ microdisks,⁴⁰ microtoroids,⁴¹ microbottles,⁶ and microtubes⁴² The microrings, microdisks, and microtoroids confine resonant light in a narrow ring along the equator of the planar structure. Such 2D planar resonators can be manufactured by means of standard photolithography techniques. By contrast, the microcavities with the diameter gradient such as microtubes, microspheres, and microbottles support 3D confinement of resonant light. In addition to the resonance in an azimuthal plane, the resonant light can simultaneously oscillate along the axis serving as a new degree of freedom for the manipulation of optical modes.

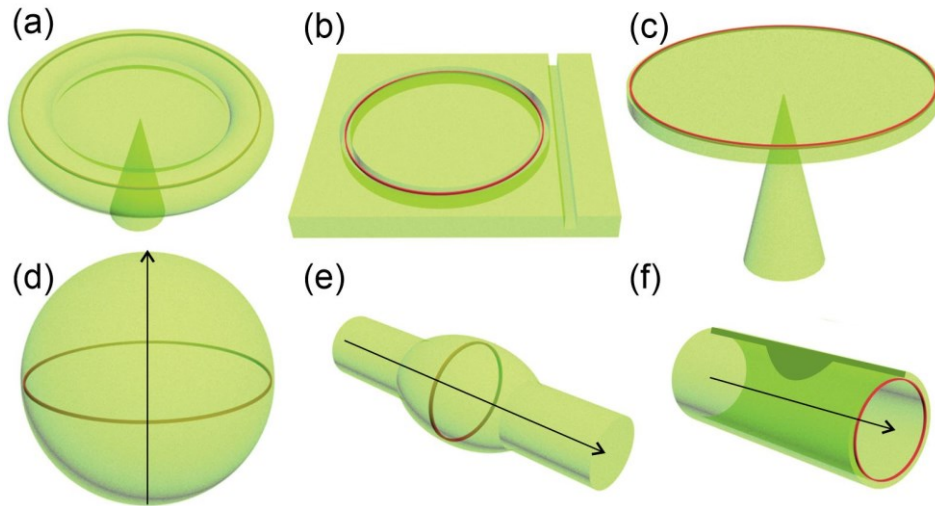


Figure 2.1. Schematic of (a) microtoroids, (b) microrings, (c) microdisks, (d) microspheres, (e) microbottles, and (f) microtubes.³⁷

2.2 Optical microtube cavities

2.2.1 General fabrication methods

Inspired by origami and kirigami (the art of paper folding and cutting), the planar nanomembrane can be assembled macroscopically into a complex 3D architecture by introducing the internal strain gradient.⁴³ In general, prestrained nanomembranes are deposited on sacrificial layers. The nanomembranes including strained and sacrificial layers are patterned via standard photolithography. By removing the sacrificial layer, the strained nanomembranes roll up into hollow-core microtube structures.

In the early stage, the sacrificial layer was dissolved in a solvent which is referred as wet-releasing nanotechnology. By this method, epitaxially semiconductor bilayer nanomembranes supporting opposite elastic forces were adopted to fabricate microtube structures.⁴⁴ As shown in Figure. 2.2, this rolled-up mechanism utilizes lattice mismatch in the heteroepitaxial crystalline bilayer.⁴³ The rolled-up nanotech can be used in other epitaxy nanomembrane systems grown by molecular beam epitaxy (MBE). However, this fabrication often requires a

selective under etching procedure which not only removes the sacrificial layer but also dissolves the strained nanomembrane itself in some cases.

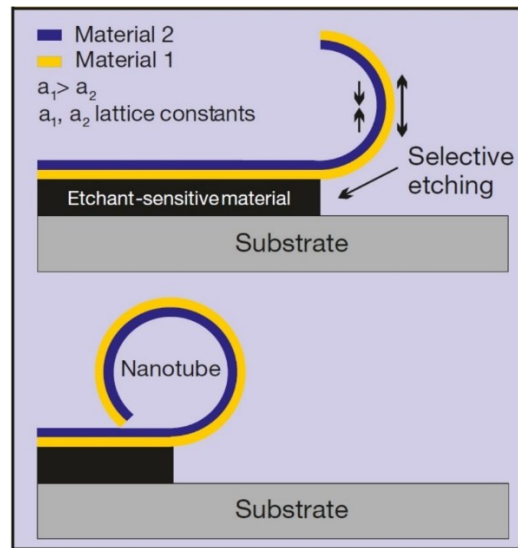


Figure 2.2. Schematic of rolled-up mechanism of tube cavities using lattice mismatch.⁴³

In order to circumvent the limitation of material choice, a polymer material of photoresist dissolved in acetone was selected as the sacrificial layer.⁴⁵ The wet-releasing nanotechnology almost covers any inorganic material and material combinations. In this case, three major parameters have an effect on the strain state of non-epitaxial nanomembranes. These parameters come from the difference in the thermal expansion between sacrificial layers and strained layers, deposition rate leading to different stress levels, and relaxation and build-up of strain during deposition.

Physical vapor deposition methods such as e-beam/thermal evaporation and sputtering technology are employed to deposit the nanomembranes.⁴⁵⁻⁴⁷ For accurate positioning, tilted deposition is usually applied to define an opening window. As shown in Figure 2.3a, by preparing strained layer in such a glancing angle deposition technique, a shadow was created at one side of the photoresist edge which provides a well-defined starting line for the rolling direction of the nanomembrane.⁴⁶

During the rolling process, the directional rolling of strained layers can be controlled by geometry design of prestrained nanomembranes and anisotropic mechanical property of sacrificial layers. For instance, when the circular pattern of sacrificial layers has a uniform thickness (left panel of Figure 2.3b), a symmetric microtube is realized with the tube wall varying symmetrically from the middle of the tube to the two ends.⁴⁷ In contrast, by employing off-center spin coating of photoresist layer, the centrifugal force gradient enables a sloped photoresist layer resulting in an asymmetric cone-like microtube cavity (right panel of Figure 2.3b) in which the spin-orbit coupling of light was demonstrated.²⁴ Besides the large-scale patterns fixing the rolling boundary, the directional control of the rolling process in nanoscale is realized by designing the nanopatterned holes array in prestrained nanomembranes (Figure 2.3c).⁴⁸ Furthermore, by introducing the strain variable nanomembranes as part of prestrained layer, the reversible shape changing between rolled and flat (unrolled) statuses was realized based on the volume expansion of rolling layer.⁴⁹

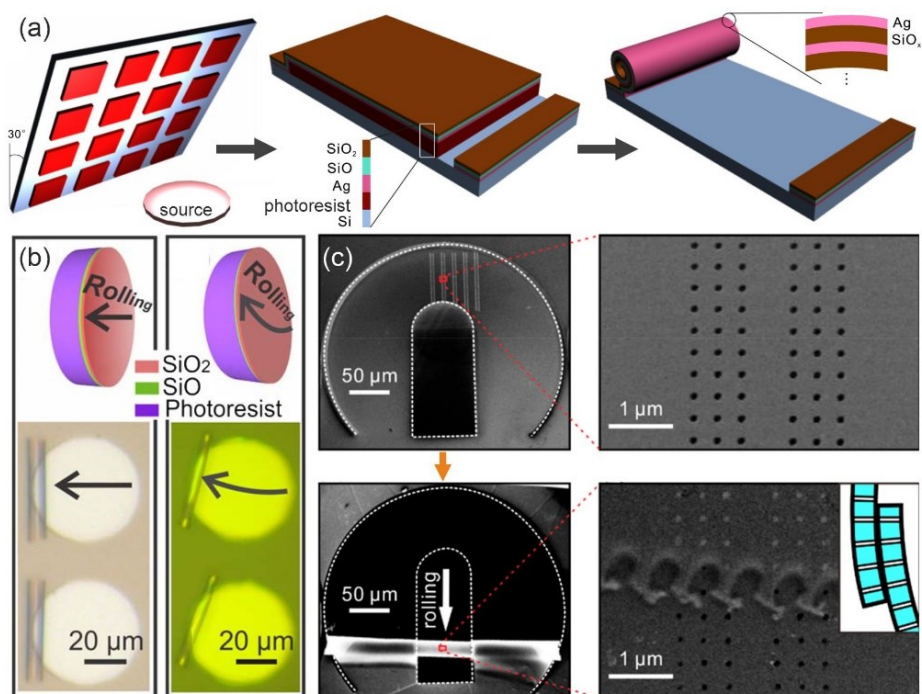


Figure 2.3. (a) Schematic of the fabrication process of a microtube by tilted deposition.⁴⁶ (b) Optical images of symmetric and asymmetric microtubes and corresponding schematics of

rolling process.⁴⁷ (c) Top panel: SEM images of the nanopatterned diamond nanomembrane and its enlarged view. Bottom panel: SEM images of the rolled-up diamond microcavity and its enlarged view.⁴⁸

Over the past few years, wet-releasing of lithographically patterned nanomembranes has been widely applied to self-assemble 3D microtube cavities. However, wet-release techniques often suffer from serious damage problems due to the liquid aggressive reagents turbulence which leads to low yield, reproducibility, and an overall deterioration of the microcavity performance.

To address these issues, dry-release methods with well-controllable fabrication on wafer-scale are explored via dry rolling of prestrained nanomembranes from a suitable sacrificial layer.⁵⁰ The main difference between wet- and dry-releasing is that the patterning of strained nanomembranes, definition of starting edge, and etching of sacrificial layer occur in plasma or gas phase atmosphere (Figure 2.4a). In a case of SiN_x microtube fabricated by dry-releasing technique, a SiN_x strained bilayer together with a top and bottom Al₂O₃ protection layer are deposited on a Si sacrificial layer, where the strain can be created by varying the deposition rate (Figure 2.4b). And then, standard lithography techniques and dry etch chemistry are applied to pattern strained nanomembranes and the sacrificial layer (Figure 2.4c). After opening a release window via reactive ion etching (RIE) to define starting rolling, the strained nanomembranes roll up into microtube by etching the sacrificial layer in a dry environment. In particular, the releasing of strained nanomembranes is determined by the reactive etching behavior between XeF₂ molecules and Si atoms in the sacrificial layer. Similar to other rolled-up microtubes, the tube diameter or its curvature is directly determined by the film thickness and the strain gradient existing along the film thickness.

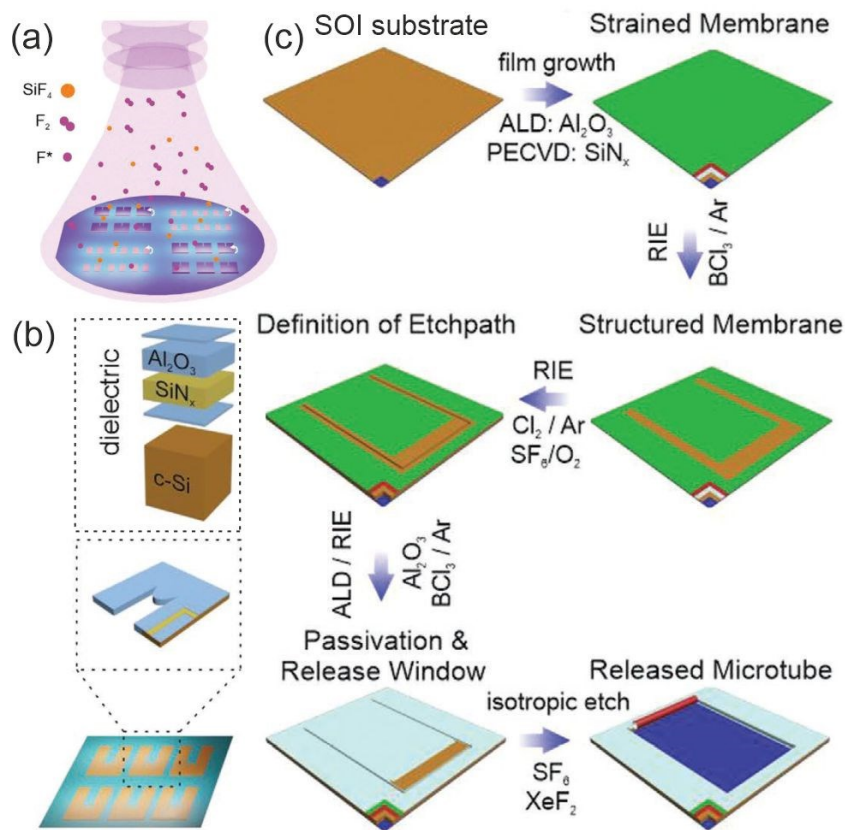


Figure 2.4. (a) Schematic of the dry release in a plasma or gas phase etch. (b) Illustration of patterning of strained layer stacks. (c) Schematic diagram showing the fabrication process (blue: SiO_2 , brown: Si, white: Al_2O_3).⁵⁰

Besides the optical microcavities, the dry-release method is developed to roll-up metallic/dielectric hybrid films for the fabrication of electronic devices. More importantly, this type of rolling-up nanotechnology can be extended to other strained materials systems (e.g., III-V, II-VI functional materials) and suitable sacrificial layers (e.g., Si, Ge, SiGe, Mo). Materials of III-V and II-VI compounds (most commonly of GaX, InX, AlX, ZnX, CdX, X=As, S, Se, N, Te, etc.), show a very high etching selectivity towards fluorine chemistry due to the high boiling points of their elemental fluorides. The strain of deposited films can be created due to lattice mismatch in hetero epitaxial films grown by metal-organic chemical vapor deposition (MOCVD) and metalorganic vapor phase epitaxy (MVPE).

2.2.2 Material sciences and engineering

Strain engineering offers a unique and fantastic platform to rearrange planar nanomembranes into 3D microtubular structures which combine the excellent properties of the constitutive materials with their unique geometries.

A bilayer consisting of one or two kinds of materials with different strains is usually employed as strained layer grown on an etchant-sensitive material. Based on the rolling geometry of microtube cavities, the corresponding strain states in bilayer can be designed and effectively implemented to realize the target mechanical behavior of either tensile and compressive prestrain, as shown in Figure 2.5a. The phenomena can be concluded into two cases of tensile or compressive prestrain, which results in compression or tension in rolled-up bilayer, respectively. When the compressive strain is introduced in thinner layer and the thicker layer supplies tensile strain, the whole nanomembrane system possesses tensile prestrain because the critical compressive strain for buckling is smaller than the critical tensile strain for fracturing, and the final rolling direction of upward or downward depends on the position of the thicker layer in bilayer, and vice versa.⁵¹⁻⁵⁴ For example, a SiO_x/Si heterobilayer is released forming a microtube structure by the downward bending of the tensile strained Si layers (Figure 2.5b).^{51, 52} In contrast, a rolled-up microtube is realized by the bending up and self-assemble of SiO/SiO₂ bilayer deposited by angled e-beam evaporation (Figure 2.5c).⁵⁴

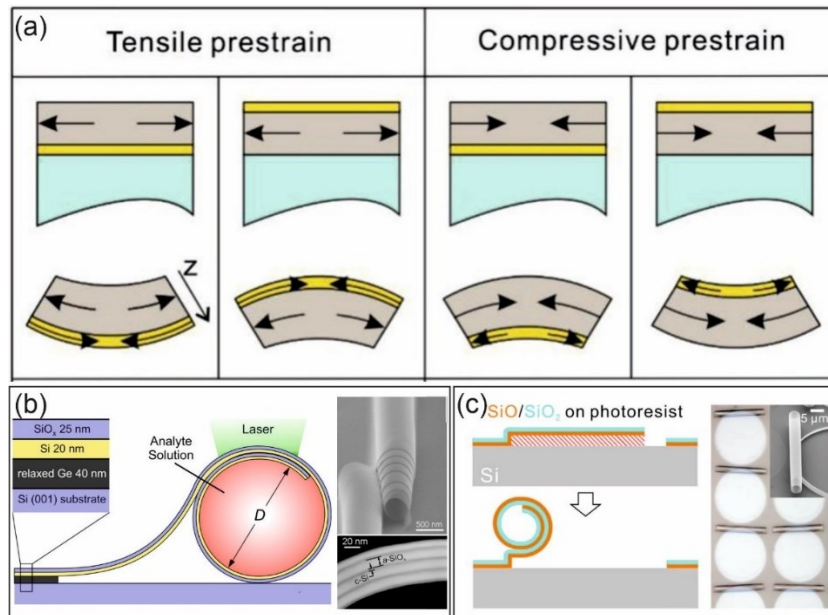


Figure 2.5. (a) Strategies for strain engineering in rolled-up bilayer. The arrow depicts the strain direction.⁵⁵ (b) A schematic illustration of the rolling of an SiO_x/Si nanomembrane into a microtube. SEM images of a rolled-down microtube.^{51, 52} (c) Schematic diagram illustrating the fabrication process of rolled-up SiO/SiO_2 microtubes. Optical microscope image of microtube arrays.⁵⁴

In a word, the keys in the rolling process of nanomembranes are the selectively etching of sacrificial layer and the releasing of strained layers depending on the designed layer stressors, which therefore limit fabrication methods of nanomembranes and the corresponding selection of materials. So far, microtube resonators have been made from many different materials and material combinations. Semiconductor materials including group IV, III-V, and II-VI grown by MBE were firstly used to fabricate microtubes where the mismatched lattice constants create a strain gradient in a bilayer. The first rolled-up microtube cavity was demonstrated by releasing prestrained layer of GaAs/InGaAs with InAs quantum dots from an AlAs sacrificial layer.⁵⁶ HF solution is selected as a good etchant to selectively etch away AlAs. In the case of releasing group IV semiconductor material of Si or SiGe, H_2O_2 solution was used to remove a Ge sacrificial layer. One of the important advantages of this epitaxial nanomembrane is that the strain can be accurately calculated based on the well-known values of the lattice constants. But

the unique growth behavior of nanomembrane in MBE process greatly restricts the choice of materials to inorganic semiconductors as strained and sacrificial layers. The photoluminescence (PL) of InAs quantum dots in GaAs/InGaAs microtubular cavity was excited by a laser beam at a low temperature of 5 K. Therefore, by combining MBE with thermal evaporation technology, a SiO_x/Si microtubular resonator in which SiO_x layers are thermally evaporated on top of the tensile strained Si layers could be excited for PL emission at room temperature by creating Si nanoclusters or nanocrystals separated out from SiO_x under post annealing.⁵²

Later on, based on the development of growing nanomembranes with e-beam evaporation, PECVD, magnetron sputtering, more non-epitaxial vapor deposition and different material systems were explored to realize room-temperature WGMs of microtube resonators. During the non-epitaxial growth process, the strain status normally depends on the experimental parameters of deposition rate and the base pressure during deposition which can be manipulated to generate the target strain gradient. For instance, utilizing photoresist as the sacrificial layer and acetone as the etchant, the material systems were largely extended to metals (Ti, Au, Ag, Pd, Fe, Pt, Au/Ag, $\text{Ni}_{80}\text{Fe}_{20}$, Pd/Fe/Pd, Ti/Au),⁵⁷ oxides (SiO_2 , TiO_2 , ZnO, Al_2O_3 , $\text{ZrO}_2/\text{Y}_2\text{O}_3$) and diamond for better surface roughness and higher light confinement of microtube cavities.⁴⁵ In particular, SiO/SiO_2 bilayers are widely used as strained layers to prepare microtube cavities with high Q factor.^{27, 58-60} The bottom and the top SiO_x layer are deposited at different rates for exerting different stress levels which can largely facilitate the rolling process. Recently, due to the strain inside SiN_x can be tuned into compression or tension by changing the deposition parameters, the SiN_x bilayer supporting different strain states fabricated by PECVD are employed as prestrained layer.⁵⁰ Thanks to the novel dry-releasing scheme yields excellent uniformity for fabricating high-quality microcavities, the SiN_x microtubular cavities exhibit optical resonances in a broad spectral range with record-high Q-factors >7800 which provide an excellent platform to construct plasmon-photon and strong optical coupling systems. Here,

several typical microtubes systems including materials of strained layers and corresponding deposition methods, the type of strain, materials of sacrificial layer and etchants used for release are summarized in Table 2.1.

Table 2.1. The summary of several typical microtubes systems (T and C is tension and compression, respectively.)

Rolling layer			Sacrificial layer		rolled direction	Ref.
material	strain	fabrication	material	etching		
(Al)GaAs/In(Al)GaAs	T/C	MBE	AlAs	HCl, HF	up	61-69
GaN/AlN	C/T	MOVPE	Si (111)	HNO ₃ /HF	down	53
Cr/Si/SiGe	T/C	thermal evaporative/MBE	Si (001)	KOH	up	70
SiO _x /Si	T	thermal evaporative/MBE	Ge	H ₂ O ₂	down	51, 52
ZnO, Al ₂ O ₃ , Si _x N _y , Ti, Au, Ag, Pd, Fe, Pt, Au/Ag, Ni ₈₀ Fe ₂₀ , Pd/Fe/Pd, Ti/Au	C	ALD, PE-CVD, e-beam evaporation, PIII&D	photoresist	acetone	up	45
SiO/SiO ₂	C	e-beam evaporation	photoresist	acetone	up	24, 27, 42, 45, 47, 54, 58-60, 71-86
SiO ₂	C	e-beam evaporation	photoresist	acetone	up	32, 87-90
ZrO ₂ /Y ₂ O ₃	C	CVD/ e-beam evaporation	photoresist	acetone	up	55, 91, 92
TiO ₂	C	ALD, e-beam evaporation	photoresist	acetone, DMSO	up	45, 93-97
Ag/SiO _x	C	e-beam evaporation	photoresist	acetone	up	45, 46
diamond	C, T	wafers with diamond	photoresist, SiO ₂	acetone, HF	up, down	48, 98
SiO/TiO ₂ /Ag, SiO/SiO ₂ /Au	C	e-beam evaporation	PMMA	burning	up	99, 100
SiN _x	T/C	PE-CVD	Si	XeF ₂	up	50

2.2.3 Construction of functional microtube cavities

Optical resonance in microtube cavities originates from the constructive light circulating and interfering along the circular trajectory. The microtube resonators can be divided into two categories of active and passive cavities. For the former one, by incorporating luminescent materials into tube walls, the microtube cavities are excited by a focused laser beam with high photon energy to generate PL, which is further coupled into the WGMs. Optical resonance is probed from the far-field WGM emission. In microtube cavities consisting of semiconductor materials, luminescent quantum dots were introduced during MEB preparation.¹⁰¹⁻¹⁰⁵ In Si-based microtube cavities (SiO_x and SiN_x), the defect centers formed during deposition of nanomembranes emit PL under pumping light. For the passive resonators, based on evanescent coupling by placing a nearfield coupler, such as a tapered fiber,⁸⁸ integrated waveguide, or prism,¹⁰⁶ in close proximity to the microtube cavity, the WGM emission signals are detected by transmission spectra through the same coupler. One of the advantages of using a coupler coupling light into the system is that the electromagnetic wave can be guided in a predetermined direction.

The functional microtube cavities are previously constructed by manual micromanipulation. With the use of fiber abrupt tapers inserted into the end of the tubes, a single rolled-up microtube can be lifted off from the host substrate and transferred to a foreign one with a controlled position.¹⁰³ As shown in Figure 2.6a, a four-port add-drop configuration was realized by manually transferring a SiO_2 microtube from the substrate to sandwiched between two fibers. The angle between the through and drop fiber leads to different coupling efficiencies. This device might serve as an optical frequency filter and vertical light transfer at telecommunication wavelengths in future 3D multi-level optical data processing.⁸⁹ Moreover, Figure 2.6b-d present a microfluidic integration system in which a set of high-quality microtubes were transferred by micro-manipulation to robust SU-8 polymeric sockets patterned on one chip.⁹⁰ After final chip

assembly and packaging with a PDMS cover, the integration of multiple channels and several microtube resonators shows the capability of multiplexed detection. In addition, owing to microtube cavities supporting resonances in a vertical plane, a selective out-of-plane optical coupling system was demonstrated by manually placing a TiO₂ microtube resonator on a planar SU-8 polymer based waveguide fabricated by lithography.⁹³ For the above-mentioned devices, the microtubes must be lifted off from the mother substrate. This mechanical process may damage the structural integrity of the microtube resonators.

Recently, in a strong coupling system formed by a microtube cavity and a microsphere, the polystyrene microsphere was manually transferred into the intrinsic hollow of rolled-up microtube structures on chip which supply a simple and flexible way for designing photonic molecules with largely mismatched sizes.⁶⁰ Besides, rolled-up microtubes can be employed for trapping and detection of cells in a solution based on the manual micromanipulation setup. As shown in Figure 2.6e, the capillary tip on an XYZ μ -manipulator was positioned at one of the open ends of a microtube to pump a cell to the opposite opening of the resonator after the pump was turned on.⁷⁴ A label-free optofluidic sensor was realized in a microtube resonator through peak sharpening and spectral shifts of WGMs under light illumination.

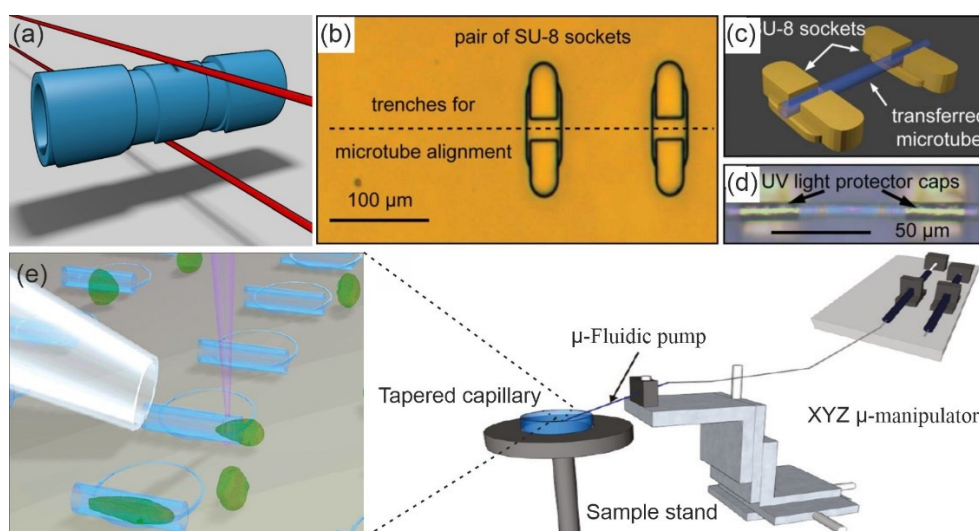


Figure 2.6. (a) Schematic of two tapered fibers in a four-port add-drop configuration coupled to a microtube cavity.⁸⁹ (b) Optical image of a pair of SU-8 sockets. (c) 3D sketch of a

transferred microtube placed into the socket structures. (d) Optical image of a transferred microtube.⁹⁰ (e) Diagram of the μ -syringe setup used for the manual manipulation. Schematic showing the image of a microtube with a cell sucked in at one end.⁷⁴

During the micromanipulation process, a precise control of manual operation is required with the aid of a CCD camera, which renders such a process time consuming and less feasible for massive integration and suffer from drawbacks of mechanical vibrations and system instability. In order to achieve applications of optical resonators at the chip level, a manual substrate-on-substrate transfer based on the gravitational force induced by the solvent in and around the tube was reported on the fabrication of InGaAs/GaAs microtube cavities on Si substrates.¹⁰²

Actually, the unique fabrication of rolled-up microtubes offers a highly flexible solution for integration on waveguide chips avoiding any manual process steps. As shown in Figure 2.7, a fancier monolithically integrated configuration has been designed and demonstrated to realize on-chip fabrication which is a crucial ingredient for advanced photonic integrated circuits. Figure 2.7a schematically presents that the on-chip Si waveguides with two grating couplers at both ends to send light and collect the transmission signal were fabricated from a SOI substrate via lithography and reactive ion-etching techniques. And then, based on maturing rolled-up nanotechnology, TiO₂ microtubes were directly built up on the Si waveguides (Figures 2.7b-d). Thus, multiple microtube cavities can be integrated on waveguide arrays (Figures 2.7e-g) which demonstrates the feasibility to integrate massive microtubes on multiple waveguides. More importantly, the monolithically integrated devices offer a much more accurate tuning of the coupling gap which is crucial for effective coupling. In this case, the optical coupling strength between the microtubes and the waveguides can be flexibly tuned by changing the thickness of the photoresist and the number of windings of the rolled-up resonators. The integration of

microtubes on multiple waveguides for parallel and multi-routing optical coupling was also reported almost at the same time in other literatures.^{29, 107}

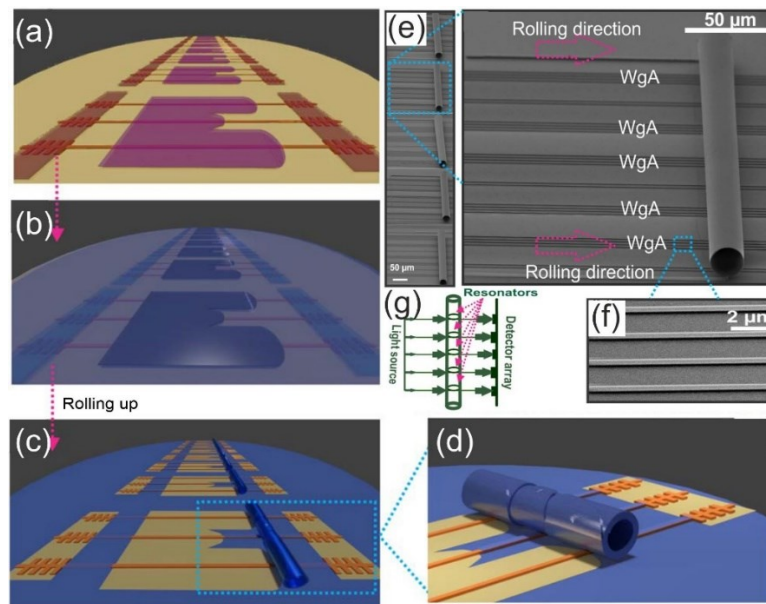


Figure 2.7. (a) Patterned photoresist arrays on waveguides. (b) Strained layer is deposited onto the waveguide chip. (c) The strained nanomembrane rolls up into microtubes. (d) Magnification of a microtube cavity on top of waveguides. (e) SEM image of several fully integrated long microcavities spanning over waveguide arrays (WgAs) and corresponding magnification of single integrated microcavity. (f) Magnification of one part of WgAs. (g) Schematic illustrating a ring resonator array along a microcavity.⁹⁶

Besides, various post modifications in microtubes have been widely explored which is particularly important for the manipulation of optical modes in practical devices. The optical modes of microtube cavities are essentially determined by the perturbation of the evanescent field, the effective refractive index and geometrical parameters of the microcavities, by which the resonant modes can be tuned.

Generally, because the microtube cavities with subwavelength wall thickness cannot strictly confine light inside the cavity but decay exponentially to outside several hundred nanometers, the homogeneous perturbation from the surrounding environment can slightly modify the

evanescent field leading to resonant modes to be perturbed. To investigate the evanescent coupling effect, a near-field probe was tangential to touch the surface of a microtube and directly interacted with the evanescent field (Figure 2.8a).⁷⁷ When the probe was scanned along the axial direction, owing to the lateral variation of the evanescent field, the redshift and tuning of each axial mode is position-dependent. The fundamental mode owing extensive volume overlap with the probe shifts more than the other axial modes (Figure 2.8b). Moreover, by moving the probe perpendicularly to the axis of the microtube, a big redshift of resonant modes over a large energy range was observed (Figure 2.8c). The similar tuning effect can be used in sensing and optofluidic applications such as, introducing polarizable molecules or particles around the microtube surface, and injecting fluidic into the hollow channel of the microtubes.

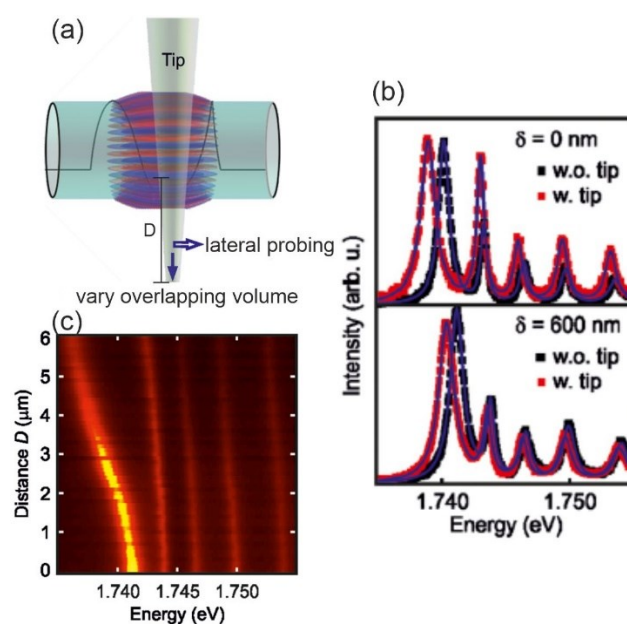


Figure 2.8. (a) Schematic of the lateral probing process and the method used to vary the overlapping volume between the probe and evanescent field. (b) Measured details of an azimuthal mode with and without the probe at two lateral positions. (c) PL intensity maps for the mode as a function of probe distance D .⁷⁷

The resonant modes of microtube cavities can also be tuned by changing the effective refractive index of the microcavity via the post-deposition of nanomembranes to slightly modify

the optical path length. Stepwise one-by-one monolayer coating by atomic layer deposition (ALD) was usually introduced to deposit Al_2O_3 on a rolled-up microtube.^{71, 87} ALD can meet the needs for atomic layer control and conformal deposition using sequential, self-limiting surface reactions.¹⁰⁸ In the ALD coating process, the precursor can disperse into the hollow core of microtube, allowing for deposition of Al_2O_3 on both inner and outer tube surfaces to increase the effective refractive index of tube wall resulting in a controllable red shift of the resonant modes.⁷¹ When Al_2O_3 was deposited from 0 to 80 nm in steps of 10 nm (Figure 2.9a), the number of observed axial modes decreased due to the weakened significance of the lobe. In the spectrum from the most thickly coated microtube (deposition of 80 nm Al_2O_3 leading to a 160 nm increase in the tube wall thickness), the resonator modes shifted into higher order radial multimode. The thicker tube wall also contributes to the presence of TE (magnetic field parallel to the tube axis) modes which is an important polarization state of resonant modes.

Furthermore, by gradually asymmetrical postdeposition SiO_2 nanocap on the top side of the microtube through e-beam evaporation (Figure 2.9b), optical resonances showed spectral blueshifts followed by redshifts, which is attributed to a competition between shape deformation and effective increase of tube wall thickness (Figure 2.9c).⁷³ Besides using these physic vapor deposition techniques, the layer-by-layer (LBL) assembly was employed to introduce poly(acrylic acid)/poly(ethylenimine) (PAA/PEI) polymer layer on the inner and outer surface of an oxide microtube walls to modify the effective refractive index of cavities.⁹² When the sandwiched microtubes were exposed to a moist surrounding, the expansion of polymers due to the absorption of water molecules lead to an increased wall thickness and a decrease of the wall's refractive index, which further enabled a profound wavelength redshift of the WGM resonances. The modified microtube cavities can be used to detect the environmental relative humidity.

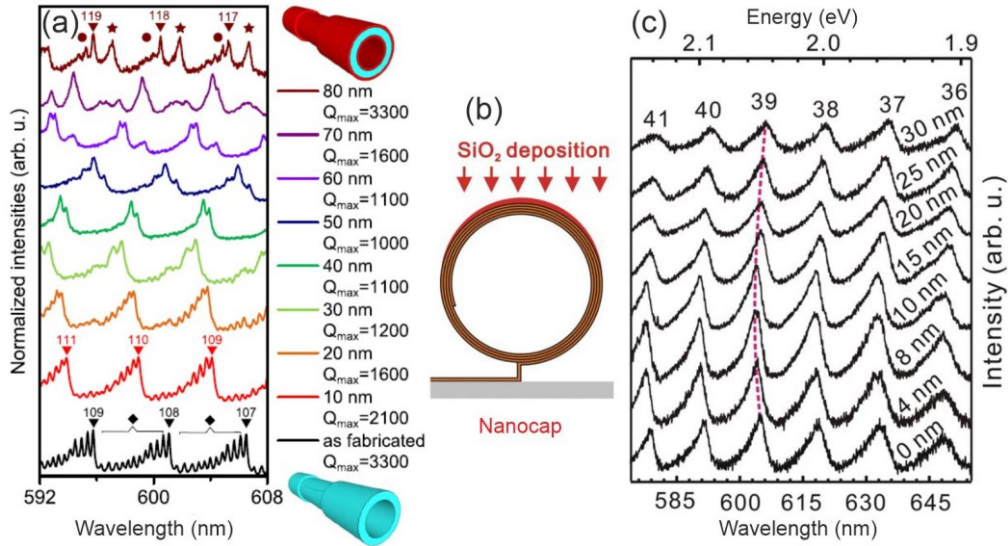


Figure 2.9. (a) Evolution of the PL spectra of the microtube cavity as a function of Al₂O₃ thickness.⁸⁷ (b) Sketch of a microtube cross section during SiO₂ deposition. (c) PL spectra of the microtube after a series of SiO₂ nanocap depositions.⁷³

Owing to the optical resonance of microtube cavities coming from the constructive interference of the light traveling along a circular trajectory, one may affect the geometry of microtubes should have a significant influence on resonant behavior. In previous reports, various shaped lobes predefined on the start and end rolling edges of 2D nanomembranes, such as triangular and parabolic segments, are designed as a new degree of freedom to tailor the confinement of light.^{26, 66, 68} In contrast to regular WGM cavities, the rotational symmetry is broken by varying rolling edges along the tube axis in the rolled-up microtubes with lobes. The complex manipulations for deforming the cavity geometry to break the chiral symmetry, such as precision lithography and introducing local scatters near the cavity boundary via micromanipulation, are not required in microtube systems.¹⁰⁹ This type of microtube cavities not only supports 3D confined resonant modes but also provides a 3D tailored spiral shape which enables a unique property of 3D directional light emission investigated in detail in previous work.⁸² In this case, a triangular-shaped rolling edge induces the light confinement in a quasi-potential well due to the effective refractive index change along the tube axial direction.

A single azimuthal mode split into fundamental and higher-order axial modes which interacts with the triangular edge at different sites and the corresponding facet orientation of the outer edge. As shown in Figure 2.10a, the fundamental mode shows a single light emission beam, but the higher order axial modes exhibit dual light emission beams symmetrically distributed at two sides of the triangular lobe. The emission directions change as the curved triangular nanomembrane edge faces into different directions which was demonstrated by the angle-resolved measurements (Figure 2.10b).

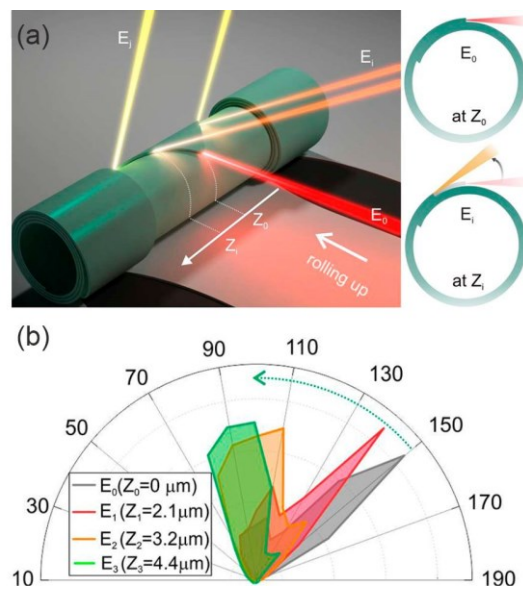


Figure 2.10. (a) Left: Schematic showing directional emission of fundamental and higher order axial modes from microtube cavity. Right: Cross-sectional views at different axial position (Z_0 , Z_i) with corresponding light emission directions. (b) The angle-resolved measurements.⁸²

The spiral asymmetry of microtube cavities can be further modified through post-shaping of cavity geometry which is highly desirable for fine-adjusting of chiral modes and directional light emission.⁸⁵ A high-index nanobelt fabricated by electron beam-induced deposition (EBID) as an additional crescent-shaped nanocap structure on top of the outer rolling edge was employed to disturb the spiral tube wall of microtube cavities. As shown in Figure 2.11a and b, before the deposition of the nanobelt, probabilistic bi-directional emission with comparable intensities occurred because of the outcoupling effect of both outer and inner rolling edges. In

contrast, the high-index crescent-shaped nanocap deforms the spiral structure with a modified resonant light leakage site which induced the nanocap-decorated outer edge as the foremost scatter and further breaks the balance between backscattering strengths of clockwise (CW) and counterclockwise (CCW) lightwaves (Figure 2.11c and d). A strong mode chirality emerges in post-modification microtube cavity while the CCW lightwave becomes the dominant component. Such a scheme of re-shaping the microcavity boundary for manipulating the properties of resonant modes can also be applied to other 3D optical microcavities and photonic devices.

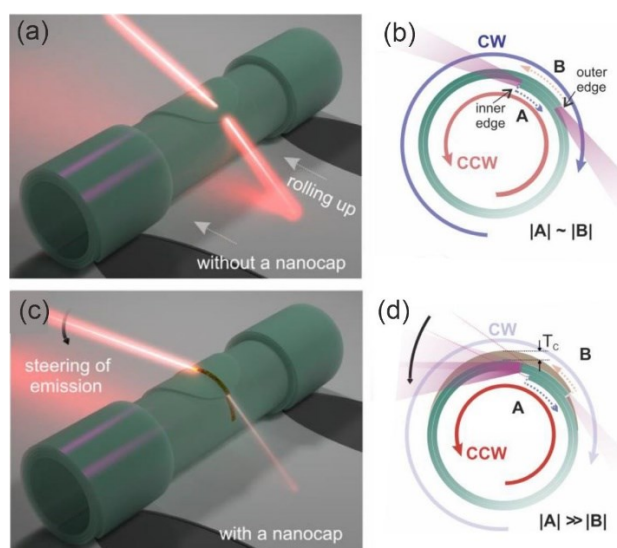


Figure 2.11. The microtube cavity without (a) with a nanobelt (c) across the tube forming a nanocap. Schematics in a cross-sectional view showing the unbalanced backscattering between CW and CCW components and corresponding emission directions: without (b) and with the nanobelt (d).⁸⁵

In addition, an external strain enabled post-modification of the geometry of microtubes is explored as an efficient and highly flexible approach for modifying the optical resonance wavelength.⁷⁹ To realize a controllable mechanical stretching process, the microtube was transferred on the polydimethylsiloxane (PDMS) substrate (Figure 2.12a). The lateral stretching leads to a modification of the cross-section of microtubes shape and the lobe width

corresponding to the width of the axial potential well. As a result, the field distributions of resonant modes and the axial free spectral ranges (FSRs) defined by the depth of potential well are efficiently tuned (Figure 2.12b). As confirmed by the evolution of axial modes upon continuously increased strain shown in Figure 2.12c, the axial modes show a continuous redshift attributed to the tube shape change from non-round to round shape upon a moderate strain (less than 12%) and then blue shift due to a shrunk cavity circumference with further increased strain. Moreover, the spacing between each axial mode continuously decreases upon increased strain owing to the strain imposed along the axial direction which reduced the depth of axial potential well. This approach of the efficient modification of the resonant modes by strain engineering potentially provides a simple and robust post-fabrication treatment for not only microtube cavities but also the other nanomembrane-based optical microcavity devices.

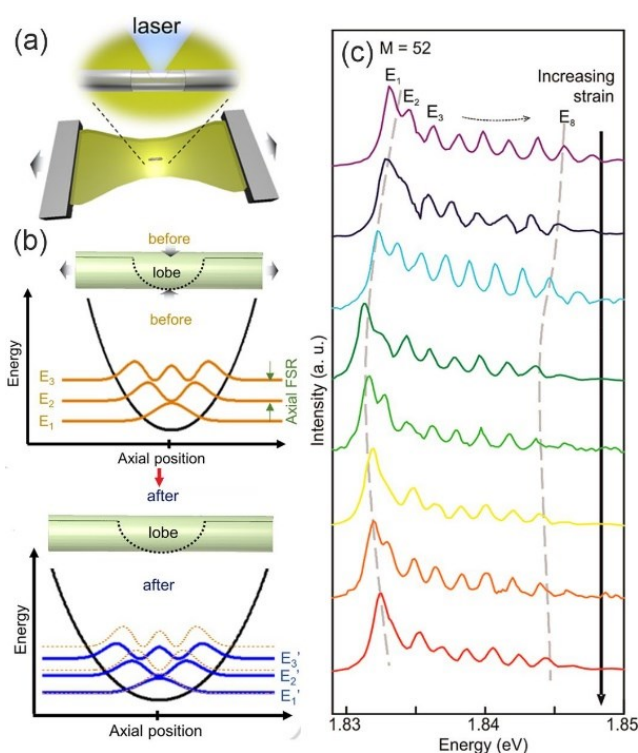


Figure 2.12. (a) A microtube was transferred on PDMS substrate for strain-enabled modification. (b) Schematics illustrating a modification of axial modes and the microtube shape along the tube. (c) Evolution of axial modes upon an increased strain.⁷⁹

2.3 Coupled microtube cavities

Coupled optical microcavities provide an intriguing platform to manipulate photons in terms of frequency and spatial distribution,¹¹⁰⁻¹¹² finding many unique photonic applications in a variety of fields, such as nonlinear optics,^{112, 113} laser physics,^{17, 39} and non-Hermitian photonics.^{20, 114-116}

Depending on the coupling strength, the resonance interaction in coupled microcavities can be divided into weak and strong coupling regimes. In general, weak coupling known as the Purcell effect is a perturbation regime where the decay rate is dependent on electromagnetic field density.^{14, 117} As the coupling strength exceeds damping rates, strong coupling regime is reached with the energy splitting between two hybrid states called Rabi splitting, in which the energy exchange rate between coupling components is very fast.^{118, 119} Anticrossing behavior is another characteristic of a strongly coupled system.^{117, 120}

Optical microcavities guiding resonant light along a ring trajectory (i.e., the path of resonant light) in carefully designed geometries form WGM resonances by self-interferences, which have been employed as a versatile photonic structure for building coupled microcavity systems and investigating resonant optical coupling phenomena.^{1, 121, 122} To construct the optical coupling systems, usually two or more WGM microcavities (e.g., microtoroids,^{11, 12} microdisks,^{123, 124} microrings,¹²⁴⁻¹²⁶ microspheres^{21, 127}) are placed in close proximity. In these coupling systems, the microcavity geometries and the inter-cavity coupling gap play important roles to ensure sufficient spectral match and efficient coupling. The above-mentioned WGM microcavities support 2D confined resonant modes where the corresponding optical coupling is fixed at one 2D plane.

Nanomembrane origami is the art of constructing 3D microstructures from 2D nanomembranes through a self-rolling process, which offers high design flexibility in

microcavity geometries.^{128, 129} The origami microtube cavities form out-of-plane WGM resonances, which is distinct from conventional circular-shaped WGM resonators that confine light in one 2D plane. Over the past decade, microtube cavities have been explored for constructing optical coupling systems. Several articles have been published with emphasis on the fundamental studies of microtube cavities,^{28, 130-136} and strong coupling behavior in coupled microcavities.^{111, 112, 117-119, 137-139} For instance, an optical coupling system is formed by trapping a microsphere into the hollow core of a microtube cavity, which possesses the internal tangent configuration different from the conventional coupled microcavities comprised of solid-core WGM microcavities with an externally tangent site (Figure 2.13a).⁶⁰ In addition to the tangent configuration, concentric ring microtubular cavities were reported to realize supermode hybridization by varying the thickness of the spacer layer (Figure 2.13b).⁸⁰ All these optical coupling systems support strong coupling of 2D confined resonant modes. In recent researches, optical coupling systems supporting out-of-plane optical coupling has been proposed to explore 3D photonic integration, for example transferring a microtube cavity positioned on a planar microring structure (Figure 2.13c).⁹³

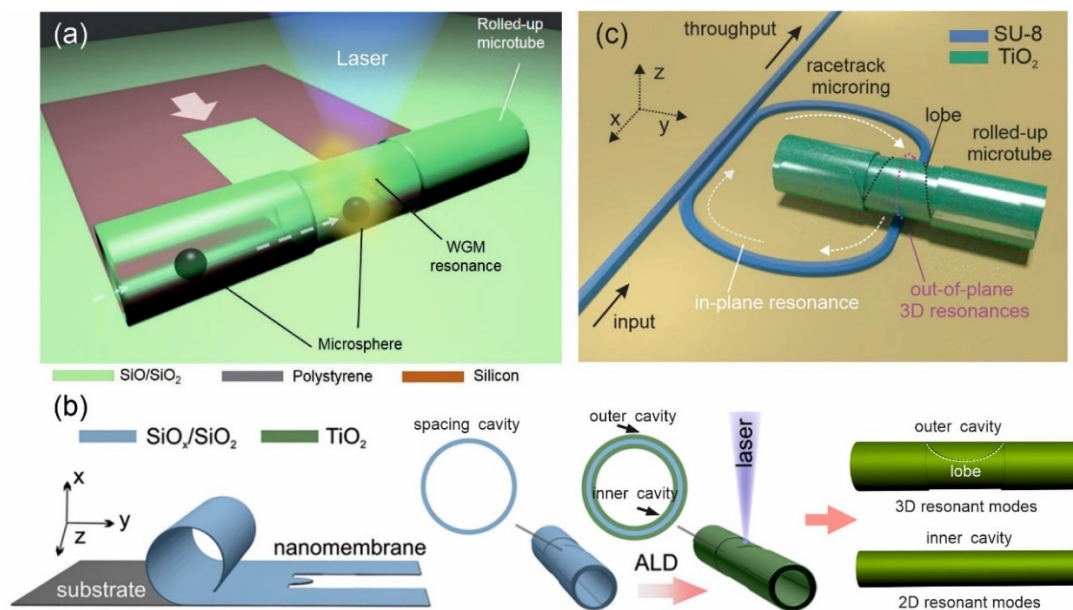


Figure 2.13. Schematic of coupled microtubular cavity systems (a) a microsphere trapped in a microtube without lobe, (b) concentric microtubular cavities, (c) a microtube onto a microring.

Owing to the mode coupling between one set of 2D and another set of 3D confined resonant modes or two sets of 2D confined resonant modes, the above-mentioned optical coupling based on microtubular cavities is still fixed at one 2D planar. Up to now, the efficient 3D confined optical coupling of resonant light has not been reported, in which the wavevector can exist in more than one direction (i.e., azimuthal and axial directions) for both fundamental and applied studies. The manipulation of wavevector with a higher degree of freedom allows for the study of topological photonic based on non-trivial evolution of wavevector, such as generating optical Berry phase, optical spin-Hall effect.^{23, 24}

The microtube cavities with axial potential wells support 3D WGM resonances along both azimuthal and axial directions,^{26, 27} offering a promising possibility to explore multichannel and multidimensional optical coupling. The axial confinement within the microtubes adds a new degree of freedom for the manipulation of optical resonances and coupling.^{24, 27-29} Specifically, the axial optical potential well in a microtube cavity splits the original azimuthal mode into fundamental and multiple higher-order axial modes with different spatial distributions,²⁷ which promises to achieve multichannel optical coupling in coupled microtube cavities. It is therefore highly desirable to explore optical coupling systems of microtube cavities for realizing simultaneously multichannel and multidimensional manipulation of photonic signals.

Chapter 3 Experimental methods

This chapter is divided into two parts. The first part presents the deposition of nanomembranes and step-by-step photolithography process for the fabrication of microtube cavities. The second part describes the characterization techniques used to determine optical properties and structural measurement.

3.1 Sample preparation

3.1.1 Nanomembranes deposition

In this thesis, the microtube cavities were fabricated by self-rolling of prestrained nanomembranes. In detail, the nanomembranes are consisted of Al_2O_3 stop layer/Si sacrificial layer/ Al_2O_3 protection layer/ SiN_x prestrained layer/ Al_2O_3 protection layer from bottom to top, as shown in Figure 3.1. The Si film serves as a sacrificial layer that can be rapidly removed by xenon difluoride. An Al_2O_3 film between the sacrificial layer and substrate was selected as the stop layer to prevent the Si/ SiO_2 substrate from being damaged by gas-phase etch. Two Al_2O_3 layers at the bottom and top of SiN_x film can protect the strained layer from corrosion by the solvents and etchants during the film patterning and film release. All the Al_2O_3 layers were deposited by PE-ALD (FlexAL, Oxford Instruments PLC, Abingdon, UK). Si and SiN_x layers were fabricated by ICPECVD SI 500 D (Sentech Instruments GmbH, Berlin, Germany). The SiN_x strained film was prepared with a compressive strain in the bottom part while a tensile strain in the upper part by adjusting the related deposition parameters such as inductively coupled plasma (ICP) power and reactive gas flow.

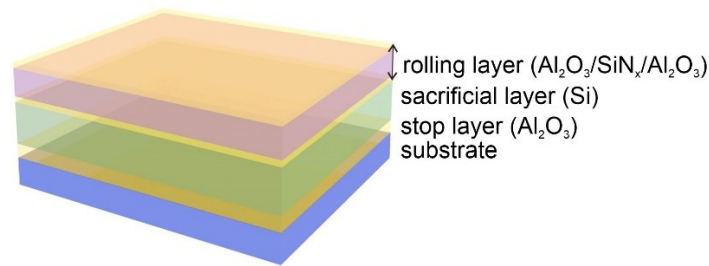


Figure 3.1. Schematic of the deposition of nanomembranes.

3.1.2 Photolithography

After the deposition of nanomembranes, standard photolithography and dry-etching were utilized to pattern the film and release the prestrained layer, as shown in Figure 3.2. The dry-etching technique possesses high yield and reproducibility enabling wafer-scale fabrication of monolithically integrated microtube cavities.

Firstly, a photoresist layer (AZ-5214E, Microchemicals GmbH, Germany) was spin-coated onto the nanomembranes. And then, the photoresist layer was patterned with different shapes according to the designed microtube configuration. The pattern was performed by a maskless aligner (MLA 100, Heidelberg Instruments Mikrotechnik GmbH, Heidelberg, Germany). RIE (Plasma Lab 100; Oxford Instruments PLC, Abingdon, UK) with chlorine and fluorine chemistry were used to structure the rolling layer under the patterned photoresist after development procedure. These trenches were etched into the sacrificial layer in similar steps to define where to start etching the sacrificial layer for releasing the prestrained films. The patterned sample was then passivated by coating an Al_2O_3 thin film to anchor the strained layer to the substrate. After opening the etching windows by RIE, the microtubular cavity was realized by a gas phase etch (Xactix e2; Orbotech LTD., Yavne, Israel) to etch away the Si sacrificial layer resulting in the rolling of prestrained nanomembranes.

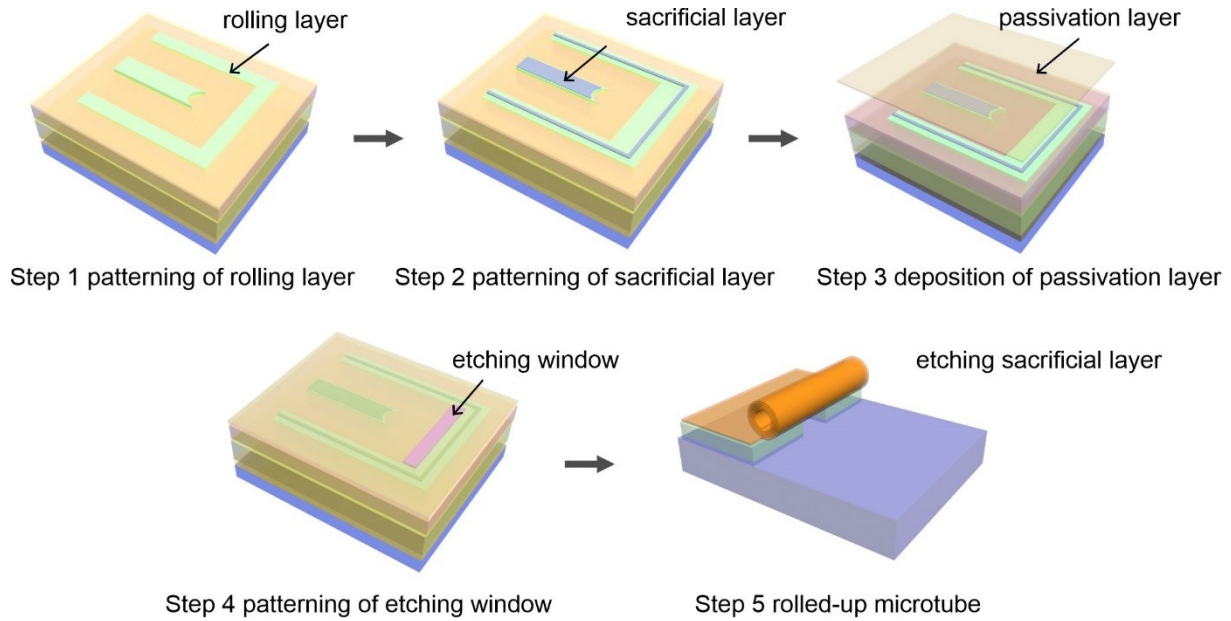


Figure 3.2. Schematic diagram illustrating the fabrication process steps of the representative SiN_x microtubular cavities.

3.2 Characterization methods

3.2.1 Scanning electron microscopy

SEM characterization and focused ion beam (FIB) cuts were performed in an NVision40 (Carl Zeiss Microscopy GmbH, Germany) for imaging the microtubular cavities. FIB cuts were made using Ga⁺ ions of 30 kV with currents of 3 nA and 700 pA. SEM images of the cross-sections were taken at 10 keV and very low current (aperture 7.5 μm) to avoid charging.

3.2.2 Optical measurement setup

Optical measurement was performed with a photoluminescence laser confocal setup (LabRAM HR Evolution, Horiba Scientific), as shown in Figure 3.3. An excitation source with 457 nm (solid-state laser) laser line was utilized to excite photoluminescence emission (in the range of ~1.5-2.5 eV) of defects in the SiN_x microtube serving as a light source to pump the optical resonances. A 50× microscope objective was used to focus the laser beam onto the microtube cavities and collect the corresponding emission light. The resonant light was guided to the

spectrometer with 600 blz/mm and an electrically cooled charge coupled device (CCD) camera. For the measurement of resonant modes with polarization states (transverse magnetic (TM) mode: electric field parallel to the tube axis; transverse electric (TE) modes: magnetic field parallel to the tube axis), a half-wave plate for 90° rotation and a polarizer were used to distinguish whether the polarization state of resonant modes was TE or TM.

The spatial distributions of the axial modes were mapped by moving the tubular microcavities with a step of 0.1 or 0.2 μm along the tube axis and collecting the far-field emission spectra at different positions of the lobe region.

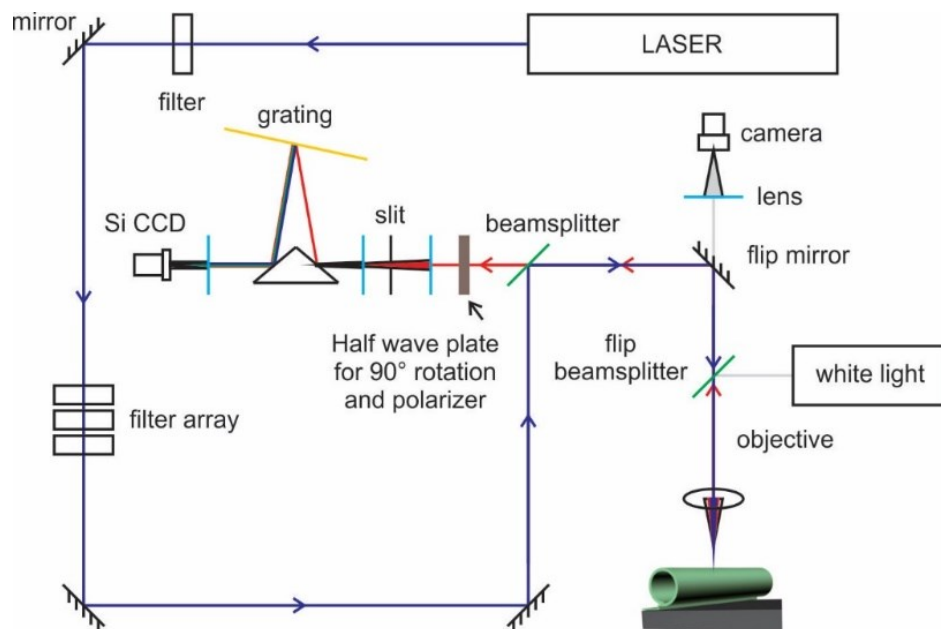


Figure 3.3. Sketch of the laser confocal setup.²⁷

Chapter 4 Nanogap Enabled Trajectory Splitting and 3D Optical Coupling in Self-Assembled Microtubular Cavities

In this work, the generation of multiple sets of 3D confined resonant modes was realized in a single microtube cavity owing to nanogap induced resonant trajectory splits. The optical field largely overlaps in the split resonant trajectories, enabling strong optical coupling of 3D confined resonant light. The anticrossing feature and modes changing-over were demonstrated as direct evidence of strong coupling. In such an optical coupling system, the spatial optical field distribution of 3D coupling modes was experimentally mapped upon the strong coupling regime, which allows direct observation of the energy transfer process between two hybrid states. Numerical calculations based on a quasi-potential model and the mode detuning process are in excellent agreement with the experimental results. The generation of multiple sets of 3D confined resonant modes and their efficient coupling in a single microcavity is of high interest for directional coupling with a higher degree of freedom to realize on-chip integration with elevated functionalities such as multiplexing, 3D lasing, and signal processing.

The results presented in this chapter have been published: X. Wang, Y. Yin, H. Dong, C. N. Saggau, M. Tang, L. Liu, H. Tang, S. Duan, L. Ma, and O. G. Schmidt, Nanogap Enabled Trajectory Splitting and 3D Optical Coupling in Self-Assembled Microtubular Cavities, *ACS Nano* 2021, 15, 18411–18418. Y.Y., L.M., and O.G.S. conceived the project. X.W., Y.Y., H.D., C.N.S., and S.D. designed the experiments and prepared the samples. L.L., and H.T. performed the structure characterizations. X.W., and Y.Y. performed the optical measurements. X.W., Y.Y., and M.T. performed the numerical simulation. X.W., Y.Y., and L.M. analyzed the data and wrote the paper. All authors participated in the discussions.

4.1 Introduction

Optical microcavities guiding resonant light along a ring trajectory (*i.e.*, the path of resonant light) in carefully designed geometries form WGM resonances by self-interferences, which have been employed as a versatile photonic structure for many applications in lasing, nonlinear optics, and light–matter interactions.^{1, 6, 40, 72, 83, 140-143} To further explore the manipulation of resonant light, optically coupled WGM microcavities with hybridized resonant trajectories were explored to tune the resonant eigenfrequency and the spatial distribution of the resonant modes, indicating a variety of nontrivial physical phenomena and practical applications ranging from mode-selective lasing to non-Hermitian photonics.^{4, 36, 39, 114, 144} In these coupling systems, the microcavity geometries (*i.e.*, microtoroids,^{11, 12} microdisks,¹³⁻¹⁷ microrings,¹⁸⁻²⁰ microspheres,^{21, 22}) and the inter-cavity coupling gap play important roles to ensure sufficient spectral match and efficient coupling. In general, the optical coupling and energy transfer happen at a tangent site of two or multiple resonant trajectories located separately in the neighboring WGM microcavities.^{12, 111, 145} It should be noted that the above-mentioned WGM microcavities support 2D confined resonant modes where the corresponding optical coupling is fixed at one 2D planar. Up to now, the efficient 3D confined optical coupling of resonant light has not been reported, in which the wavevector can exist in more than one direction (*i.e.*, azimuthal and axial directions) for both fundamental and applied studies such as non-trivial evolution of wavevector and direction-selective coupling.^{23, 24}

As one type of WGM microcavities, microtubular cavities fabricated by self-rolling of prestrained nanomembranes provide 3D confinement of light simultaneously resonating in the circular cross-section and along the microtube axis. This is distinct from conventional circular-shaped WGM resonators that confine light in one 2D plane. The axial dimension of the microtube cavity supports the manipulation of resonant modes with a new degree of freedom.^{24,}

^{42, 50, 59, 81, 96, 130, 136, 146, 147} Thus, it is of high interest to design and regulate resonant trajectories

of 3D confined light supported by microtubular cavities for the investigation of 3D optical coupling of resonant modes. In this work, the occurrence of multiple sets of 3D confined resonant modes and their coupling was enabled based on resonant trajectory split in a single microtube cavity. Owing to the existence of an interlayer nanogap in the tube wall, the resonant trajectory partially splits at the nanogap region while sharing the same trajectory in the rest part of the cavity. As all the split trajectories experience axial confinement in the tube cavity, they are all simultaneously confined and resonating along the axial direction. As a result, multiple sets of 3D confined resonant modes were generated which is different from previous reports in microtube cavities.^{27, 42, 66, 85} More interestingly, strong optical coupling between two sets of 3D confined resonant modes was observed from a single microtube cavity. The corresponding spectral anticrossing feature and the changing-over of coupled modes were revealed as direct evidence of strong coupling where the interaction strength overcomes the losses. In particular, the spatial optical field distribution of 3D coupling modes was experimentally mapped upon the strong coupling regime, which shows the corresponding energy transfer process between the two hybrid states. Numerical calculations based on the quasi-potential model and the mode detuning process are in excellent agreement with the experimental results. The occurrence of multiple sets of 3D resonant modes and their efficient coupling based on partial trajectory split provides a compact design, assuming an excellent platform to engineer 3D photonic integration systems for a variety of potential applications in lasing, sensing, and optical switching.

4.2 Experimental section

Fabrication of Microtubular cavities: The microtubular cavities (11-13 μm in diameter) with and without interlayer nanogaps in the tube wall were fabricated by dry-etching⁵⁰ with a controlled nanomembrane release. Firstly, the nanomembranes consisted of Al_2O_3 stop layer (~ 15 nm), Si sacrificial layer and rolling layer (double Al_2O_3 protection layer (~ 4 nm) and SiN_x strained layer (~ 40 nm)) from bottom to top were deposited onto precleaned Si/ SiO_2 wafer as

the substrate. All the Al_2O_3 layers were deposited by PE-ALD (FlexAL, Oxford Instruments PLC, Abingdon, UK). Si and SiN_x layers were fabricated by ICPECVD SI 500 D (Sentech Instruments GmbH, Berlin, Germany). And then a photoresist layer about 1.3 μm in thickness (AZ-5214E, Microchemicals GmbH, Germany) was spin-coated onto the nanomembranes, followed by a U-shape patterning with a parabolic lobe which was performed by a maskless aligner (MLA 100, Heidelberg Instruments Mikrotechnik GmbH, Heidelberg, Germany). RIE (Plasma Lab 100; Oxford Instruments PLC, Abingdon, UK) with chlorine and fluorine chemistry were used to structure the patterned nanomembranes. Next, the structured sample was passivated by a 4 nm thick Al_2O_3 layer to protect the unstructured sacrificial layer. After opening the etching window by RIE, the microtubular cavity was released by a gas phase etch (Xactix e2; Orbotech LTD., Yavne, Israel) to etch away the Si sacrificial layer resulting in the rolling of nanomembranes. In addition, the Al_2O_3 layer was grown by ALD deposition on the surface of the microtube to tune the resonant frequencies and the coupling strength of coupled microtubular cavities.

Characterization: Scanning electron microscopy images in cross-sectional view were obtained after cutting by the focused ion beam. Optical measurement was performed with a microphotoluminescence laser confocal setup (LabRAM HR Evolution, Horiba Scientific) with an excitation wavelength of 457 nm to excite the photoluminescence of defects in the SiN_x microtube, in which a 50x microscope objective was used to focus the laser beam onto the microtubular cavities and collect the corresponding emission light.

4.3 Results and discussion

Microtubular cavities were prepared by a dry chemistry-rolling method⁵⁰ through a well-controlled nanomembrane release. The schematic of the microfabrication process is illustrated in Figure 4.1, and more detailed preparation information is provided in the Experimental section.

In brief, a 15-nm-thick Al_2O_3 film between the sacrificial layer and substrate was selected as the stop layer to prevent the Si/SiO₂ substrate from being damaged by gas-phase etch. The prestained SiN_x nanomembrane (40 nm thick) was deposited on a silicon sacrificial layer by plasma-enhanced chemical vapor deposition, which was in turn patterned by photolithography and dry etch chemistry. The patterned sample was passivated by 4 nm Al_2O_3 film. Followed by opening a release window to define the starting rolling edge, the strained SiN_x patterns together with a top and bottom Al_2O_3 protection layer roll up into microtubular structures through removing the sacrificial layer by XeF_2 vapor etching. A parabolic-shaped lobe structure was designed on the SiN_x pattern which induces axial confinement in the rolled-up microtube cavities.^{25, 50}

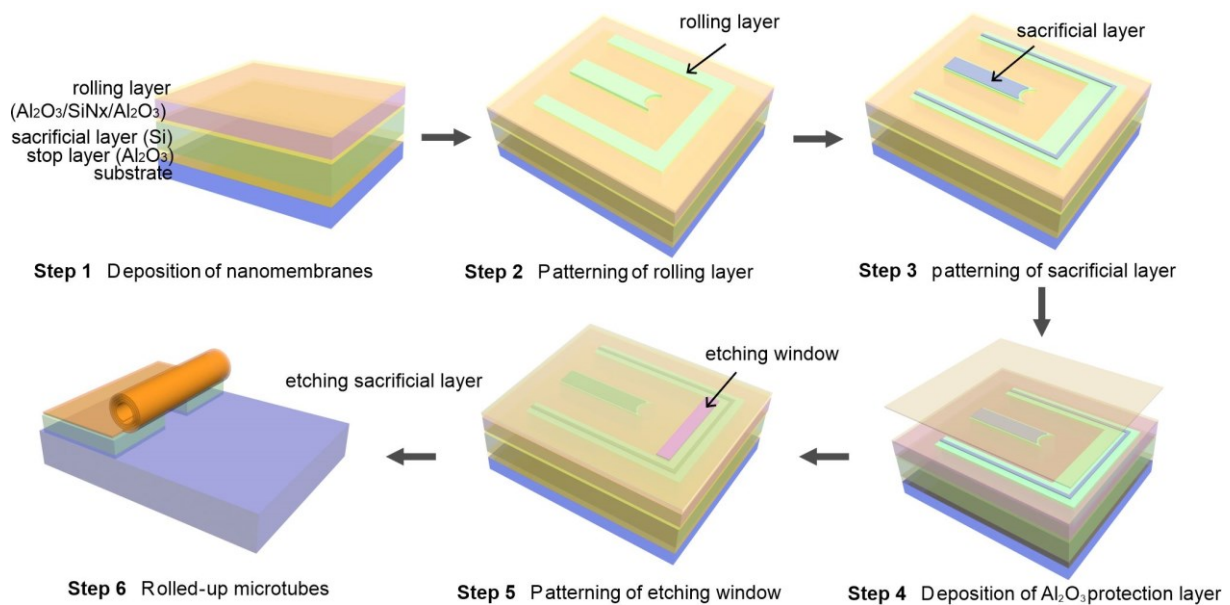


Figure 4.1. Schematic diagram illustrating the fabrication process steps of the SiN_x microtubular cavities.

During the roll-up process (see Figure 4.2a), the release of the strained nanomembranes undergoes several well-controlled pulsed etching cycles with 30 s per cycle and 3 Torr XeF_2 vapor pressure. After each etching cycle, the release process of the strained nanomembranes is suspended for ten seconds. The duration of each etching cycle and the pressure of XeF_2 etching

gas are fixed in the preparation of all microtubular cavities. The rolling speed and steps (equal to etching cycles) are determined by the reactive etching behavior between XeF_2 molecules and Si atoms in the sacrificial layer. As such, the final geometry structure of the microtubular cavity is determined by the photolithographic patterning and release process of the strained SiN_x nanomembranes.^{26, 50} Figure 4.2b shows a representative SiN_x microtube prepared by the well-controlled rolling.

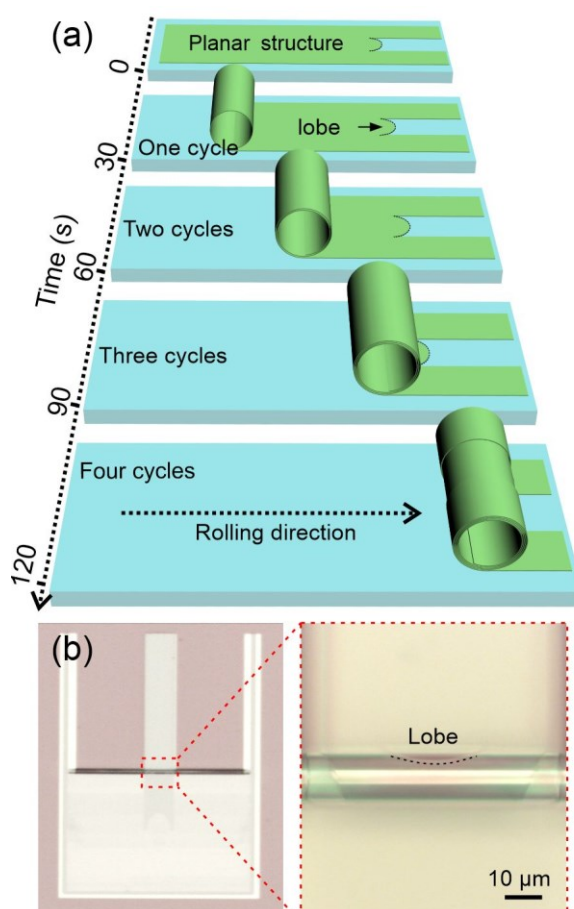


Figure 4.2. (a) Schematic diagram illustrating a controllable roll-up process of a SiN_x microtubular cavity. (b) Optical microscopy image of a rolled-up microtube and a magnified image of the middle tube segment where a lobe structure is located.

By adjusting the etching cycles, three types of microtube cavities are obtained. For the tube fabricated with less than four etching cycles, it possesses a tight interlayer structure of tube wall which accommodates one resonant trajectory, as shown in Figure 4.3a and b. For optical

characterizations, a 457 nm laser is used to excite photoluminescence (PL) emission (in the range of ~ 1.5 - 2.5 eV) from the SiN_x layer in the tube wall. The conventional microtubular cavity without nanogap only supports one set of 3D confined polarized modes (see Figure 4.3c). With the increase of etching cycles, the interlayer nanogap structure occurs in the tube wall due to the pulsed rolling process which is shown in the corresponding cross-sectional SEM image (see Figure 4.3d). The interlayer nanogap enables the resonant trajectory to partially split into double ones while sharing the axial confinement induced by the same lobe structure (see Figure 4.3e). The splitting trajectories support two sets of 3D confined resonant modes as shown in Figure 4.3f, which is distinct from the previous reports.^{27, 42, 50, 80} Further increasing the etching cycles generate more interlayer nanogaps in the tube wall. As shown in Figure 4.3g and h, a microtube with more than one interlayer nanogap is observed which supports three partially split resonant trajectories. As a result, three sets of 3D confined resonant modes are generated in a single microtubular cavity (see Figure 4.3i).

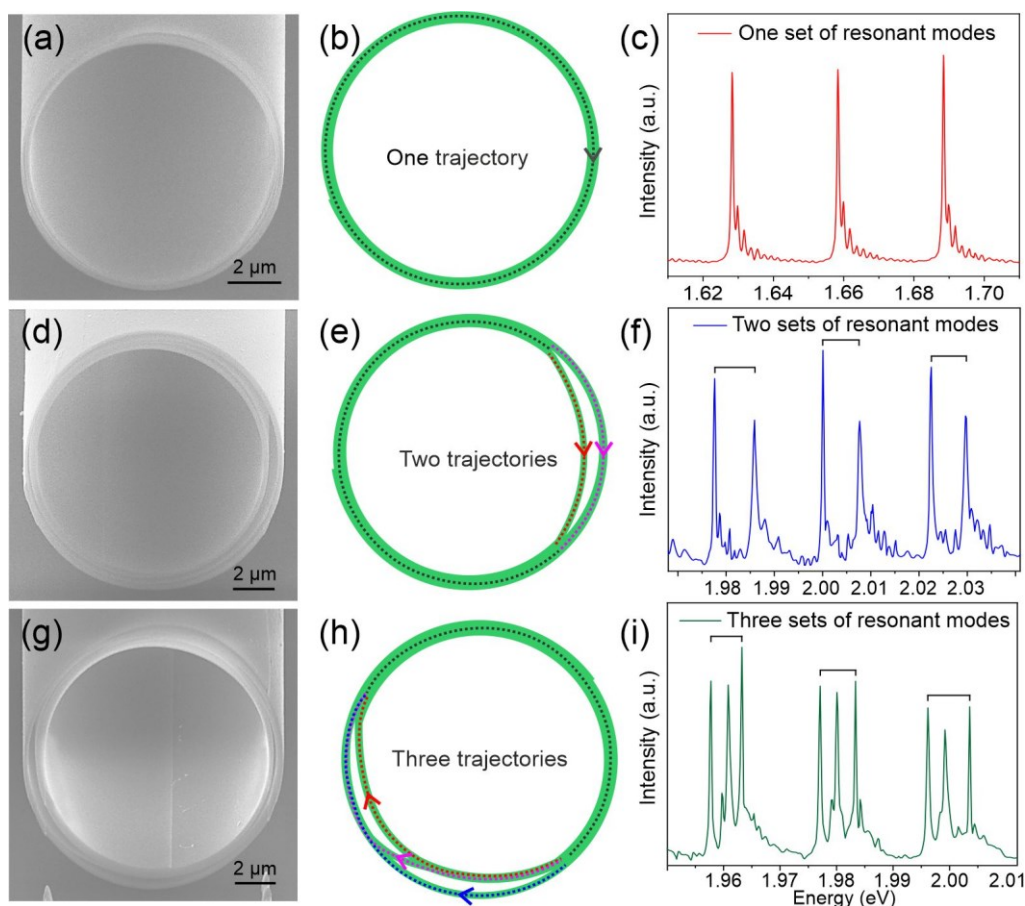


Figure 4.3. SEM images of the three types of microtubular cavities without (a) and with one (d), two (g) interlayer nanogap in the tube wall in cross-sectional view after cutting by the focused ion beam. (b), (e), and (h) Schematic showing the corresponding cross-sectional structure and resonant trajectories. The measured resonant spectra of three types of microtubular cavities supporting one (c), two (f), and three (i) sets of 3D confined TM (electric field parallel to the tube axis) polarized modes.

The formation of the three types of microtubular cavities is further systematically investigated considering the parameters of the rolling step length and the ratio of total rolling length (L) to diameter (D) which are adjusted during the roll-up process. The rolling step length is defined as the rolling length of the strained nanomembranes in one etching cycle of 30 s, which is related to the thickness of the sacrificial layer. L/D is used to reflect the winding number of the tube wall where the interlayer nanogap in the tube wall is formed during the pulsed release. Both the rolling step length and L/D determine the etching cycles which is relevant to the number of sets of 3D confined resonant modes. The corresponding results were plotted in a phase diagram shown in Figure 4.4. The diagram is divided into three regions corresponding to microtube cavities supporting one, two, and three sets of resonant modes, respectively. As sketched in the red region, the tube cavities fabricated with a small ratio L/D (<7.3) only support one set of resonant modes. As the L/D increases, interlayer nanogaps start to occur in the tube wall. These microtubular cavities support more than one set of resonant modes due to the split resonant trajectories. At the same time, as the rolling step length becomes smaller (less than 35 μm), more etching cycles are required during the roll-up process, which generates more than one interlayer nanogap in the tube wall. As a result, two or three sets of resonant modes are observed from a single microtube cavity depending on the occurrence of one or more nanogaps in the tube wall.

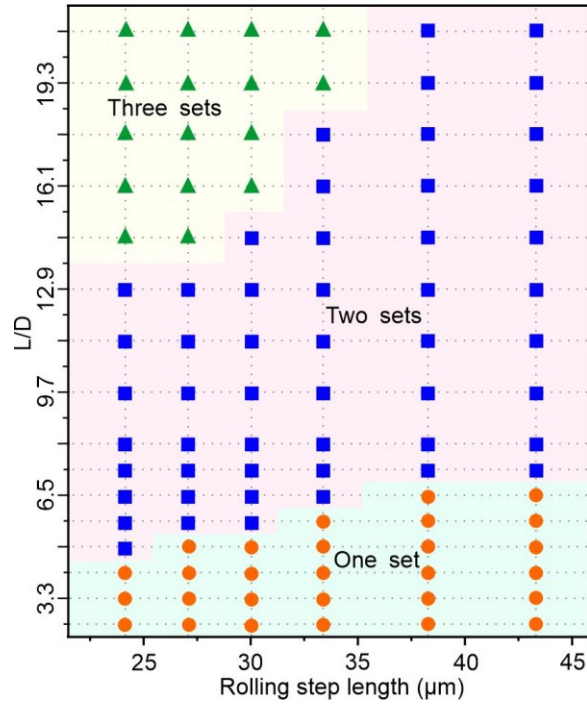


Figure 4.4. Diagram of three types of the microtubular cavity with different rolling step lengths and the ratio of rolling length (L) to diameter (D). The circles, squares, and triangles represent a microtubular cavity that supports one, two, and three sets of 3D resonant modes, respectively.

A detailed transition of the optical resonant spectra of three types of microtubular cavities with different ratios of rolling lengths to diameter changing from 2.5 to 20.9 and the same rolling step lengths of 30 μm per etching cycle is shown in Figure 4.5. As shown in the green region, the tube cavities with the ratio L/D from 2.5 to 4.9 only support one set of resonant modes. In the red region, these microtubular cavities become to support two sets of resonant modes with the increase of ratio L/D from 5.7 to 14.5. Moreover, in the yellow region, three sets of resonant modes are observed from a single microtube cavity with further increased L/D from 16.1 to 20.9.

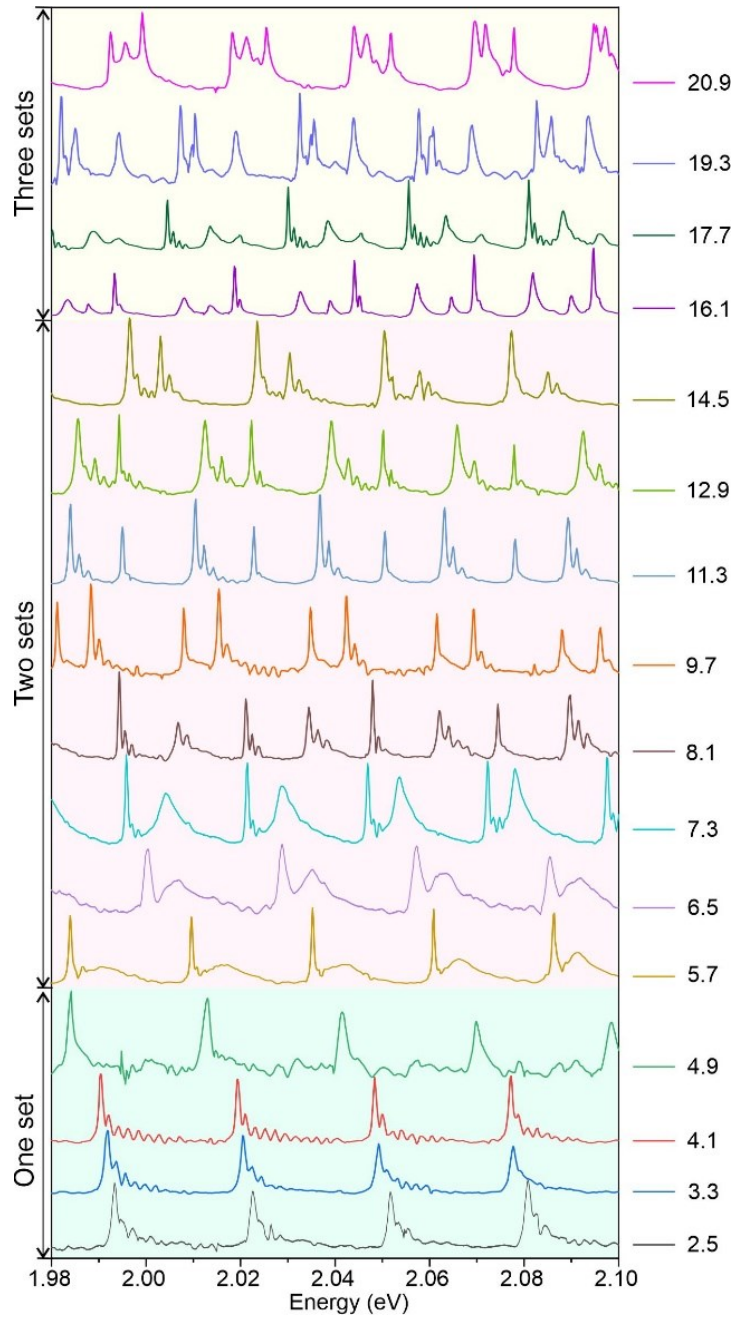


Figure 4.5. The detailed optical resonant spectra of three types of microtubular cavities by changing the ratios of rolling lengths to diameter.

Optical field distributions in these three types of microtubular cavities were calculated by a finite element method based on the commercial software COMSOL. Because all the azimuthal modes have similar behavior and to save calculation time, a representative resonant mode with a smaller mode number is selected to calculate the optical field distributions.^{27, 80} Owing to the spatial overlapping of the optical field, the simulated optical field distribution of the

microtubular cavities is slightly hybridized which can reflect the split of resonant trajectories induced by the interlayer nanogap. As shown in Figure 4.6a, one resonant trajectory is observed in the microtube cavity without a wall nanogap. In the microtube with a wall nanogap, the resonant trajectory split is revealed by a distinct difference in the optical field distribution. As shown in Figure 4.6b, most of the optical field is overlapping in the tube wall while it gets split into an inner and outer part at the nanogap location. Similarly, three partially split resonant trajectories are formed when more nanogaps occur in the tube wall, as shown in Figure 4.6c.

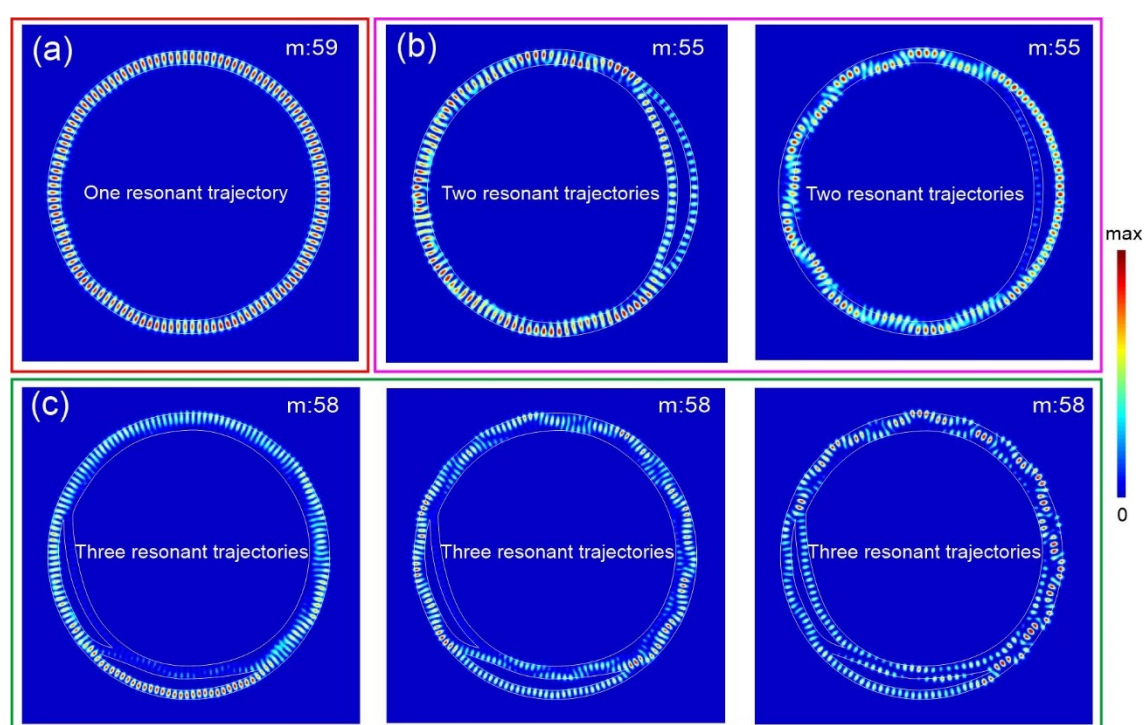


Figure 4.6. Calculated optical field distributions in the cross-section of the tube wall of three types of microtubular cavities with one (a), double (b), and three (c) resonant trajectories, respectively.

To further analyze the observed multiple sets of 3D resonant modes, the spatial distributions of the axial modes supported by the three types of the microtubular cavities were mapped by collecting the far-field emission spectra in the lobe region with a scanning step of $0.2 \mu\text{m}$ along the tube axis, as shown in the top panels of Figure 4.7. For comparison, the axial modes of the microtube cavity supporting one set of 3D resonant modes are shown in Figure 4.7a. For the

tube cavity supporting two sets of 3D resonant modes, the axial modes are partially overlapping with each other in the lobe region (see Figure 4.7b). This mapping result indicates that the two sets of resonant modes are confined by two quasi-potential wells induced by trajectory split sharing the same lobe structure. Similarly, for the microtubular cavity supporting three sets of 3D resonant modes, three independent quasi-potential wells, rather than being a sum of three quasi-potential wells are clearly observed from a single microtubular cavity (Figure 4.7c).

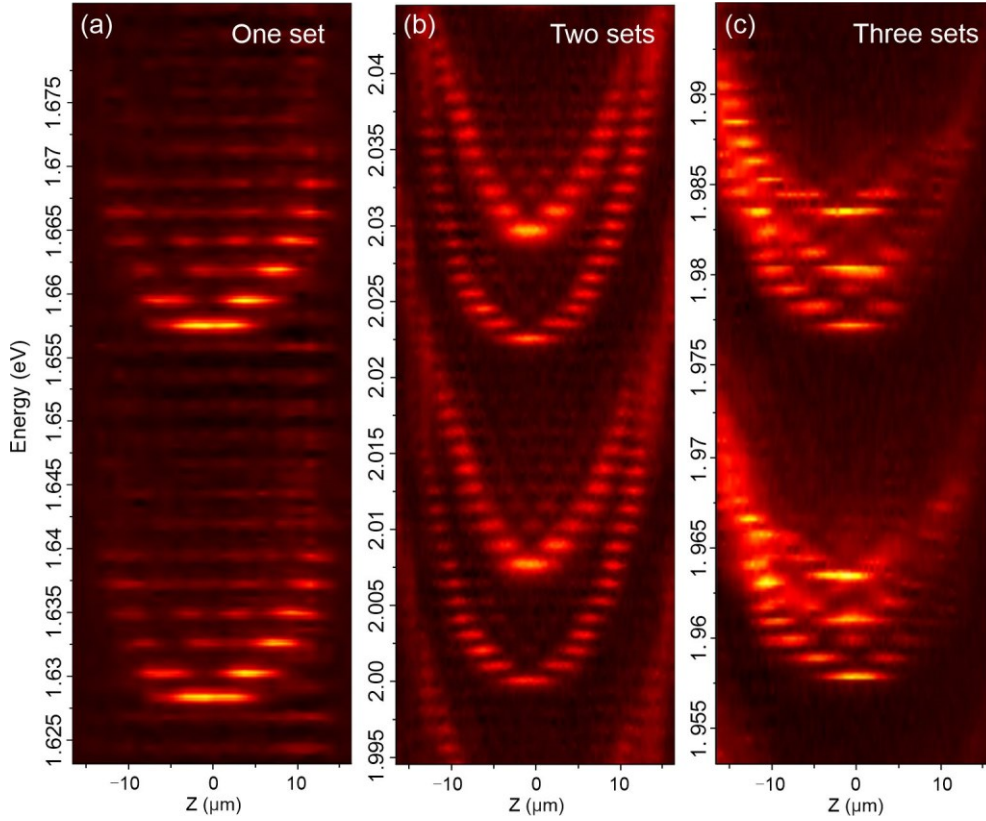


Figure 4.7. The measured spatial field distributions of axial modes in the lobe region for three types of microtubular cavities supporting one (a), two (b), and three (c) sets of resonant modes, respectively.

To verify the experimental results, a theoretical model is developed based on adiabatic approximation.^{25, 27} In brief, the optical electric field can be separated into $r\phi$ -plane and z components. For each position z along the tube axis, the optical field $\phi(r, \phi)$ in the r - ϕ plane is described by the function $-(1/n^2)\nabla^2\phi(r, \phi) = k_{circ}^2(r, \phi)\phi(r, \phi)$, where n is the refractive

index, $k_{circ}(z)$ is the quasi-potential. Then the axial propagation determined by the lobe structure is described by a quasi-Schrodinger equation, $-(1/n^2)(\partial^2/\partial z^2)\Psi(z) + k_{circ}^2(z)\psi(z) = k^2(z)\psi(z)$, where $k(z)$ is the eigenenergy, $\Psi(z)$ is an eigenstate of the axial mode. Considering the geometrical parameters of the microtubular cavities diameter as well as the quasi-potential well, the antinode distributions of axial modes of the three types of the microtubular cavities are calculated, as shown in the top panels of Figure 4.8a-c. The calculation results show an excellent agreement with the corresponding experimental measurements (see the bottom panels of Figure 4.8a-c).

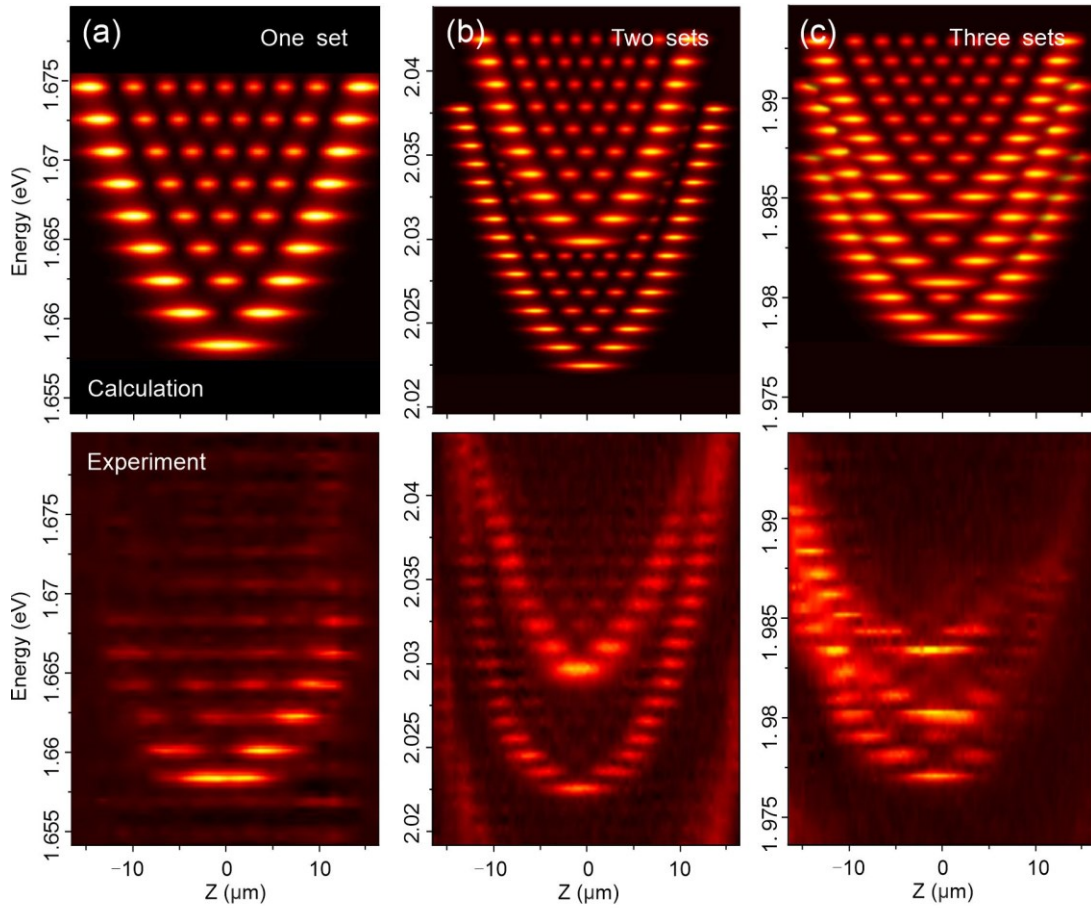


Figure 4.8. Top panels: calculated antinode distributions of axial modes for three types of the microtubular cavity supporting one (a), two (b), and three (c) sets of 3D confined resonant modes, respectively. Bottom panels: measured spatial distributions of axial modes in the lobe region for the experimentally investigated microcavities.

Furthermore, optical coupling between two sets of 3D resonant modes supported by a single microtubular cavity is investigated. The coupling strength is mainly dependent on the difference in resonant frequency and the spatial overlapping of the optical field.^{117, 119, 148, 149} The interlayer nanogap directly determines the difference in free spectral range (FSR) and mode spacing between multiple sets of 3D confined resonant modes. The optical coupling occurs when the frequencies of two sets of 3D confined resonant modes are approaching each other. As shown in Figure 4.9, the coupling strength is tuned by step-by-step Al₂O₃ coating on the rolled-up microtube by ALD.⁸⁷ In the ALD coating process, the precursor can disperse into the hollow core of microtubes, allowing for the deposition of Al₂O₃ on both inner and outer tube surfaces. As the thickness of Al₂O₃ increases from 1 to 6 nm, the effective refractive index gradually increases leading to the continuous redshift of the whole modes. The two sets of resonant modes experience different spectral shifts as the double sets of resonant modes have unequal sensitivities to the perturbations induced by Al₂O₃ coating. The spacing between the two neighboring fundamental modes firstly decreases and then increases, which shows a clear anticrossing trend with the evolution of Al₂O₃ coating thickness. In addition, the mode intensity of the coupled modes was exchanged with each other during the process. The corresponding spectral anticrossing feature together with the modes changing-over show direct evidence of strong optical coupling in the single microtubular cavity.

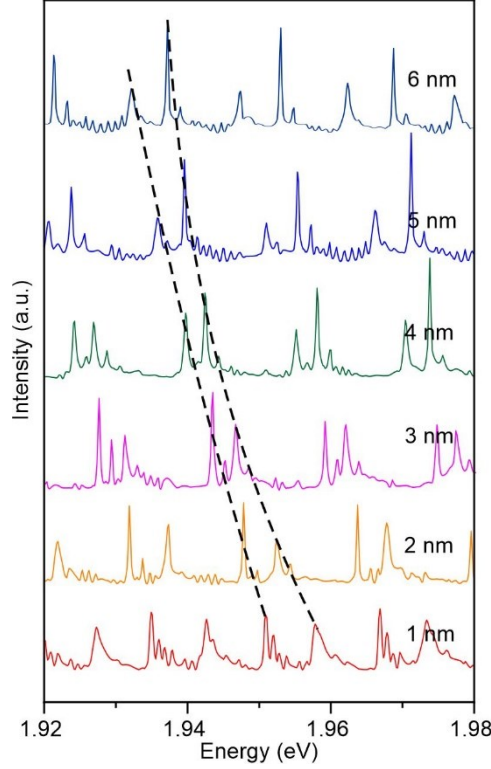


Figure 4.9. Transition of resonant modes measured from a microtubular cavity supporting two sets of resonant modes upon Al_2O_3 coating (from 1 to 6 nm with a step of 1 nm).

The mode coupling behavior in the coupled cavity is modeled by a Hamiltonian matrix $H = \begin{bmatrix} E_1 - i\gamma_1 & V_1 \\ V_2 & E_2 - i\gamma_2 \end{bmatrix}$,⁸⁰ where E_1 and E_2 are the initial eigenenergies, γ_1 and γ_2 are the decay rates. V_1 and V_2 are the coupling constants and $V_2 = V_1^*$, ensuring that the coupling strength $\sqrt{V_1 V_2}$ is a real number. The coupled eigenstates were described by $E_{\pm} = E_+ - i\gamma_+ \pm \sqrt{(E_- - i\gamma_-)^2 + V_1 V_2}$, where $E_{\pm} = (E_1 \pm E_2)/2$ and $\gamma_{\pm} = (\gamma_1 \pm \gamma_2)/2$. The anticrossing trend and the modes intensity changing-over were obtained in the modeling results, showing an excellent agreement with experimental measurements (see Figure 4.10). In particular, as shown in the inserts of Figure 4.10, the stronger modes hybridization between two sets of resonant modes is observed at zero detuning of the best-coupled modes.

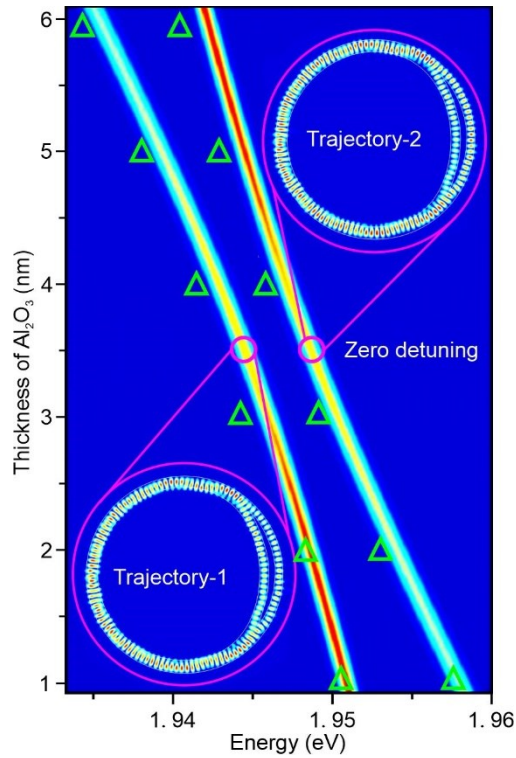


Figure 4.10. Evolution of modeled coupling modes obtained by transfer matrix modeling. The triangles represent the experimental results in Figure 4.9. The inserts show the simulated optical field distribution of the microtube at zero detuning of the best-coupled mode.

To further examine the coupling and energy transfer of the coupling system, the evolution of the measured and calculated spatial optical field distribution of coupling modes was analyzed together with the corresponding resonant mode spectra (see Figure 4.11). The spacing of coupled fundamental modes firstly shrinks from 3.73 to 2.71 meV and then increases to 3.22 meV accompanied by the exchange of modes intensity. For instance, when the coupled microtube cavities are in the strong coupling regime with the minimum mode spacing (Al_2O_3 coating thickness ~ 4 nm), high-order axial modes of the coupled microcavities are spatially overlapping representing efficient energy transfer between the two sets of modes. The coupling of the resonant modes becomes so strong that their mode profiles are significantly blurred which is also a sign of energy transfer under strong mode hybridization.

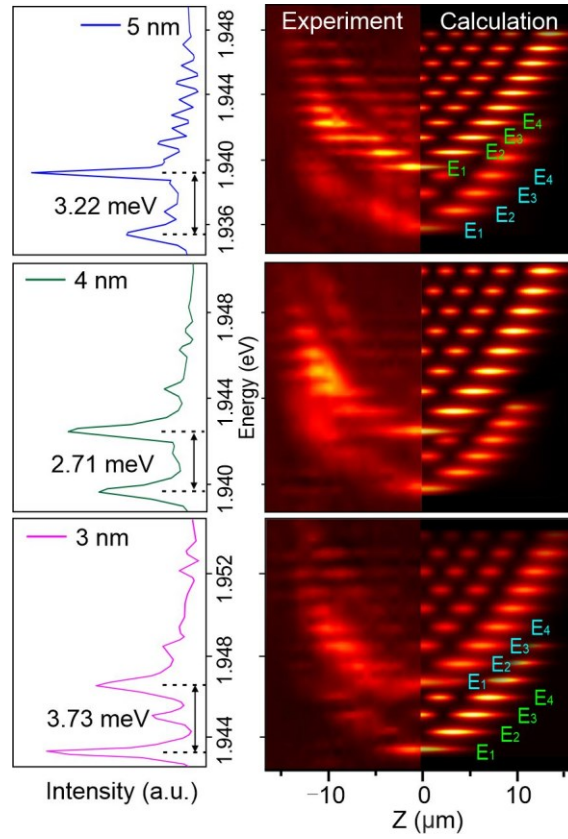


Figure 4.11. The evolution of measured (left panel) and calculated (right panel) spatial optical field distribution of the coupling modes together with the corresponding resonant mode spectra.

The strong optical coupling of 3D resonant light was also realized in the microtube cavity supporting three sets of resonant modes. The corresponding evolution of measured resonant spectra of the microtubular cavity supporting three sets of resonant modes upon Al₂O₃ thickness from 1 to 10 nm with a step of 1 nm were shown in Figure 4.12. A clear anticrossing trend is observed with the increase of Al₂O₃ thickness. Moreover, the mode intensity of the coupled modes was exchanged with each other during the process. The spectral anticrossing feature together with the modes changing-over are revealed as the direct evidence to verify the strong optical coupling in the microtubular cavity supporting three sets of 3D confined resonant modes.

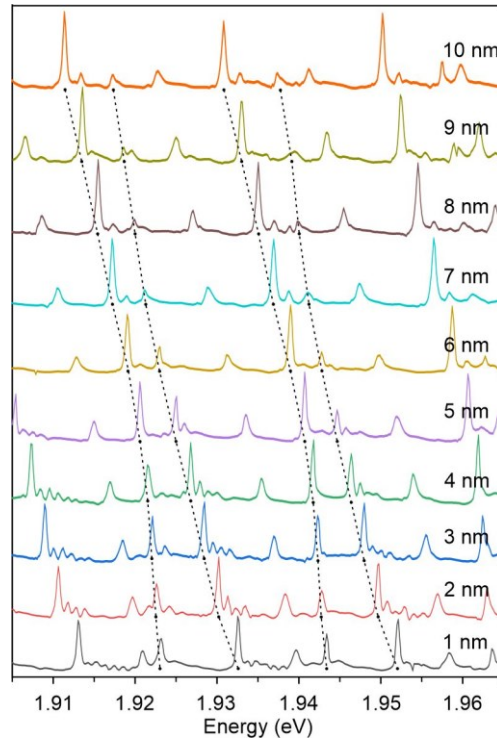


Figure 4.12. The evolution of measured resonant spectra of the microtubular cavity supporting three sets of resonant modes upon Al_2O_3 thickness from 1 to 10 nm.

4.4 Conclusion

In summary, microtubular cavities with interlayer nanogaps in the tube wall were fabricated by a well-controlled nanomembrane release. The interlayer nanogap in the tube wall causes the resonant trajectory to partially split into two or three ones while sharing the same axial confinement, which results in the occurrence of multiple sets of 3D confined resonant modes in a single microtube cavity. The co-existence of two or three independent quasi-potential wells was revealed in experiments and further verified by the numerical calculations. The largely overlapping optical field in two or three ring trajectories in a single microtubular cavity enables strong optical coupling of 3D confined resonant modes. The anticrossing feature and the modes changing-over were demonstrated as direct evidence of strong coupling. The 3D optical coupling is particularly interesting for directional coupling with a higher degree of freedom. Moreover, the manipulation of wavevector with a higher degree of freedom allows for the study

of topological photonic based on non-trivial evolution of wavevector, such as generating optical Berry phase, optical spin-Hall effect.^{23, 24} Our work offers a compact and robust scheme for realizing multiple sets of 3D confined resonant modes and their coupling in a single microtube cavity, which is of high interest for promising applications such as optical modulations, multiplexing, lasing, sensing, and on-chip 3D integration.

Chapter 5 Collective Coupling of 3D Confined Optical Modes in Monolithic Twin Microtube Cavities Formed by Nanomembrane Origami

Coupled optical microcavities have been extensively explored as an ideal platform to manipulate photons in terms of the resonant eigenfrequencies and spatial distributions. However, the effective energy exchange channels between coupled microcavities are usually fixed by a nanogap at a tangent site between the neighboring resonant trajectories, which severely hinders the parallel manipulation of photonic modes. In this chapter, we study the monolithic fabrication of twin microtube cavities by a nanomembrane origami method for achieving collective coupling of 3D confined optical modes. The well-designed nanomembrane origami produces *in situ* wafer-scale twin microcavity coupling systems. The unique parallel configuration of twin microtubes enables large spatial overlapping of optical fields at a one-dimensional nanogap along the tube axis. Owing to the well-aligned twin geometries, two sets of 3D confined optical modes in twin microtubes are spectrally and spatially matched, by which both the fundamental and higher-order axial modes are respectively coupled with each other. Multiple groups of the coupling modes provide multiple effective channels for energy exchange between coupled microcavities, which are illustrated by the measured spatial optical field distributions. The spectral anticrossing and changing-over features of each group of coupled modes are revealed in experiments and calculations, indicating the occurrence of strong coupling. In addition, the simulated 3D mode profiles of twin microcavities confirm the collective strong coupling behavior, which is in good agreement with the experimental results. The collective coupling of 3D confined resonant modes promises broad applications in multichannel optical signal processing, nonlinear optics, and 3D non-Hermitian systems.

The results presented in this chapter have been submitted: X. Wang, Z. Wang, H. Dong, C. N. Saggau, H. Tang, M. Tang, L. Liu, S. Baunack, L. Bai, J. Liu, Y. Yin, L. Ma, and O. G. Schmidt, Collective Coupling of 3D Confined Optical Modes in Monolithic Twin Microtube Cavities Formed by Nanomembrane Origami, Nano Letters (submitted). Y.Y., L.M., and O.G.S. conceived the project. X.W., Z.W., Y.Y., and H.D. designed the experiments and prepared the samples. H.T., L.L., and S.B. performed the structure characterizations. X.W. performed the optical measurements. X.W., C.N.S., and M.T. performed the numerical simulation. X.W., Z.W., H.D., and L.M. analyzed the data and wrote the paper. All authors participated in the discussions.

5.1 Introduction

Strong interactions between coupled optical microcavities provide an intriguing platform to manipulate photons in terms of frequency and spatial distribution,¹¹⁰⁻¹¹² finding many unique photonic applications in a variety of fields, such as nonlinear optics,^{112, 113} laser physics,^{17, 39} and non-Hermitian photonics.^{20, 114-116} WGM microcavities supporting resonances along a ring trajectory have been identified as ideal candidates for building those coupled microcavity systems and investigating resonant optical coupling phenomena.^{1, 121, 122} The strong interactions between two resonant modes can arise from the surface backscattering or nonlinear coupling in a single WGM microcavity.¹⁵⁰⁻¹⁵⁴ In general, to construct the optical coupling systems, two or more WGM microcavities (e.g., microtoroids,^{11, 12} microdisks,^{123, 124} microrings,^{125,126} microspheres^{21, 127}) are placed in close proximity to explore the WGM optical coupling.¹⁵⁵ The WGM optical resonance is confined within a 2D azimuthal plane.^{16,156} The corresponding coherent coupling is constrained to a tangent site between neighboring microcavities, where the single channel of energy exchange severely hinders the parallel processing of photonic signals.

Nanomembrane origami is the art of constructing 3D microstructures from 2D nanomembranes through self-rolling process, which offers high design flexibility in microcavity geometries.^{128, 129} The origami microtube cavities with axial potential wells support 3D WGM resonances along both azimuthal and axial directions,^{26, 27} offering a promising possibility to explore multichannel and multidimensional optical coupling. The axial confinement within the microtubes adds a new degree of freedom for the manipulation of optical resonances and coupling.^{24, 27-29} Specifically, the axial optical potential well in a microtube cavity splits the original azimuthal mode into fundamental and multiple higher-order axial modes with different spatial distributions,²⁷ which promises to achieve multichannel optical coupling in coupled microtube cavities. It is therefore highly desirable to explore optical

coupling systems of microtube cavities for realizing simultaneously multichannel manipulation of photonic signals in 3D space.

In this work, we demonstrate the collective optical coupling of 3D confined resonant modes in monolithic twin microtube cavities. Using a nanomembrane origami approach,^{3, 50} the twin microtubes with axial potential wells are obtained by self-rolling of prestrained nanomembranes from two opposite directions, which simplifies the fabrication flow and enables *in situ* wafer-scale fabrication of coupling systems. The 3D microtube geometry provides a large coupling region along the tangent line between two neighboring microcavities, which creates multiple spatial channels for optical coupling. With almost the same geometries, the twin microtube cavities allow good spectral matching of multiple axial modes. As a result, the fundamental and higher order axial modes supported by the twin microcavities (cavity-I and II) are simultaneously coupled with each other. Through mode detuning, spectral anticrossing and changing-over features of multiple groups of coupling modes are observed in both experimental and simulations, revealing the occurrence of strong coupling. The well-aligned collective strong coupling offers multiple coupling channels for efficient energy exchange between coupled microcavities, which is illustrated by the spatial optical field distributions. The simulated 3D mode profiles in the twin microtubes agree well with the experimental results. Our work provides a unique platform for realizing collective strong coupling of 3D confined resonant modes in a monolithically integrated coupling system, which is of high interest for promising applications in nonlinear optics, 3D coupled non-Hermitian systems and multichannel optical signal processing.

5.2 Experimental section

Sample fabrication: The tubular twin microcavities were fabricated by self-rolling of prestrained SiN_x nanomembranes with top and bottom Al₂O₃ protection layer from two opposite

directions. As previously reported in detail,^{50, 157} dry-etching with high yield and reproducibility was utilized to pattern thin films and etch Si sacrificial layer in gas phase atmosphere. The nanomembranes consist of Al₂O₃ stop layer/Si sacrificial layer/Al₂O₃ protection layer/SiN_x strained layer/Al₂O₃ protection layer from bottom to top. The Si sacrificial layer (400 nm) and SiN_x layer (40 nm) were deposited using chemical vapor deposition (CVD, SI 500 D, Sentech Instruments). The Al₂O₃ stop layer (15 nm), protection layer (4 nm) and passivation layer (4 nm) were fabricated by atomic layer deposition (ALD, FlexAL, Oxford Instruments PLC, Abingdon, UK). A photoresist layer with a thickness of 1.3 μm (AZ-5214E, Microchemicals GmbH, Germany) was first spin-coated onto the prepared nanomembranes. The photoresist was exposed by a Maskless Aligner exposure system (MLA 100, Heidelberg Instruments Mikrotechnik GmbH, Heidelberg, Germany) and developed in AZ 726 MIF developer (Microchemicals). The obtained photoresist pattern with double lobe structure was etched into the sacrificial layer by reactive ion etching (RIE, Plasma Lab 100; Oxford Instruments PLC, Abingdon, UK). And then the whole sample was passivated by Al₂O₃ layer. The SiN_x strained layer rolled up from two opposite directions at the same time by opening two etching windows, which was performed by etching Si sacrificial layer inside a xenon difluoride etching system (Xactix e2; Orbotech Ltd., Yavne, Israel).

Characterization: Scanning electron microscopy characterization was performed in a Zeiss DSM982. The samples were imaged after sputter coating with Cr (~10 nm) to improve conductivity and contrast. In addition, the resonant spectra were carried out using a confocal photoluminescence setup (LabRAM HR Evolution, HORIBA Scientific). A laser beam at an excitation wavelength of 457 nm was focused onto the microcavity surface through a 50× long working distance objective lens. The spatial distributions of the axial modes were mapped by moving the tubular microcavities from -5 to 5 μm with a step of 0.1 μm along the tube axis and collecting the spectra at different positions of the lobe region.

5.3 Results and discussion

Figure 5.1a illustrates an optical coupling system consisting of parallel twin microtube cavities. A lobe structure modified on the microtube provides an axial optical potential well (i.e. potential well-1 and 2 in cavity-I and II, respectively) which supports optical axial resonances in addition to the azimuthal WGM ones. The unique configuration of parallel twin microtubes enables the spatial overlapping of evanescent fields at the whole tangent line along the tube axis. Due to the axial position-dependent field distribution in the twin microtube cavities, optical coupling between two sets of 3D confined modes can occur when the resonant modes are spectrally and spatially matched.^{158, 159} In the case of strong coupling, the resonant modes get hybridized in the twin microcavity system and culminate in the emergence of modes splitting (Figure 5.1b).^{112, 119} As shown in Figure 5.1c and d, the fundamental modes E_0 and E_0' interact with each other to form a doublet of two hybrid states of E_{0-} and E_{0+} , while each higher-order axial modes (e.g. E_1, E_2) confined in potential well-1 couple with the same order axial modes (i.e., E_1', E_2') in potential well-2, resulting in hybridized states ($E_{1-}, E_{1+}; E_{2-}, E_{2+}$). In other words, a collective strong coupling of aligned 3D confined resonant modes, including fundamental modes and higher-order axial modes, can occur in the twin microtube cavity system.

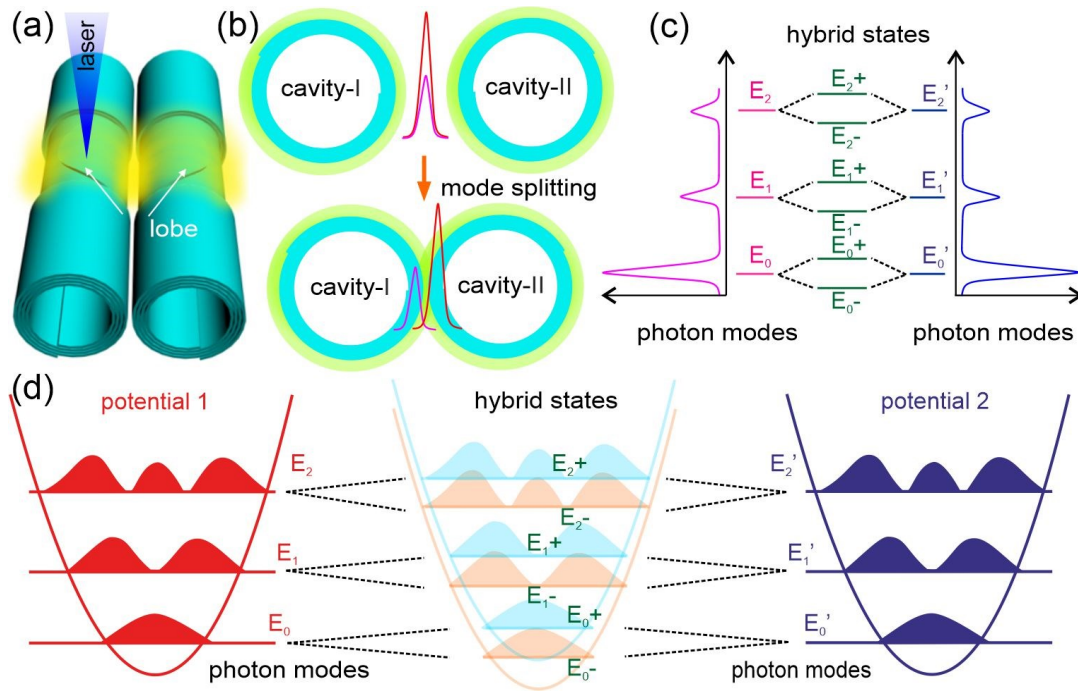


Figure 5.1. (a) Schematic of optical coupling via a tangent line and (b) the resultant mode splitting in an optical coupling system consisting of parallel twin microcavities under laser excitation. (c, d) Schematic illustration of the collective mode coupling between two sets of 3D confined resonant modes

To obtain the target optical coupling systems, the nanomembrane origami method is employed for the preparation of parallel twin microtubes.⁵⁰ The key to realize the unique configuration lies in the clever predefinition of the nanomembranes before the rolling process, which influences the resonant modes and their corresponding optical coupling behaviors in twin microcavities.²⁵ As illustrated in Figure 5.2, the prestrained SiN_x films (~40 nm) with top and bottom double Al₂O₃ protection layers (~4 nm) are firstly deposited on a silicon sacrificial layer. Two identical parabolic-shaped lobes are patterned on the middle part of the strained layer by standard photolithography. Then, the whole sample is passivated by a 4 nm thick Al₂O₃ layer via ALD. By opening two windows as the starting rolling edges, the patterned nanomembrane is rolled up into parallelly aligned twin microtubes from two opposite directions each with the same rolling length.

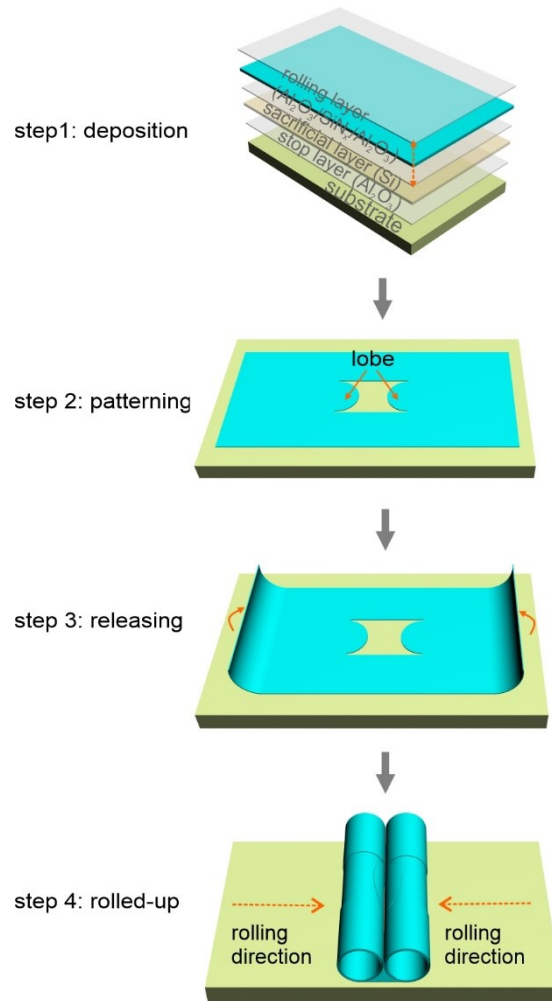


Figure 5.2. Schematic diagram of the fabrication steps of the twin microcavities.

Rolled-up nanotechnology enables *in situ* mass fabrication of monolithically integrated twin microtubes with high yield and quality, as shown in the scanning electron microscopy (SEM) images (Figure 5.3a and b). The patterned double parabolic-shaped lobes are located in the middle region of the twin microtubes (Figure 5.3c and d) providing light confinement along the tube axis.^{56, 66} Accordingly, both of the twin microtubes can support 3D confined resonant modes. With almost the same geometries, such as diameters ($\sim 10 \mu\text{m}$) and lobes, the twin microtube cavities allow for simultaneous spectral matching of multiple axial modes including fundamental and higher-order axial modes.¹⁵⁸ Besides, the two coupled microtubes are well aligned parallelly (Figure 5.3b-d), which facilitates good spatial matching of two sets of 3D confined resonant modes.¹⁵⁹ Overall, the spectral and spatial matching can enable the

occurrence of the collective optical coupling between two sets of 3D confined optical modes in twin microtube systems.

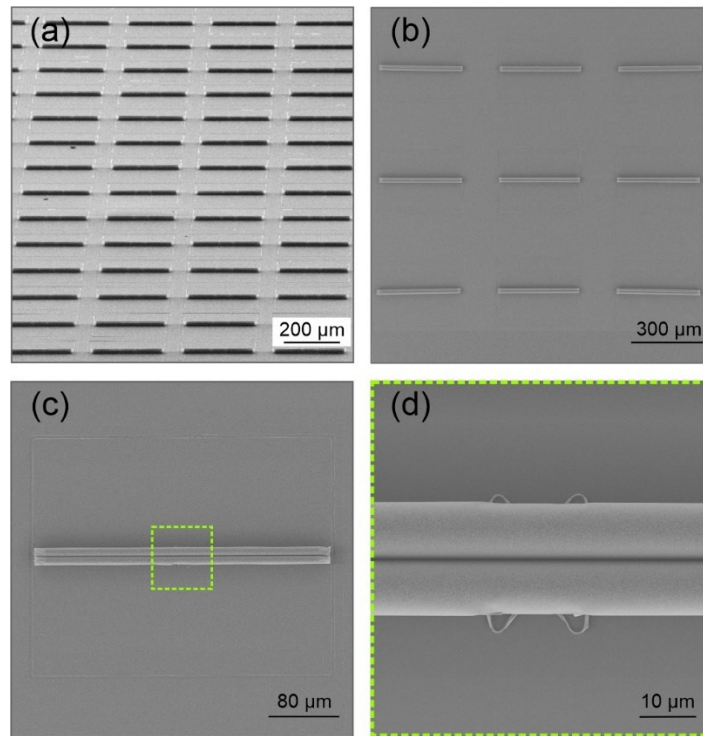


Figure 5.3. SEM images of (a) a large-area twin microtubes array seen under 75° , (b) a small-area twin microtubes, and (c, d) individual twin microtubes and the corresponding zoom-in central segment.

The resonant spectra in both isolated and coupled microtubes are investigated to reveal the optical coupling behavior in the twin microcavities. Isolated single microtubes fabricated by the same preparation parameters exhibit almost the same diameter ($\sim 10 \mu\text{m}$) shown in Figure 5.4a and b. In a laser confocal setup, an excitation laser beam at 457 nm is used to excite photoluminescence (PL) emission from the SiN_x layer in the tube wall, serving as the light source to the pump optical resonances. Figure 5.4c shows the PL spectrum of an isolated microtube cavity. Similar to conventional microtube cavities,^{24, 27} the single microtube cavity supports one set of 3D confined resonant modes with transverse magnetic (TM, defined as the electric field parallel to the tube axis) polarization. For the twin microtubes, the laser excitation and emission measurement spots are focused onto only one microtube cavity (see schematic in

Figure 5.1a), while the collected PL spectrum can be deconvoluted into two sets of 3D confined resonant modes (Figure 5.4d). This phenomenon indicates twin microtubes possess a suitable coupling gap which enables the large overlap of the optical fields along the tangent line. The appropriate quality (Q) factor ($\sim 2000-3000$) of fundamental and higher-order modes facilitate the spectral match of two sets of optical modes. Moreover, the resonant frequencies of two sets of 3D confined optical modes approach each other. Both the neighboring fundamental and higher-order modes have small mode spacing yielding a good spectral matching for efficient mode coupling between twin microtube cavities.

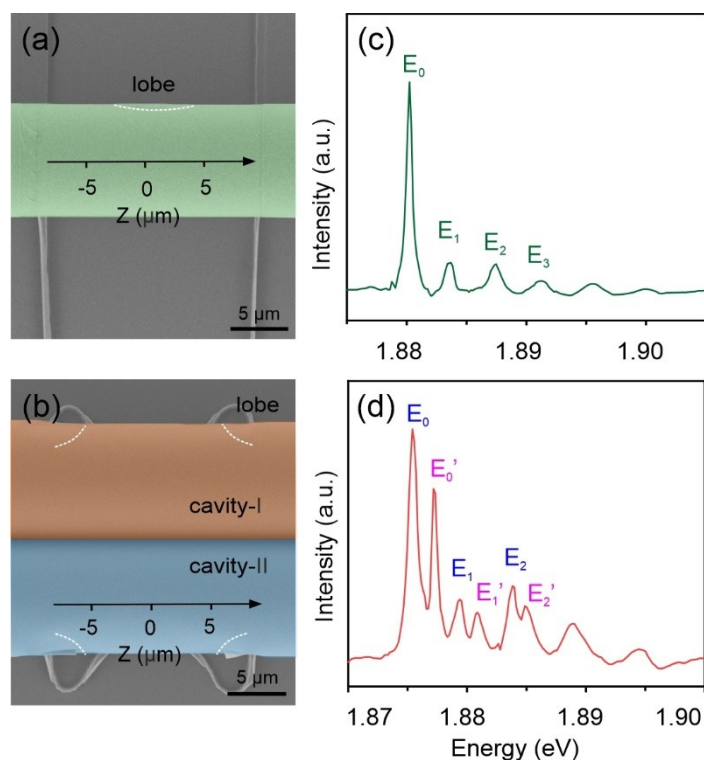


Figure 5.4. SEM images of a single (a) and twin (b) microcavities at the lobe region indicating the mapping measurement regions. Measured resonant spectra of a single (c) and twin (d) microcavities.

Spatial distributions of the axial modes supported by single and twin microcavities were characterized by mapping the PL spectra along the microtube axis (indicated in Figure 5.4a and b). The spectra and spatial distributions in a wider resonant frequency range supported by one

isolated and twin microtubular cavities can be found in Figure 5.5. Figure 5.5a and b show the PL spectra and mapping PL result of the isolated microtube, where one set of 3D resonant modes, including the fundamental mode E_0 and higher-order axial modes E_i ($i \geq 1$), are clearly observed due to the optical confinement in an axial potential well. In contrast, a distinct result is observed in the twin microcavities, i.e. two sets of 3D confined resonant modes are formed due to the efficient optical coupling confined in two potential wells in the twin microtubes (Figure 5.5a and c). The two sets of resonant modes largely overlap with each other in the lobe region of neighboring microtubes. Overall, the large spatial overlapping together with the spectral matching of two sets of 3D confined optical modes may result in effective multichannel mode coupling in the twin microtube cavities.

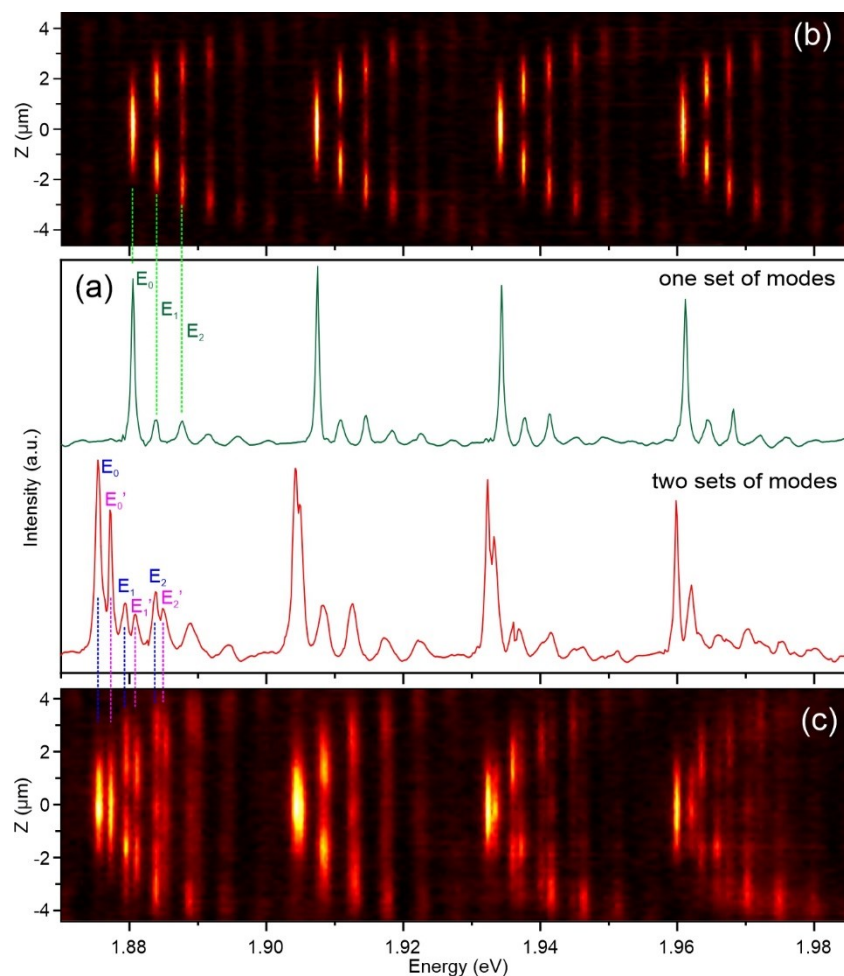


Figure 5.5. (a) The measured resonant spectra of one isolated and twin microcavities supporting one and two sets of 3D confined resonant modes, respectively. The measured spatial distributions of resonant modes in the lobe region for one single (b) and twin (c) microcavities.

To further investigate the optical coupling in twin microtube cavities, the spectral detuning between two sets of 3D optical modes was examined via step-by-step Al_2O_3 coating on the twin microcavities by ALD which changes the effective refractive index and coupling strength.^{80, 108} Figure 5.6 shows the variation of resonant spectra of the coupled microtubes with the increase of Al_2O_3 layer thickness. Both sets of 3D confined resonant modes undergo continuous redshifts due to the increased effective refractive index of the microtube cavities.

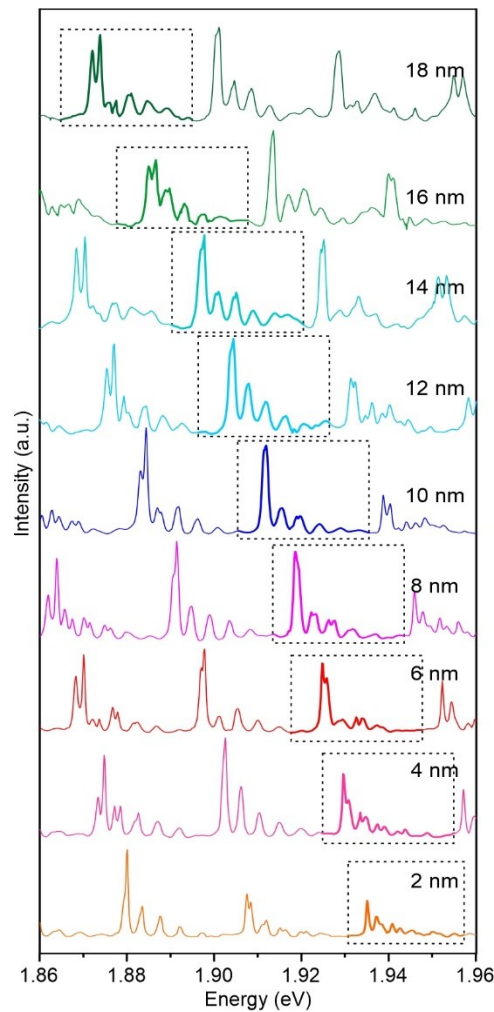


Figure 5.6. Evolution of resonant spectra of a twin microcavity measured by varying Al_2O_3 coating thickness from 2 to 18 nm.

For the resonant modes framed by the dotted boxes in Figure 5.6, the mode energy and spacing of the neighboring fundamental modes and the first two orders of axial modes are extracted as a function of Al₂O₃ thickness, as shown in Figure 5.7. It is found that the spacing between two fundamental modes first shrinks from 2.24 to 0.41 meV at an Al₂O₃ thickness of 10 nm, and then increases to 1.67 meV for an 18 nm thick Al₂O₃ coating (Figure 5.7a). The higher-order axial modes exhibit similar behaviors in mode spacing with Al₂O₃ coating (Figure 5.7b and c). Clear anticrossing trends are observed for both fundamental and higher-order axial modes. In addition, the mode intensity of the coupled fundamental modes reverses when the Al₂O₃ thickness increases from 2 to 18 nm (see Figure 5.6). The spectral anticrossing feature together with the mode changing-over serves directly proves the occurrence of strong optical coupling in the twin microtube cavities.^{119, 138} The minimum mode spacing for the three groups of coupling modes is reached for an Al₂O₃ thickness of 10 nm, which indicates that the mode coupling evolves synchronously over the detuning process.

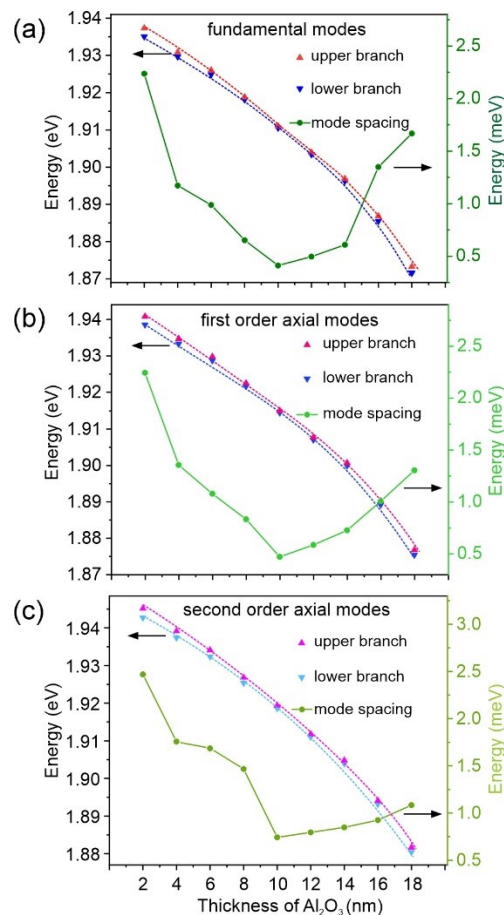


Figure 5.7. Mode energy and mode spacing as a function of the thickness of Al₂O₃ coating for the coupled fundamental (a), first (b) and second (c) order axial modes. The lower and upper branches correspond to the lower and higher energy modes of each group of coupled modes, respectively.

To theoretically understand the collective mode coupling behavior, the optical coupling of fundamental modes and higher-order axial modes in the twin microcavities were separately modeled by a Hamiltonian matrix.^{160, 161} The optical coupling between two resonant modes can be described as:

$$H = \begin{pmatrix} E_1 & V \\ W & E_2 \end{pmatrix},$$

where W and V are coupling constants. E_1 and E_2 are the complex energies, \sqrt{VW} is the coupling strength with the off-diagonal elements $W=V^*$. Real part of E_1 and E_2 are the initial eigenenergies of coupling modes extracted from experimental data (Figure 5.7). The hybrid states of coupled modes can be expressed as:

$$E_{\pm} = \frac{E_1 + E_2}{2} \pm \sqrt{\frac{(E_1 - E_2)^2}{4} + VW}.$$

For each group of the coupling modes, two distinct resonant branches exist as the upper and lower branches (Figure 5.8a-c). Both branches can be fit very well by the anticrossing trend. The mode intensity of the lower branch decreases as the Al₂O₃ coating increases, while that of the upper branch increases during the process. The spectral anticrossing feature and the modes intensity changing-over confirm the occurrence of strong coupling behavior between each group of the coupling modes. Figure 5.8d shows the evolution of three groups of strongly coupled modes over the detuning process. In the case of zero detuning, the strongest coupled states of three coupling systems are realized synchronously at an Al₂O₃ thickness of about 10 nm. Numerical calculations of the mode anticrossing behavior show good agreement with

experimental measurements (see Figure 5.7), further verifying the collective strong coupling between two sets of 3D confined optical modes.

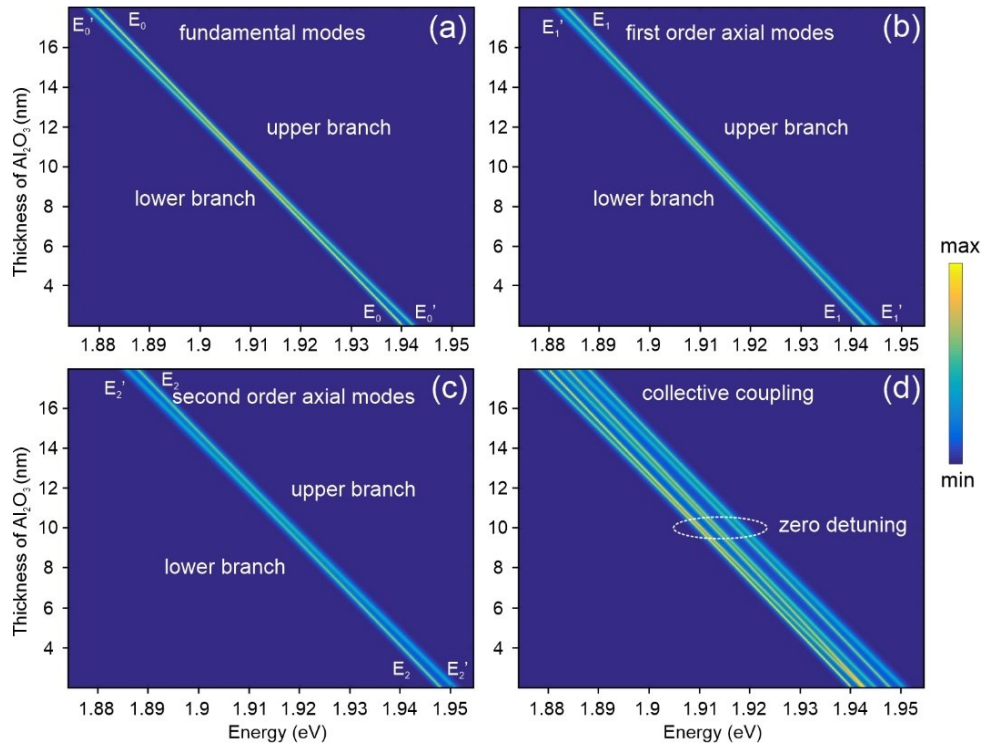


Figure 5.8. Calculated detuning of coupled fundamental (a), first (b) and second (c) order modes obtained by transfer matrix modeling. (d) The modeled evolution of three groups of coupling modes over the detuning process.

Further insight into the strong interaction between two sets of 3D confined resonant modes in the twin microtube system is gained from a detailed analysis of the mode intensity changing-over behavior (Figure 5.9-5.11). Figure 5.9 displays two representative resonant spectra and corresponding spatial distributions with Al_2O_3 coating thicknesses of 2 and 18 nm (beginning and ending of the tuning). At the beginning of the spectral detuning process (Al_2O_3 coating thickness 2 nm), two sets of resonant modes are slightly hybridized, which are fitted by Lorentzian functions indicating the fundamental modes ($E_0; E_0'$) and individual axial modes ($E_1, E_2; E_1', E_2'$). The lower branch (E_0, E_1, E_2) in each group of coupled modes initially has a higher mode intensity than that of the upper branch (E_0', E_1', E_2'). In contrast, the mode intensity of the lower branch becomes smaller than that of the upper branch with an Al_2O_3

coating thickness of 18 nm (Figure 5.9a). Such mode changing-over behavior during the spectral detuning process is a typical characteristic of strong optical coupling. When the coupled twin microtubes are in the weak coupling regime, the optical fields of two sets of 3D optical modes overlap less spatially with each other, which represents less energy exchange between coupled modes (Figure 5.9b).

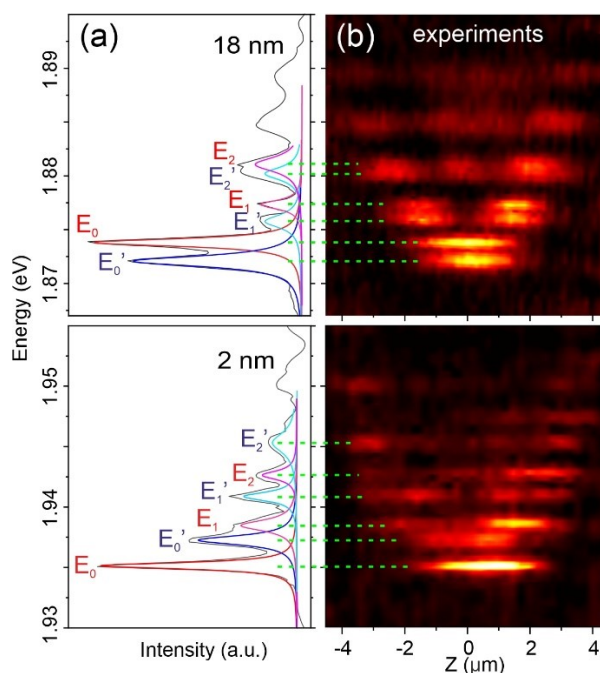


Figure 5.9. Evolution of resonant spectra (a) and measured (b) spatially optical field distribution of the coupling modes with Al_2O_3 coating thicknesses of 2 and 18 nm.

With increasing Al_2O_3 layer thickness (8 and 10 nm Al_2O_3 coating, closest mode splitting), the optical field is highly hybridized resulting in the emergence of hybrid states of 3D confined optical modes exhibiting mode splitting in the resonant spectra (Figure 5.10). The hybrid resonant modes including fundamental and higher-order axial modes collectively exchange energy with each other, which is manifested in the changing-over of the mode intensity between each group of coupling modes (Figure 5.10a). This phenomenon indicates that all coupling systems have entered the strong coupling regime with the minimum coupling spacing. In the regime with strong coupling strength, the optical fields of each group of coupled modes largely overlap with each other generating efficient energy exchange between coupled modes (Figure

5.10b). Consequently, a collective strong coupling of both the fundamental modes and higher-order axial modes is realized in the twin microtube cavities. Each group of coupling modes can be treated as a single strong coupling system providing an effective path for efficient energy exchange between coupled microcavities. The multichannel strong coupling can simultaneously modify the spatial distributions of the potential energy and resonant eigenfrequency of 3D coupled modes, which would enable the parallel manipulation of photonic signals in 3D space.

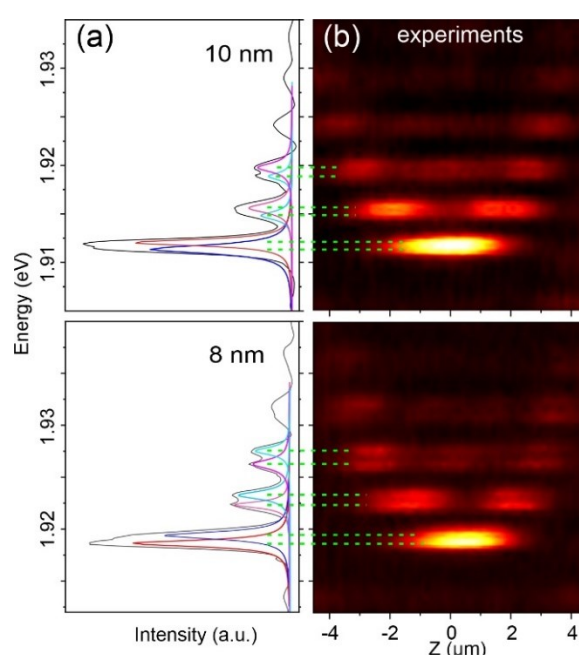


Figure 5.10. Evolution of resonant spectra (a) and measured (b) spatially optical field distribution of the coupling modes with Al_2O_3 coating thicknesses of 8 and 10 nm.

Figure 5.11 show a detailed analysis of the mode intensity changing-over behavior between two sets of 3D confined optical modes. Similarly, the resonant spectra with different Al_2O_3 coating thicknesses are fitted by Lorentzian functions indicating the evolution of mode intensity of coupled modes during the detuning process. For the Al_2O_3 coating thickness less than 8 nm (Figure 5.9-5.11), the lower branch in each group of coupled modes has a higher mode intensity than that of the upper branch. In contrast, when the Al_2O_3 coating thickness exceeds 10 nm, the mode intensity of the lower branch is smaller than that of the upper branch. The mode intensity

changing-over behavior demonstrates the occurrence of collective strong coupling between two sets of 3D confined optical modes in the twin microtube cavities.

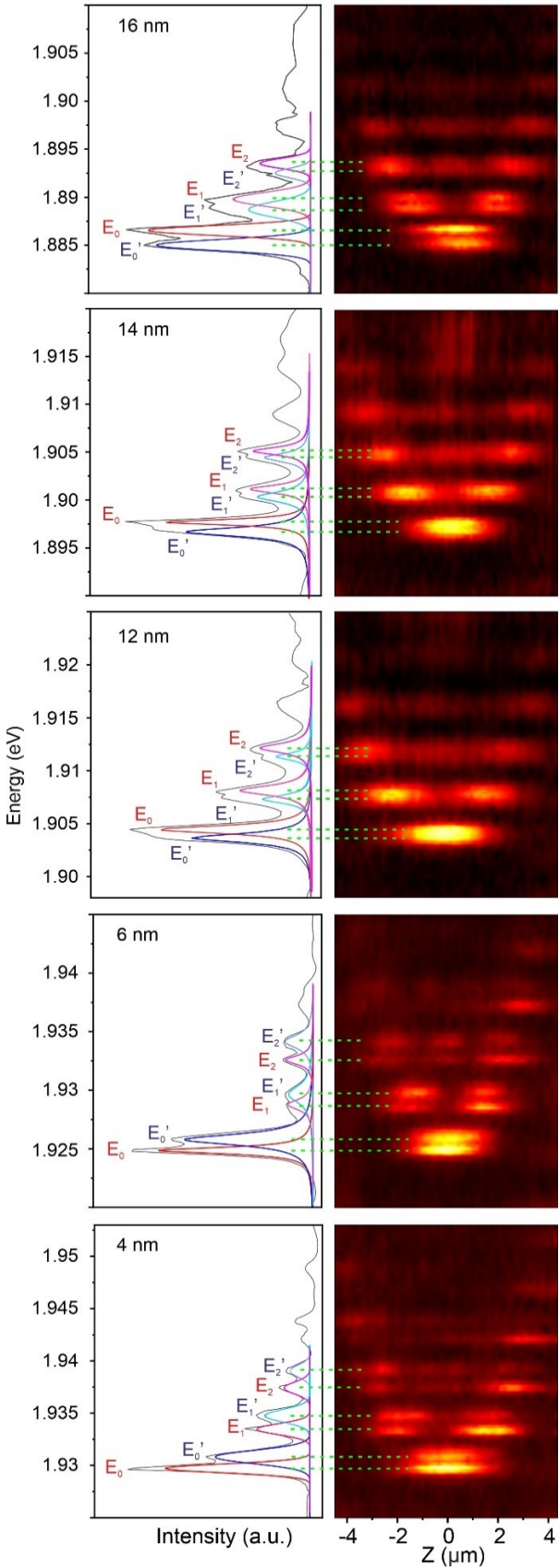


Figure 5.11. The resonant spectra and measured spatial distributions of the twin microtube cavities over detuning process.

The experimental results about the mode changing-over behavior can be well explained by a theoretical model based on the adiabatic approximation. The field distribution in the microtube cavities along the axial direction is determined by the axial potential well as described by a quasi-Schrödinger equation,²⁷ $-(1/n^2)(\partial^2/\partial z^2)\Psi(z) + k_{circ}^2(z)\psi(z) = k^2(z)\psi(z)$, where $k(z)$ is the eigenenergy, $\psi(z)$ is an eigenstate of the axial modes, $k_{circ}(z)$ is the quasipotential calculated by solving the optical field $\phi(r, \varphi)$ in the r - φ plane with the equation $-(1/n^2)\nabla^2\phi(r, \varphi) = k_{circ}^2(r, \varphi)\phi(r, \varphi)$. Figure 5.12a shows the calculated spatial distributions of two sets of 3D confined resonant modes in twin microtubes by considering the geometrical parameters of each microcavity. According to the measured PL spectra, different quality factors are assigned to the two sets of resonant modes to show the mode changing-over behavior. The calculation results clearly reveal the collective mode changing-over by the evolution of the spatial optical field with the increase of the Al₂O₃ coating, which is in good agreement with the experimental observations (Figure 5.12a and b).

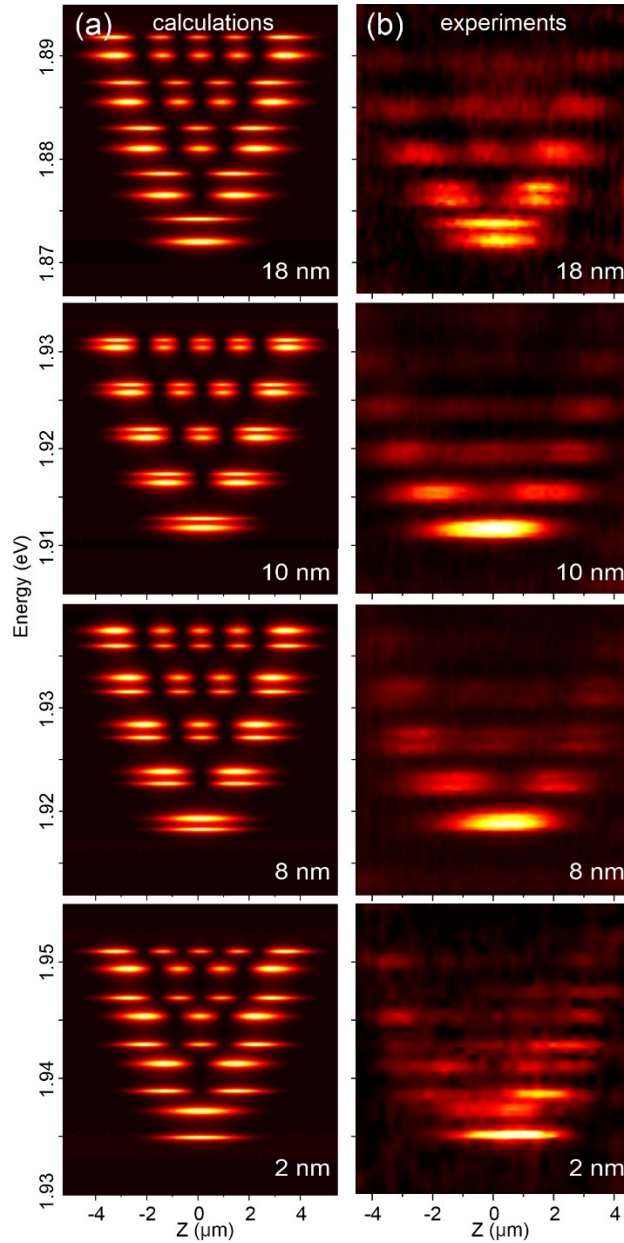


Figure 5.12. Evolution of measured (a) and calculated (b) spatially optical field distribution of the coupled modes with Al_2O_3 coating thicknesses of 2, 8, 10, and 18 nm.

To better visualize the collective strong coupling, 3D optical field distribution in the twin microtube systems were simulated via the FDTD method. In order to save computational time, a model of microtube cavity is set to a tube wall thickness of 100 nm and a diameter of 3 μm . The second microtube cavity is the axial mirror of the first one. The refractive index of the model was set to be 2.0. The coupling gap between twin microtubes was set as 90 nm. One of the twin microcavities was driven by a coupled waveguide. Figure 5.13 present the simulated

3D mode profiles of the fundamental and first two higher-order axial modes. By pumping one cavity (cavity-I) of the twin microtubes, the optical fields of all resonant modes distribute over the twin microtubes (cavity-I and II) along the ring trajectory and axial direction instead of localizing in the excited microcavity (cavity-I), which indicates strong interactions between two sets of 3D confined optical modes confined by axial potential wells.

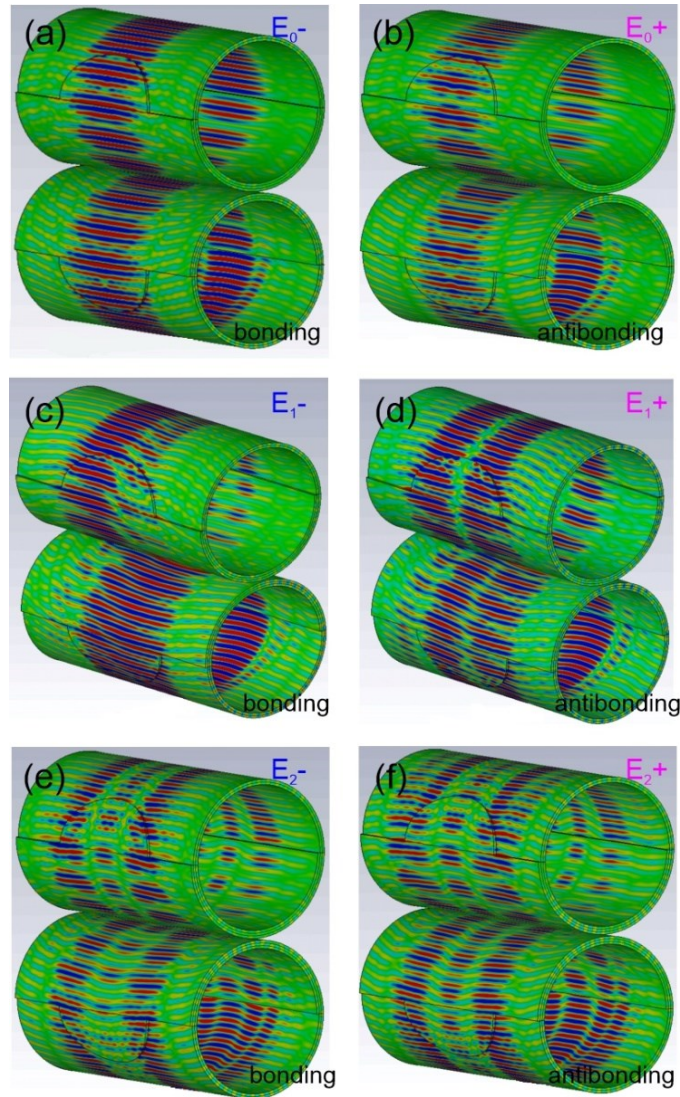


Figure 5.13. Mode profiles of the bonding and antibonding modes for the fundamental modes (a, b), first-order (c, d) and second-order axial modes (e, f) revealed by 3D simulation.

The coherent coupling between twin microtubes splits each degenerate optical state of the individual microcavity into two nondegenerate states with different eigenfrequencies and

phases,^{162, 163} corresponding to the mode splitting of fundamental and higher-order axial modes in the measured and calculated resonant spectra (Figure 5.6 and Figure 5.14). The low- and high-energy states of each group of coupled modes are respectively the bonding (E_{0-} , E_{1-} , E_{2-}) and antibonding (E_{0+} , E_{1+} , E_{2+}) modes, in analogy to the hybrid orbits in multi-atomic molecular systems.^{164, 165}

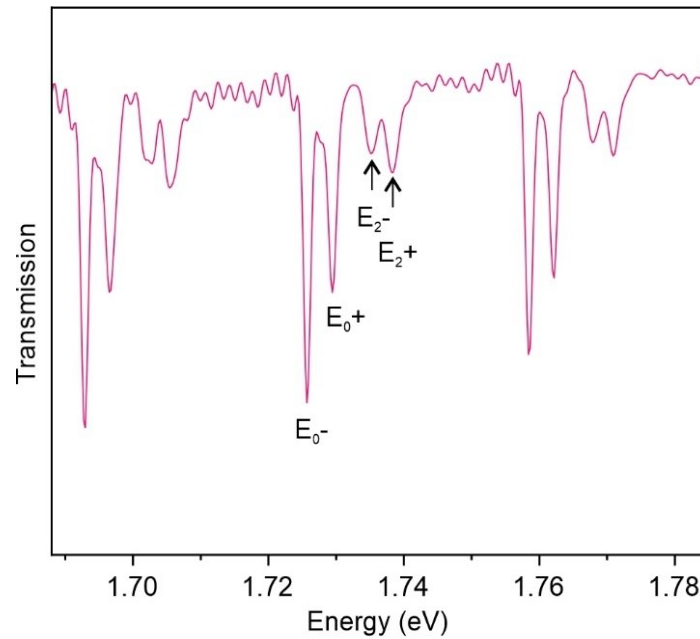


Figure 5.14. The calculated transmission spectra of the coupled twin microtubes.

The cross-sectional view of 3D mode profiles shown in Figure 5.15 indicates the hybrid optical field around the tangent position between twin microcavities. The bonding modes exhibit the optical field in phase having a nonzero intensity in the coupling gap region, while the optical field of the antibonding modes is out of phase and appears repulsive at the coupling region due to phase mismatch.^{166, 167} Note that both the fundamental and higher-order axial modes support bonding (E_{0-} , E_{1-} , E_{2-}) and antibonding states (E_{0+} , E_{1+} , E_{2+}), which is a signature of collective strong coupling in the twin microcavities.

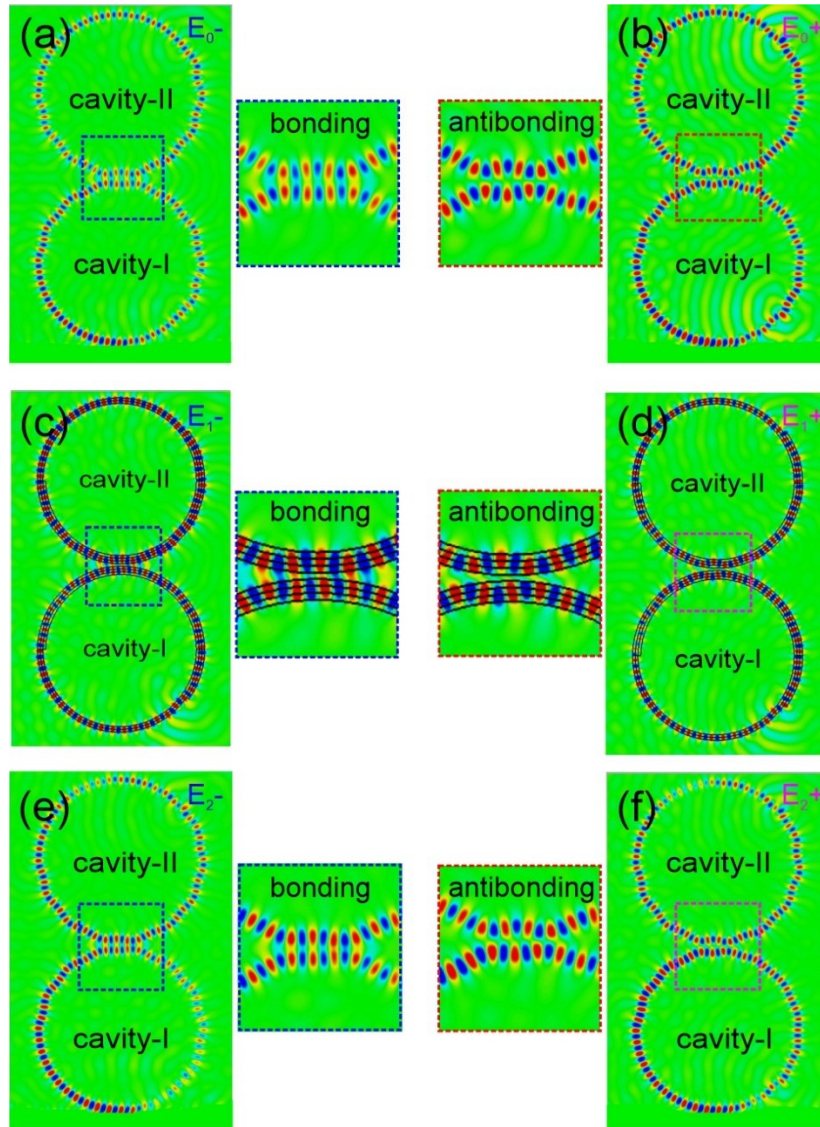


Figure 5.15. The cross-sectional view of 3D mode profiles of the bonding and antibonding modes for the fundamental modes (a, b), first-order (c, d) and second-order axial modes (e, f).

In addition, the mode anticrossing and changing-over features of multiple groups of coupling modes as direct evidence of strong coupling are clearly identified by spectral detuning via continuously changing the permittivity (effective refractive index) of one cavity (see Figure 5.16). Overall, the simulations of mode hybridization demonstrate the collective strong coupling of 3D confined resonant modes in good agreement with the experimental results.

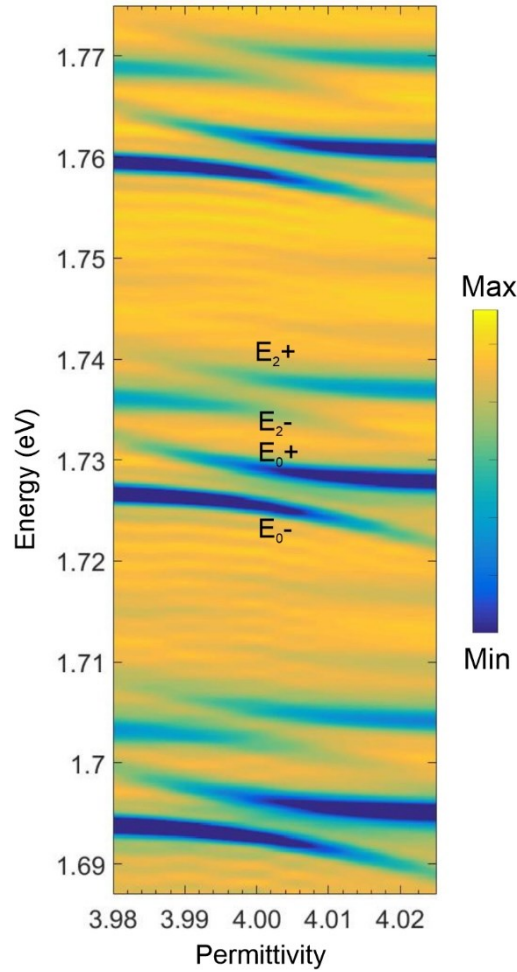


Figure 5.16. Map of the resonant frequency as a function of permittivity of modeled twin microtubes

5.4 Conclusion

In summary, collective strong coupling between two sets of 3D confined resonant modes is realized in monolithically integrated twin microtube cavities which are fabricated *in situ* by the self-rolling of prestrained SiN_x nanomembranes from two opposite directions based on standard photolithography. This unique parallel configuration enables optical coupling to occur at the tangent line of twin microtubes along tube axis increasing the coupling region. Owing to the aligned twin geometries of the double microtube cavities, two sets of 3D confined resonant modes are spectrally and spatially matched. Both the fundamental and higher-order axial modes are strongly coupled with each other, namely as collective strong coupling. During the detuning

process, the spectral anticrossing feature and the modes changing-over of each group coupling system as direct evidence of strong coupling are revealed in experiments and calculations. The measured evolution of spatial optical field distributions allows the direct observation of the energy exchange between each group of coupling modes in the collective strong coupling regime. Each group of coupling modes can be treated as an independent strong coupling system providing an effective path for energy exchange between coupled microcavities. Moreover, 3D mode profiles of twin microcavities simulated via the FDTD method are in excellent agreement with the experimental results. Our work offers a compact design of monolithic twin microcavities for realizing collective strong coupling of 3D confined optical modes, which could be exploited for manipulating higher-order optical coupling, multichannel optical signal processing, and 3D non-Hermitian systems.

Chapter 6 Summary and Outlook

This is the final chapter including the basic conclusions for previous chapters and the potential outlook of the research topic.

6.1 Summary

Optical coupling microcavities have been explored as an ideal platform to manipulate the resonant light. Whispering-gallery mode (WGM) microcavities supporting resonances along a ring trajectory have been identified as ideal candidates for building those coupled microcavity systems and investigating resonant optical coupling phenomena. As one type of WGM microcavities, microtube cavities with axial potential wells can support 3D optical resonances in an azimuthal plane and along the tube axis, offering a promising possibility to explore multichannel and multidimensional optical coupling. The axial confinement within the microtubes adds a new degree of freedom for the manipulation of optical resonances and coupling. Specifically, the axial optical potential well in a microtube cavity splits the original azimuthal mode into fundamental and multiple higher-order axial modes with different spatial distributions, which promises to achieve multichannel optical coupling in coupled microtube cavities. It is therefore highly desirable to explore optical coupling systems of microtube cavities for realizing simultaneously multichannel and multidimensional manipulation of photonic signals.

The focus of this doctoral thesis is on the optical coupling of 3D confined resonant modes based on microtube cavities fabricated by self-rolling of prestrained nanomembranes. In contrast to the optical coupling fixed at one 2D planar, the microtube cavities with interlayer nanogap support the efficient strong coupling of 3D resonant modes. The 3D optical coupling enables the wavevector to exist in more than one direction (i.e., azimuthal and axial directions),

which are promising for both fundamental and applied studies such as non-trivial evolution of wavevector and direction-selective coupling. In addition, a collective optical coupling of 3D confined resonant modes is realized in monolithic twin microtube cavities. Both the fundamental and higher-order axial modes are strongly coupled with each other. Multiple groups of the coupling modes provide multiple effective channels for energy exchange between coupled microcavities. Our work provides a unique platform for realizing strong coupling of 3D confined resonant modes in a monolithically integrated coupling system, which is of high interest for promising applications in nonlinear optics, 3D non-Hermitian systems and multichannel optical signal processing.

These studies include the following aspects:

(1) In the first optical coupling system, the generation of multiple sets of 3D confined resonant modes and their coupling was enabled based on resonant trajectory split in a single microtube cavity. Owing to the existence of an interlayer nanogap in the tube wall, the resonant trajectory partially splits at the nanogap region while sharing the same trajectory in the rest part of the cavity. As all the split trajectories experience axial confinement in the tube cavity, they are all simultaneously confined and resonating along the axial direction. As a result, multiple sets of 3D confined resonant modes were generated in a single microtube cavities. Moreover, strong optical coupling between two sets of 3D confined resonant modes was observed. The corresponding spectral anticrossing feature and the changing-over of coupled modes were revealed as direct evidence of strong coupling. In particular, the spatial optical field distribution of 3D coupling modes was experimentally mapped upon the strong coupling regime, which shows the corresponding energy transfer process between the two hybrid states. Numerical calculations based on the quasi-potential model and the mode detuning process are in excellent agreement with the experimental results. The 3D optical coupling is particularly interesting for directional coupling with a higher degree of freedom. The manipulation of wavevector with a

higher degree of freedom allows for the study of topological photonic based on non-trivial evolution of wavevector, such as generating optical Berry phase, and optical spin-Hall effect.

(2) A collective strong coupling between two sets of 3D confined resonant modes is realized in monolithically integrated twin microtube cavities which are fabricated *in situ* by the self-rolling of prestrained SiN_x nanomembranes from two opposite directions based on standard photolithography. This unique parallel configuration enables optical coupling to occur at the tangent line of twin microtubes along the tube axis increasing the coupling region. Owing to the aligned twin geometries of the double microtube cavities, two sets of 3D confined resonant modes are spectrally and spatially matched. Both the fundamental and higher-order axial modes are strongly coupled with each other, namely as collective strong coupling. During the detuning process, the spectral anticrossing feature and the modes changing-over of each group coupling system as direct evidence of strong coupling are revealed in experiments and calculations. The measured evolution of spatial optical field distributions allows the direct observation of the energy exchange between each group of coupling modes in the collective strong coupling regime. Each group of coupling modes can be treated as an independent strong coupling system providing an effective path for energy exchange between coupled microcavities. Moreover, 3D mode profiles of twin microcavities simulated via the FDTD method are in excellent agreement with the experimental results. Our work offers a compact design of monolithic twin microcavities for realizing collective strong coupling of 3D confined optical modes, which could be exploited for manipulating higher-order optical coupling, multichannel optical signal processing, and 3D non-Hermitian systems.

6.2 Outlook

Microtube cavities fabricated by self-rolling of prestrained nanomembranes have gained considerable interest because of a variety of unique properties including rich materials available, the capability of on-chip fabrication, and hollow-core structure, and the subwavelength walls.⁸²

Owing to the optical resonance of microtube cavities coming from the constructive interference of the light traveling along a circular trajectory, one may affect the geometry of microtubes should have a significant influence on resonant behavior. As shown in Figure 6.1a and b, the interlayer nanogap in the tube wall enables the trajectory splitting in a single microtube. The resonant frequency and spatial distribution of resonant modes lie in the nanogap position and size. By pressuring a fiber on the microtube cavity, the interlayer nanogap can be changed. The two sets of resonant modes show a clear mode shift and spatial distribution change, which can reflect the effect of pressure (Figure 6.1c). On this basis, the microtube cavities with interlayer nanogap can be used for sensing applications based on the spectral evolution.

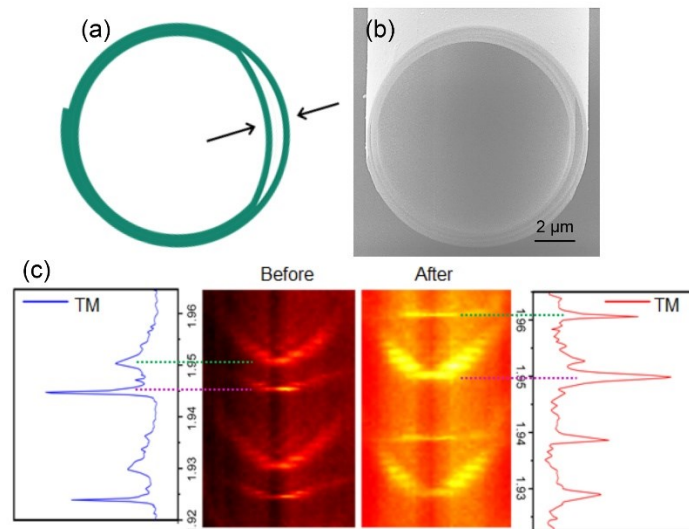


Figure 6.1. (a) Schematic showing the cross-sectional structure of a microtube cavity with interlayer nanogap. (b) The corresponding SEM image of the microtube. (c) The resonant

spectra and measured spatially optical field distribution of the microtube before and after applying the pressure.

In addition, because of the subwavelength walls, the optical field cannot be strongly confined within the wall of microtube cavities but exponentially decays outside the tube wall in the form of evanescent fields. Microtube cavities present high sensitivities to the perturbation from the surrounding environment. The hollow-core structure of microtubes naturally provides built-in microfluidic channels which enables a clear advantage in optofluidic by filling either liquid or gas into cavities. The coupled microtube cavities mentioned in this thesis can define two new types of optofluidic sensors. With the high sensitivities of evanescent fields to perturbation, the sensor action can work through the evolution of coupled modes within the optical coupling systems.

Bibliography

1. Vahala, K. J., Optical Microcavities. *Nature* **2003**, *424*, 839.
2. Artemyev, M. V.; Woggon, U.; Wannemacher, R.; Jaschinski, H.; Langbein, W., Light Trapped in a Photonic Dot: Microspheres Act as a Cavity for Quantum Dot Emission. *Nano Letters* **2001**, *1*, 309.
3. Dong, H.; Saggau, C. N.; Zhu, M.; Liang, J.; Duan, S.; Wang, X.; Tang, H.; Yin, Y.; Wang, X.; Wang, J.; Zhang, C.; Zhao, Y. S.; Ma, L.; Schmidt, O. G., Perovskite Origami for Programmable Microtube Lasing. *Adv. Funct. Mater.* **2021**, *2109080*.
4. Du, Y.; Zou, C.; Zhang, C.; Wang, K.; Qiao, C.; Yao, J.; Zhao, Y. S., Tuneable Red, Green, and Blue Single-Mode Lasing in Heterogeneously Coupled Organic Spherical Microcavities. *Light Sci. Appl.* **2020**, *9*, 151.
5. Gu, F.; Xie, F.; Lin, X.; Linghu, S.; Fang, W.; Zeng, H.; Tong, L.; Zhuang, S., Single Whispering-Gallery Mode Lasing in Polymer Bottle Microresonators *via* Spatial Pump Engineering. *Light Sci. Appl.* **2017**, *6*, e17061.
6. Sumetsky, M., Lasing Microbottles. *Light Sci. Appl.* **2017**, *6*, e17102.
7. Li, Y. ; Abolmaali, F.; Limberopoulos, N. I.; Urbas, A. M.; Astratov, V. N., Coupling Properties and Sensing Applications of Photonic Molecules. *2015 National Aerospace and Electronics Conference* **2015**, *102*.
8. Srinivasan, K.; Painter, O., Linear and Nonlinear Optical Spectroscopy of a Strongly Coupled Microdisk–Quantum Dot System, *Nature* **2007**, *450*, 862.
9. Hoang, T. X.; Nagelberg, S. N.; Kolle, M.; Barbastathis, G., Fano Resonances from Coupled Whispering-Gallery Modes in Photonic Molecules. *Opt. Express* **2017**, *25*, 13125.
10. Kang, T. Y.; Lee, W.; Ahn, H.; Shin, D. M.; Kim, C. S.; Oh, J. W.; Kim, D.; Kim, K., Plasmon-Coupled Whispering Gallery Modes on Nanodisk Arrays for Signal Enhancements. *Sci. Rep.* **2017**, *7*, 11737.

11. Yang, C.; Jiang, X.; Hua, Q.; Hua, S.; Chen, Y.; Ma, J.; Xiao, M., Realization of Controllable Photonic Molecule based on Three Ultrahigh-Q Microtoroid Cavities. *Laser Photonics Rev.* **2017**, *11*, 1600178.
12. Peng, B.; Özdemir, Ş. K.; Lei, F.; Monifi, F.; Gianfreda, M.; Long, G. L.; Fan, S.; Nori, F.; Bender, C. M.; Yang, L., Parity–Time-Symmetric Whispering-Gallery Microcavities. *Nature Phys.* **2014**, *10*, 394.
13. Benyoucef, M.; Shim, J. B.; Wiersig, J.; Schmidt, O. G., Quality-Factor Enhancement of Supermodes in Coupled Microdisks. *Opt. Lett.* **2011**, *36*, 1317
14. Lin, H.; Chen, J.; Chao, S.; Lo, M., Lin, S., Chang, W., Strong Coupling of Different Cavity Modes in Photonic Molecules Formed by Two Adjacent Microdisk Microcavities. *Opt. Express* **2010**, *18*, 23948.
15. Roiz, M.; Monakhov, A.; Kunitsyna, E.; Yakovlev, Y.; Teissier, R.; Baranov, A., Strong Optical Coupling between Semiconductor Microdisk Lasers: From Whispering Gallery Modes to Collective Modes. *J. Appl. Phys.* **2020**, *127*, 173105.
16. Ishii, S.; Baba, T., Bistable Lasing in Twin Microdisk Photonic Molecules. *Appl. Phys. Lett.* **2005**, *87*, 181102.
17. Zhang, N.; Gu, Z.; Wang, K.; Li, M.; Ge, L.; Xiao, S.; Song, Q., Quasiparity-Time Symmetric Microdisk Laser. *Laser Photonics Rev.* **2017**, *11*, 1700052.
18. Lee, W.; Li, H.; Suter, J. D.; Reddy, K.; Sun, Y.; Fan, X., Tunable Single Mode Lasing from an on-Chip Optofluidic Ring Resonator Laser. *Appl. Phys. Lett.* **2011**, *98*, 061103.
19. Chandralalim, H.; Fan, X., Reconfigurable Solid-State Dye-Doped Polymer Ring Resonator Lasers. *Sci. Rep.* **2015**, *5*, 18310.
20. Hodaei, H.; Hassan, A. U.; Wittek, S.; Garcia-Gracia, H.; El-Ganainy, R.; Christodoulides, D. N.; Khajavikhan, M., Enhanced sensitivity at higher-order exceptional points. *Nature* **2017**, *548*, 187.

21. Li, Y.; Abolmaali, F.; Allen, K. W.; Limberopoulos, N. I.; Urbas, A.; Rakovich, Y.; Maslov, A. V.; Astratov, V. N., Whispering Gallery Mode Hybridization in Photonic Molecules. *Laser Photonics Rev.* **2017**, *11*, 1600278.
22. Ward, J.; Benson, O., WGM Microresonators: Sensing, Lasing and Fundamental Optics with Microspheres. *Laser Photonics Rev.* **2011**, *5*, 553.
23. Bliokh, K. Y.; Rodríguez-Fortuño, F. J.; Nori, F.; Zayats, A. V., Spin–Orbit Interactions of Light. *Nature Photon.* **2015**, *9*, 796.
24. Ma, L.; Li, S.; Fomin, V. M.; Hentschel, M.; Gotte, J. B.; Yin, Y.; Jorgensen, M. R.; Schmidt, O. G., Spin-Orbit Coupling of Light in Asymmetric Microcavities. *Nat. Commun.* **2016**, *7*, 10983.
25. Strelow, C.; Schultz, C. M.; Rehberg, H.; Sauer, M.; Welsch, H.; Stemmann, A.; Heyn, C.; Heitmann, D.; Kipp, T., Light Confinement and Mode Splitting in Rolled-up Semiconductor Microtube Bottle Resonators. *Phys. Rev. B* **2012**, *85*, 155329.
26. Strelow, C.; Rehberg, H.; Schultz, C. M.; Welsch, H.; Heyn, C.; Heitmann, D.; Kipp, T., Optical Microcavities Formed by Semiconductor Microtubes Using a Bottlelike Geometry. *Phys. Rev. Lett.* **2008**, *101*, 127403.
27. Yin, Y.; Li, S.; Bottner, S.; Yuan, F.; Giudicatti, S.; Saei Ghareh Naz, E.; Ma, L.; Schmidt, O. G., Localized Surface Plasmons Selectively Coupled to Resonant Light in Tubular Microcavities. *Phys. Rev. Lett.* **2016**, *116*, 253904.
28. Wang, J.; Zhan, T.; Huang, G.; Chu, P. K.; Mei, Y., Optical Microcavities with Tubular Geometry: Properties and Applications. *Laser Photonics Rev.* **2014**, *8*, 521.
29. Yu, X.; Goddard, L. L.; Li, X.; Chen, X., Enhanced Axial Confinement in a Monolithically Integrated Self-Rolled-up SiN_x Vertical Microring Photonic Coupler. *Appl. Phys. Lett.* **2016**, *109*, 111104.
30. He, L.; Özdemir, Ş. K.; Yang, L., Whispering gallery microcavity lasers. *Laser Photonics Rev.* **2013**, *7*, 60.

31. Smith, N. D., A Technique for Continuous Measurement of the Quality Factor of Mechanical Oscillators. *Rev. Sci. Instrum.* **2015**, *86*, 053907.
32. Böttner, S.; Li, S.; Trommer, J.; Kiravittaya, S.; Schmidt, O. G., Sharp Whispering-Gallery Modes in Rolled-up Vertical SiO₂ Microcavities with Quality Factors Exceeding 5000. *Opt. Lett.* **2012**, *37*, 3.
33. Choi, H.; Heuck, M.; Englund, D., Self-Similar Nanocavity Design with Ultrasmall Mode Volume for Single-Photon Nonlinearities. *Phys. Rev. Lett.* **2017**, *118*, 223605.
34. Garrett, C. G. B.; Kaiser, W.; Bond, W. L., Stimulated Emission into Optical Whispering Modes of Spheres. *Phys. Rev.* **1961**, *124*, 1807.
35. Chen, W.; Kaya Ozdemir, S.; Zhao, G.; Wiersig, J.; Yang, L., Exceptional Points Enhance Sensing in an Optical Microcavity. *Nature* **2017**, *548*, 192.
36. He, X.; Harris, G. I.; Baker, C. G.; Sawadsky, A.; Sfindla, Y. L.; Sachkou, Y. P.; Forstner, S.; Bowen, W. P., Strong Optical Coupling through Superfluid Brillouin Lasing. *Nature Phys.* **2020**, *16*, 417.
37. Yang, S.; Wang, Y.; Sun, H., Advances and Prospects for Whispering Gallery Mode Microcavities. *Adv. Opt. Mater.* **2015**, *3*, 1136.
38. Cao, Q.; Liu, R.; Wang, H.; Lu, Y. K.; Qiu, C. W.; Rotter, S.; Gong, Q.; Xiao, Y., Reconfigurable Symmetry-Broken Laser in a Symmetric Microcavity. *Nat. Commun.* **2020**, *11*, 1136.
39. Hodaei, H.; Miri, M. A.; Heinrich, M.; Christodoulides, D. N.; Khajavikhan, M., Parity-Time-Symmetric Microring Lasers. *Science* **2014**, *346*, 975.
40. Zhao, J.; Yan, Y.; Wei, C.; Zhang, W.; Gao, Z.; Zhao, Y. S., Switchable Single-Mode Perovskite Microlasers Modulated by Responsive Organic Microdisks. *Nano Lett.* **2018**, *18*, 1241.

41. Jiang, X.; Shao L.; Zhang, S.; Yi, X.; Wiersig, J.; Wang, L.; Gong, Q.; Lončar, M.; Yang, L.; Xiao, Y., Chaos-Assisted Broadband Momentum Transformation in Optical Microresonators. *Science* **2017**, *358*, 344.
42. Ma, L.; Li, S.; Quinones, V. A.; Yang, L.; Xi, W.; Jorgensen, M.; Baunack, S.; Mei, Y.; Kiravittaya, S.; Schmidt, O. G., Dynamic Molecular Processes Detected by Microtubular Opto-Chemical Sensors Self-Assembled from Prestrained Nanomembranes. *Adv. Mater.* **2013**, *25*, 2357.
43. Schmidt, O. G.; Eberl, K., Thin Solid Films Roll up into Nanotubes. *Nature* **2001**, *410*, 168.
44. Prinz, V.Y.; Seleznev, V. A.; Gutakovsky, A. K.; Chehovskiy, A. V.; Preobrazhenskii, V. V.; Putyato, M. A.; Gavrilova, T. A., Free-Standing and Overgrown InGaAs/GaAs Nanotubes, Nanohelices and Their Arrays. *Physica E* **2000**, *6*, 828.
45. Mei, Y.; Huang, G.; Solovev, A. A.; Ureña, E. B.; Mönch, I.; Ding, F.; Reindl, T.; Fu, R. K. Y.; Chu, P. K.; Schmidt, O. G., Versatile Approach for Integrative and Functionalized Tubes by Strain Engineering of Nanomembranes on Polymers. *Adv. Mater.* **2008**, *20*, 4085.
46. Zhang, Y.; Han, D.; Du, D.; Huang, G.; Qiu, T.; Mei, Y., Rolled-up Ag-SiO_x Hyperbolic Metamaterials for Surface-Enhanced Raman Scattering. *Plasmonics* **2015**, *10*, 949.
47. Quiñones, V. A. B.; Ma, L.; Li, S.; Jorgensen, M.; Kiravittaya, S.; Schmidt, O. G., Enhanced Optical Axial Confinement in Asymmetric Microtube Cavities Rolled up from Circular-Shaped Nanomembranes. *Opt. Lett.* **2012**, *37*, 4284.
48. Tian, Z.; Li, S.; Kiravittaya, S.; Xu, B.; Tang, S.; Zhen, H.; Lu, W.; Mei, Y., Selected and Enhanced Single Whispering-Gallery Mode Emission from a Mesostuctured Nanomembrane Microcavity. *Nano Lett.* **2018**, *18*, 8035.
49. Xu, B.; Tian, Z.; Wang, J.; Han, H.; Lee, T.; Mei, Y., Stimuli-Responsive and on-Chip Nanomembrane Micro-Rolls for Enhanced Macroscopic Visual Hydrogen Detection. *Sci. Adv.* **2018**, *4*, eaap8203.

50. Saggau, C. N.; Gabler, F.; Karnaushenko, D. D.; Karnaushenko, D.; Ma, L.; Schmidt, O. G., Wafer-Scale High-Quality Microtubular Devices Fabricated via Dry-Etching for Optical and Microelectronic Applications. *Adv. Mater.* **2020**, *32*, e2003252.
51. Bernardi, A.; Kiravittaya, S.; Rastelli, A.; Songmuang, R.; Thurmer, D. J.; Benyoucef, M.; Schmidt, O. G., On-Chip Si/SiO_x Microtube Refractometer. *Appl. Phys. Lett.* **2008**, *93*, 094106.
52. Songmuang, R.; Rastelli, A.; Mendach, S.; Schmidt, O. G., SiO_x/Si Radial Superlattices and Microtube Optical Ring Resonators. *Appl. Phys. Lett.* **2007**, *90*, 091905.
53. Mei, Y.; Thurmer, D. J.; Deneke, C.; Kiravittaya, S.; Chen, Y.; Dadgar, A.; Bertram, F.; Bastek, B.; Krost, A.; Christen, J.; Reindl, T.; Stoffel, M.; Coric, E.; Schmidt, O. G., Fabrication, Self-Assembly, and Properties of Ultrathin AlN/GaN Porous Crystalline Nanomembranes: Tubes, Spirals, and Curved Sheets. *ACS Nano* **2009**, *3*, 1663.
54. Huang, G.; Kiravittaya, S.; Bolaños Quiñones, V. A.; Ding, F.; Benyoucef, M.; Rastelli, A.; Mei, Y.; Schmidt, O. G., Optical Properties of Rolled-up Tubular Microcavities from Shaped Nanomembranes. *Appl. Phys. Lett.* **2009**, *94*, 141901.
55. Wang, L.; Tian, Z.; Zhang, B.; Xu, B.; Wang, T.; Wang, Y.; Li, S.; Di, Z.; Mei, Y., On-Chip Rolling Design for Controllable Strain Engineering and Enhanced Photon-Phonon Interaction in Graphene. *Small* **2019**, *15*, e1805477.
56. Kipp, T.; Welsch, H.; Strelow, C.; Heyn, C.; Heitmann, D., Optical modes in semiconductor microtube ring resonators. *Phys. Rev. Lett.* **2006**, *96*, 077403.
57. Yin, Y.; Qiu, T.; Ma, L.; Lang, X.; Zhang, Y.; Huang, G.; Mei, Y.; Schmidt, O. G., Exploring Rolled-up Au–Ag Bimetallic Microtubes for Surface-Enhanced Raman Scattering Sensor. *J. Phys. Chem. C* **2012**, *116*, 25504.
58. Yin, Y.; Li, S. L.; Giudicatti, S.; Jiang, C. Y.; Ma, L. B.; Schmidt, O. G., Strongly Hybridized Plasmon-Photon Modes in Optoplasmonic Microtubular Cavities. *Phys. Rev. B* **2015**, *92*, 241403.

59. Yin, Y.; Chen, Y.; Saei Ghareh Naz, E.; Lu, X.; Li, S.; Engemaier, V.; Ma, L.; Schmidt, O. G., Silver Nanocap Enabled Conversion and Tuning of Hybrid Photon–Plasmon Modes in Microtubular Cavities. *ACS Photonics* **2017**, *4*, 736.
60. Wang, J.; Yin, Y.; Hao, Q.; Zhang, Y.; Ma, L.; Schmidt, O. G., Strong Coupling in a Photonic Molecule Formed by Trapping a Microsphere in a Microtube Cavity. *Adv. Opt. Mater.* **2018**, *6*, 170082.
61. Tian, Z.; Veerasubramanian, V.; Bianucci, P.; Mukherjee, S.; Mi, Z.; Kirk, A. G.; Plant, D. V., Single Polled-up InGaAs/GaAs Quantum Dot Microtubes Integrated with Silicon-on-Insulator Waveguides. *Opt. Express* **2011**, *19*, 8.
62. Zhong, Q.; Tian, Z.; Dastjerdi, M. H.; Mi, Z.; Plant, D. V., Characterization of Azimuthal and Longitudinal Modes in Rolled-up InGaAs/GaAs Microtubes at Telecom Wavelengths. *Opt. Express* **2013**, *21*, 18909.
63. Zhong, Q.; Tian, Z.; Dastjerdi, M. H. T.; Mi, Z.; Plant, D. V., Counterpropagating Whispering-Gallery-Modes of Rolled-up Semiconductor Microtubes. *IEEE Photon. Technol. Lett.* **2013**, *25*, 1691.
64. Zhong, Q.; Tian, Z.; Veerasubramanian, V.; Dastjerdi, M. H.; Mi, Z.; Plant, D. V., Thermally Controlled Coupling of a Rolled-up Microtube Integrated with a Waveguide on a Silicon Electronic-Photonic Integrated Circuit. *Opt. Lett.* **2014**, *39*, 2699.
65. Wang, H.; Zhen, H.; Li, S.; Jing, Y.; Huang, G.; Mei, Y.; Lu, W., Self-Rolling and Light-Trapping in Flexible Quantum Well–Embedded Nanomembranes for Wide-Angle Infrared Photodetectors. *Sci. Adv.* **2016**, *2*, e1600027.
66. Strelow, C.; Schultz, C. M.; Rehberg, H.; Welsch, H.; Heyn, C.; Heitmann, D.; Kipp, T., Three Dimensionally Confined Optical Modes in Quantum-Well Microtube Ring Resonators. *Phys. Rev. B* **2007**, *76*, 045303.

67. Strelow, C.; Sauer, M.; Fehring, S.; Korn, T.; Schüller, C.; Stemmann, A.; Heyn, C.; Heitmann, D.; Kipp, T., Time-Resolved Studies of a Rolled-up Semiconductor Microtube Laser. *Appl. Phys. Lett.* **2009**, *95*, 221115.
68. Dietrich, K.; Strelow, C.; Schliehe, C.; Heyn, C.; Stemmann, A.; Schwaiger, S.; Mendach, S.; Mews, A.; Weller, H.; Heitmann, D.; Kipp, T., Optical Modes Excited by Evanescent-Wave-Coupled PbS Nanocrystals in Semiconductor Microtube Bottle Resonators. *Nano Lett.* **2010**, *10*, 627.
69. Strelow, C.; Kietzmann, S.; Schramm, A.; Seher, R.; Penttinen, J. P.; Hakkarainen, T. V.; Mews, A.; Kipp, T., AlInP-based Rolled-up Microtube Resonators with Colloidal Nanocrystals Operating in the Visible Spectral Range. *Appl. Phys. Lett.* **2012**, *101*, 113114.
70. Golod, S. V.; Prinz, V. Y.; Wägli, P.; Zhang, L.; Kirfel, O.; Deckhardt, E.; Glaus, F.; David, C.; Grützmacher, D., Freestanding SiGe/Si/Cr and SiGe/Si/SixNy/Cr Microtubes. *Appl. Phys. Lett.* **2004**, *84*, 3391.
71. Bolaños Quiñones, V. A.; Huang, G.; Plumhof, J. D.; Kiravittaya, S.; Rastelli, A.; Mei, Y.; Schmidt, O. G., Optical Resonance Tuning and Polarization of Thin-Walled Tubular Microcavities. *Opt. Lett.* **2009**, *34*, 2345.
72. Huang, G.; Bolaños Quiñones, V. A.; Ding, F.; Kiravittaya, S.; Mei, Y.; Schmidt, O. G., Rolled-up Optical Microcavities with Subwavelength Wall Thicknesses for Enhanced Liquid Sensing Applications. *ACS Nano* **2010**, *4*, 3123.
73. Ma, L.; Kiravittaya, S.; Bolaños Quiñones, V. A.; Li, S.; Mei, Y.; Schmidt, O. G., Tuning of Optical Resonances in Asymmetric Microtube Cavities. *Opt. Lett.* **2011**, *36*, 3840.
74. Smith, E. J.; Schulze, S.; Kiravittaya, S.; Mei, Y.; Sanchez, S.; Schmidt, O. G., Lab-in-a-Tube: Detection of Individual Mouse Cells for Analysis in Flexible Split-Wall Microtube Resonator Sensors. *Nano Lett.* **2011**, *11*, 4037.

75. Bolaños Quiñones, V. A.; Ma, L.; Li, S.; Jorgensen, M.; Kiravittaya, S.; Schmidt, O. G., Localized Optical Resonances in Low Refractive Index Rolled-up Microtube Cavity for Liquid-Core Optofluidic Detection. *Appl. Phys. Lett.* **2012**, *101*, 151107.
76. Harazim, S. M.; Xi, W.; Schmidt, C. K.; Sanchez, S.; Schmidt, O. G., Fabrication and Applications of Large Arrays of Multifunctional Rolled-up SiO/SiO₂ Microtubes. *J. Mater. Chem.* **2012**, *22*, 2878.
77. Li, S.; Ma, L.; Zhen, H.; Jorgensen, M. R.; Kiravittaya, S.; Schmidt, O. G., Dynamic Axial Mode Tuning in a Rolled-up Optical Microcavity. *Appl. Phys. Lett.* **2012**, *101*, 231106.
78. Miao, S.; Chen, D.; Madani, A.; Jorgensen, M. R.; Bolaños Quiñones, V. A.; Ma, L.; Hickey, S. G.; Eychmüller, A.; Schmidt, O. G., Optofluidic Sensor: Evaporation Kinetics Detection of Solvents Dissolved with Cd₃P₂ Colloidal Quantum Dots in a Rolled-up Microtube. *Adv. Opt. Mater.* **2015**, *3*, 187.
79. Wang, J.; Yin, Y.; Hao, Q.; Huang, S.; Saei Ghareh Naz, E.; Schmidt, O. G.; Ma, L., External Strain Enabled Post-Modification of Nanomembrane-based Optical Microtube Cavities. *ACS Photonics* **2018**, *5*, 2060.
80. Wang, J.; Yin, Y.; Hao, Q.; Yang, Y. D.; Valligatla, S.; Saei Ghareh Naz, E.; Li, Y.; Saggau, C. N.; Ma, L.; Schmidt, O. G., Curved Nanomembrane-based Concentric Ring Cavities for Supermode Hybridization. *Nano Lett.* **2018**, *18*, 7261.
81. Yin, Y.; Wang, J.; Lu, X.; Hao, Q.; Saei Ghareh Naz, E.; Cheng, C.; Ma, L.; Schmidt, O. G., *In Situ* Generation of Plasmonic Nanoparticles for Manipulating Photon-Plasmon Coupling in Microtube Cavities. *ACS Nano* **2018**, *12*, 3726.
82. Wang, J.; Yin, Y.; Yang, Y.; Hao, Q.; Tang, M.; Wang, X.; Saggau, C. N.; Karnaushenko, D.; Yan, X.; Huang, Y.; Ma, L.; Schmidt, O. G., Deterministic Yet Flexible Directional Light Emission from Spiral Nanomembrane Cavities. *ACS Photonics* **2019**, *6*, 2537.

83. Yin, Y.; Pang, J.; Wang, J.; Lu, X.; Hao, Q.; Saei Ghareh Naz, E.; Zhou, X.; Ma, L.; Schmidt, O. G., Graphene-Activated Optoplasmonic Nanomembrane Cavities for Photodegradation Detection. *ACS Appl. Mater. Interfaces* **2019**, *11*, 15891.
84. Yin, Y.; Wang, J.; Wang, X.; Li, S.; Jorgensen, M. R.; Ren, J.; Meng, S.; Ma, L.; Schmidt, O. G., Water Nanostructure Formation on Oxide Probed *in situ* by Optical Resonances. *Sci. Adv.* **2019**, *5*, eaax6973.
85. Wang, J.; Tang, M.; Yang, Y. D.; Yin, Y.; Chen, Y.; Saggau, C. N.; Zhu, M.; Yuan, X.; Karnaushenko, D.; Huang, Y. Z.; Ma, L.; Schmidt, O. G., Steering Directional Light Emission and Mode Chirality through Postshaping of Cavity Geometry. *Laser Photonics Rev.* **2020**, *14*, 2000118.
86. Huang, G.; Mei, Y.; Thurmer, D. J.; Coric, E.; Schmidt, O. G., Rolled-up Transparent Microtubes as Two-Dimensionally Confined Culture Scaffolds of Individual Yeast Cells. *Lab Chip* **2009**, *9*, 263.
87. Trommer, J.; Bottner, S.; Li, S.; Kiravittaya, S.; Jorgensen, M. R.; Schmidt, O. G., Observation of Higher Order Radial Modes in Atomic Layer Deposition Reinforced Rolled-up Microtube Ring Resonators. *Opt. Lett.* **2014**, *39*, 6335.
88. Böttner, S.; Li, S.; Jorgensen, M. R.; Schmidt, O. G., Polarization Resolved Spatial Near-Field Mapping of Optical Modes in an on-Chip Rolled-up Bottle Microcavity. *Appl. Phys. Lett.* **2014**, *105*, 121106.
89. Böttner, S.; Li, S.; Jorgensen, M. R.; Schmidt, O. G., Vertically Aligned Rolled-up SiO₂ Optical Microcavities in Add-Drop Configuration. *Appl. Phys. Lett.* **2013**, *102*, 251119.
90. Harazim, S. M.; Bolanos Quinones, V. A.; Kiravittaya, S.; Sanchez, S.; Schmidt, O. G., Lab-in-a-Tube: on-Chip Integration of Glass Optofluidic Ring Resonators for Label-Free Sensing Applications. *Lab Chip* **2012**, *12*, 2649.

91. Lin, X.; Fang, Y.; Zhu, L.; Zhang, J.; Huang, G.; Wang, J.; Mei, Y., Self-Rolling of Oxide Nanomembranes and Resonance Coupling in Tubular Optical Microcavity. *Adv. Opt. Mater.* **2016**, *4*, 936.
92. Zhang, J.; Zhong, J.; Fang, Y. F.; Wang, J.; Huang, G. S.; Cui, X. G.; Mei, Y. F., Roll up Polymer/Oxide/Polymer Nanomembranes as a Hybrid Optical Microcavity for Humidity Sensing. *Nanoscale* **2014**, *6*, 13646.
93. Valligatla, S.; Wang, J.; Madani, A.; Naz, E. S. G.; Hao, Q.; Saggau, C. N.; Yin, Y.; Ma, L.; Schmidt, O. G., Selective Out-of-Plane Optical Coupling between Vertical and Planar Microrings in a 3D Configuration. *Adv. Opt. Mater.* **2020**, *8*, 2000782.
94. Madani, A.; Ma, L.; Miao, S.; Jorgensen, M. R.; Schmidt, O. G., Luminescent Nanoparticles Embedded in TiO₂ Microtube Cavities for the Activation of Whispering-Gallery-Modes Extending from the Visible to the Near Infrared. *Nanoscale* **2016**, *8*, 9498.
95. Madani, A.; Bolaños Quiñones, V. A.; Ma, L. B.; Miao, S. D.; Jorgensen, M. R.; Schmidt, O. G., Overlapping Double Potential Wells in a Single Optical Microtube Cavity with Vernier-Scale-Like Tuning Effect. *Appl. Phys. Lett.* **2016**, *108*, 171105.
96. Madani, A.; Kleinert, M.; Stolarek, D.; Zimmermann, L.; Ma, L.; Schmidt, O. G., Vertical Optical Ring Resonators Fully Integrated with Nanophotonic Waveguides on Silicon-on-Insulator Substrates. *Opt. Lett.* **2015**, *40*, 3826.
97. Madani, A.; Bottner, S.; Jorgensen, M. R.; Schmidt, O. G., Rolled-up TiO₂ Optical Microcavities for Telecom and Visible Photonics. *Opt. Lett.* **2014**, *39*, 189.
98. Jorgensen, M. R.; Giudicatti, S.; Schmidt, O. G., Diamond Lattice Photonic Crystals from Rolled-up Membranes. *Phys. Rev. A* **2013**, *87*, 041803.
99. Zhang, J.; Li, J.; Tang, S.; Fang, Y.; Wang, J.; Huang, G.; Liu, R.; Zheng, L.; Cui, X.; Mei, Y., Whispering-Gallery Nanocavity Plasmon-Enhanced Raman Spectroscopy. *Sci. Rep.* **2015**, *5*, 15012.

100. Li, J.; Zhang, J.; Gao, W.; Huang, G.; Di, Z.; Liu, R.; Wang, J.; Mei, Y., Dry-Released Nanotubes and Nanoengines by Particle-Assisted Rolling. *Adv. Mater.* **2013**, *25*, 3715.
101. Chun, I. S.; Bassett, K.; Challa, A.; Li, X., Tuning the Photoluminescence Characteristics with Curvature for Rolled-up GaAs Quantum well Microtubes. *Appl. Phys. Lett.* **2010**, *96*, 251106.
102. Vicknesh, S.; Li, F.; Mi, Z., Optical Microcavities on Si Formed by Self-Assembled InGaAs/GaAs Quantum Dot Microtubes. *Appl. Phys. Lett.* **2009**, *94*, 081101.
103. Tian, Z.; Li, F.; Mi, Z.; Plant, D. V., Controlled Transfer of Single Rolled-Up InGaAs–GaAs Quantum-Dot Microtube Ring Resonators Using Optical Fiber Abrupt Tapers. *IEEE Photonics Technology Letters* **2010**, *22*, 311.
104. Li, F.; Mi, Z., Optically Pumped Rolled-up InGaAs/GaAs Quantum Dot Microtube Lasers. *Opt. Express* **2009**, *17*, 19933.
105. Li, F.; Mi, Z.; Vicknesh, S., Coherent Emission from Ultrathin-Walled Spiral InGaAs/GaAs Quantum Dot Microtubes. *Opt. Lett.* **2009**, *34*, 2915.
106. Ling, T.; Guo, L. J., A Unique Resonance Mode Observed in a Prism-Coupled Microtube Resonator Sensor with Superior Index Sensitivity. *Opt. Express* **2007**, *15*, 17424.
107. Yu, X.; Arbabi, E.; Goddard, L. L.; Li, X.; Chen, X., Monolithically Integrated Self-Rolled-up Microtube-based Vertical Coupler for Three-Dimensional Photonic Integration. *Appl. Phys. Lett.* **2015**, *107*, 031102.
108. Wang, J.; Huang, G.; Mei, Y., Modification and Resonance Tuning of Optical Microcavities by Atomic Layer Deposition. *Chem. Vap. Deposition* **2014**, *20*, 103.
109. Hosoda, M.; Shigaki, T., Degeneracy Breaking of Optical Resonance Modes in Rolled-up Spiral Microtubes. *Appl. Phys. Lett.* **2007**, *90*, 181107.
110. Totsuka, K.; Kobayashi, N.; Tomita, M., Slow Light in Coupled-Resonator-Induced Transparency. *Phys. Rev. Lett.* **2007**, *98*, 213904.

111. Rakovich, Y. P.; Donegan, J. F., Photonic Atoms and Molecules. *Laser Photonics Rev.* **2009**, *4*, 179.
112. Ge, F.; Han, X.; Xu, J., Strongly Coupled Systems for Nonlinear Optics. *Laser Photonics Rev.* **2021**, *15*, 2000514.
113. Xu, X.; Li, Y., Strong Photon Antibunching of Symmetric and Antisymmetric Modes in Weakly Nonlinear Photonic Molecules. *Phys. Rev. A* **2014**, *90*, 033809.
114. Feng, L.; El-Ganainy, R.; Ge, L., Non-Hermitian Photonics based on Parity–Time Symmetry. *Nature Photon.s* **2017**, *11*, 752.
115. Ozdemir, S. K.; Rotter, S.; Nori, F.; Yang, L., Parity-Time Symmetry and Exceptional Points in Photonics. *Nat. Mater.* **2019**, *18*, 783.
116. El-Ganainy, R.; Makris, K. G.; Khajavikhan, M.; Musslimani, Z. H.; Rotter, S.; Christodoulides, D. N., Non-Hermitian Physics and PT Symmetry. *Nature Phys.* **2018**, *14*, 11.
117. Dovzhenko, D. S.; Ryabchuk, S. V.; Rakovich, Y. P.; Nabiev, I. R., Light-Matter Interaction in the Strong Coupling Regime: Configurations, Conditions, and Applications. *Nanoscale* **2018**, *10*, 3589.
118. Pelton, M.; Storm, S. D.; Leng, H., Strong Coupling of Emitters to Single Plasmonic Nanoparticles: Exciton-Induced Transparency and Rabi Splitting. *Nanoscale* **2019**, *11*, 14540.
119. Yu, X.; Yuan, Y.; Xu, J.; Yong, K.-T.; Qu, J.; Song, J., Strong Coupling in Microcavity Structures: Principle, Design, and Practical Application. *Laser Photonics Rev.* **2019**, *13*, 1800219.
120. Aoki, T.; Dayan, B.; Wilcut, E.; Bowen, W. P.; Parkins, A. S.; Kippenberg, T. J.; Vahala, K. J.; Kimble, H. J., Observation of Strong Coupling between one Atom and a Monolithic Microresonator. *Nature* **2006**, *443*, 671.
121. Peng, B.; Özdemir Ş, K.; Rotter, S.; Yilmaz, H.; Liertzer, M.; Monifi, F.; Bender, C. M.; Nori, F.; Yang, L., Loss-Induced Suppression and Revival of Lasing. *Science* **2014**, *346*, 328.

122. Grossmann, T.; Wienhold, T.; Bog, U.; Beck, T.; Friedmann, C.; Kalt, H.; Mappes, T., Polymeric Photonic Molecule Super-Mode Lasers on Silicon. *Light Sci. Appl.* **2013**, *2*, e82.
123. Gao, R.; Guan, J.; Yao, N.; Deng, L.; Lin, J.; Wang, M.; Qiao, L.; Wang, Z.; Liang, Y.; Zhou, Y.; Cheng, Y., On-Chip Ultra-Narrow-Linewidth Single-Mode Microlaser on Lithium Niobate on Insulator. *Opt. Lett.* **2021**, *46*, 3131.
124. Wang, M.; Yao, N.; Wu, R.; Fang, Z.; Lv, S.; Zhang, J.; Lin, J.; Fang, W.; Cheng, Y., Strong Nonlinear Optics in on-Chip Coupled Lithium Niobate Microdisk Photonic Molecules. *New J. Phys.* **2020**, *22*, 073030.
125. Zhang, C.; Zou, C.; Zhao, Y.; Dong, C.; Wei, C.; Wang, H.; Liu, Y.; Guo, G.; Yao, J.; Zhao, Y., Organic Printed Photonics: from Microring Lasers to Integrated Circuits. *Sci. Adv.* **2015**, *1*, e1500257.
126. Hassan, A. U.; Hodaei, H.; Miri, M.-A.; Khajavikhan, M.; Christodoulides, D. N., Nonlinear Reversal of the PT-Symmetric Phase Transition in a System of Coupled Semiconductor Microring Resonators. *Phys. Rev. A* **2015**, *92*, 063807.
127. Zhou, B.; Zhong, Y.; Jiang, M.; Zhang, J.; Dong, H.; Chen, L.; Wu, H.; Xie, W.; Zhang, L., Linearly Polarized Lasing based on Coupled Perovskite Microspheres. *Nanoscale* **2020**, *12*, 5805.
128. Xu, B.; Zhang, X.; Tian, Z.; Han, D.; Fan, X.; Chen, Y.; Di, Z.; Qiu, T.; Mei, Y., Microdroplet-Guided Intercalation and Deterministic Delamination Towards Intelligent Rolling Origami. *Nat. Commun.* **2019**, *10*, 5019.
129. Gabler, F.; Karnaushenko, D. D.; Karnaushenko, D.; Schmidt, O. G., Magnetic Origami Creates High Performance Microdevices. *Nat. Commun.* **2019**, *10*, 3013.
130. Huang, G.; Mei, Y., Electromagnetic Wave Propagation in a Rolled-up Tubular Microcavity. *J. Mater. Chem. C* **2017**, *5*, 2758.
131. Zhao, F.; Zhan, T.; Huang, G.; Mei, Y.; Hu, X., Liquid Sensing Capability of Rolled-up Tubular Optical Microcavities: a Theoretical Study. *Lab Chip* **2012**, *12*, 3798.

132. Xu, C.; Wu, X.; Huang, G.; Mei, Y., Rolled-up Nanotechnology: Materials Issue and Geometry Capability. *Adv. Mater. Technol.* **2019**, *4*, 1800486.
133. Fang, Y.; Lin, X.; Tang, S.; Xu, B.; Wang, J.; Mei, Y., Temperature-Dependent Optical Resonance in a Thin-Walled Tubular Oxide Microcavity. *Prog. Nat. Sci.* **2017**, *27*, 498.
134. Smith, E. J.; Xi, W.; Makarov, D.; Monch, I.; Harazim, S.; Bolanos Quinones, V. A.; Schmidt, C. K.; Mei, Y.; Sanchez, S.; Schmidt, O. G., Lab-in-a-Tube: Ultracompact Components for on-Chip Capture and Detection of Individual Micro-/Nanoorganisms. *Lab Chip* **2012**, *12*, 1917.
135. Böttner, S.; Jorgensen, M. R.; Schmidt, O. G., Rolled-up Nanotechnology: 3D Photonic Materials by Design. *Scr. Mater.* **2016**, *122*, 119.
136. Li, X., Self-Rolled-up Microtube Ring Resonators: a Review of Geometrical and Resonant Properties. *Adv. Opt. Photon.* **2011**, *3*, 366.
137. Torma, P.; Barnes, W. L., Strong Coupling between Surface Plasmon Polaritons and Emitters: a Review. *Rep. Prog. Phys.* **2015**, *78*, 013901.
138. Bitton, O.; Gupta, S. N.; Haran, G., Quantum Dot Plasmonics: from Weak to Strong Coupling. *Nanophotonics* **2019**, *8*, 559.
139. Galbiati, M.; Ferrier, L.; Solnyshkov, D. D.; Tanese, D.; Wertz, E.; Amo, A.; Abbarchi, M.; Senellart, P.; Sagnes, I.; Lemaître, A.; Galopin, E.; Malpuech, G.; Bloch, J., Polariton Condensation in Photonic Molecules. *Phys. Rev. Lett.* **2012**, *108*, 126403.
140. Kozyreff, G.; Dominguez-Juarez, J. L.; Martorell, J., Nonlinear optics in spheres: from Second Harmonic Scattering to Quasi-Phase Matched Generation in Whispering Gallery Modes. *Laser Photonics Rev.* **2011**, *5*, 737.
141. Zhang, X.; Cao, Q.; Wang, Z.; Liu, Y.; Qiu, C.; Yang, L.; Gong, Q.; Xiao, Y., Symmetry-Breaking-Induced Nonlinear Optics at a Microcavity Surface. *Nature Photon.* **2018**, *13*, 21.

142. Baranov, D. G.; Wersäll, M.; Cuadra, J.; Antosiewicz, T. J.; Shegai, T., Novel Nanostructures and Materials for Strong Light–Matter Interactions. *ACS Photonics* **2017**, *5*, 24.
143. Xing, P.; Ma, D.; Ooi, K. J. A.; Choi, J. W.; Agarwal, A. M.; Tan, D., CMOS-Compatible PECVD Silicon Carbide Platform for Linear and Nonlinear Optics. *ACS Photonics* **2019**, *6*, 1162.
144. Dannenberg, P. H.; Liapis, A. C.; Martino, N.; Kang, J.; Wu, Y.; Kashiparekh, A.; Yun, S., Multilayer Fabrication of a Rainbow of Microdisk Laser Particles Across a 500 nm Bandwidth. *ACS Photonics* **2021**, *8*, 1301.
145. Siegle, T.; Schierle, S.; Kraemmer, S.; Richter, B.; Wondimu, S. F.; Schuch, P.; Koos, C.; Kalt, H., Photonic Molecules with a Tunable Inter-Cavity Gap. *Light Sci. Appl.* **2017**, *6*, e16224.
146. Wang, J.; Karnaushenko, D.; Medina-Sanchez, M.; Yin, Y.; Ma, L.; Schmidt, O. G., Three-Dimensional Microtubular Devices for Lab-on-a-Chip Sensing Applications. *ACS Sensor* **2019**, *4*, 1476.
147. Yu, M.; Huang, Y.; Ballweg, J.; Shin, H.; Huang, M.; Savage, D. E.; Lagally, M. G.; Dent, E. W.; Blick, R. H.; Williams, J. C., Semiconductor nanomembrane tubes: three-dimensional confinement for controlled neurite outgrowth. *ACS Nano* **2011**, *5*, 2447.
148. Du, H.; Zhang, X.; Chen, G.; Deng, J.; Chau, F. S.; Zhou, G., Precise control of coupling strength in photonic molecules over a wide range using nanoelectromechanical systems. *Sci. Rep.* **2016**, *6*, 24766.
149. Wang, C.; Ren, J.; Cao, J., Nonequilibrium Energy Transfer at Nanoscale: A Unified Theory from Weak to Strong Coupling. *Sci. Rep.* **2015**, *5*, 11787.
150. Farnesi, D.; Barucci, A.; Righini, G. C.; Berneschi, S.; Soria, S.; Nunzi Conti, G., Optical Frequency Conversion in Silica-Whispering-Gallery-Mode Microspherical Resonators. *Phys. Rev. Lett.* **2014**, *112*, 093901.

151. Ramelow, S.; Farsi, A.; Vernon, Z.; Clemmen, S.; Ji, X.; Sipe, J. E.; Liscidini, M.; Lipson, M.; Gaeta, A. L., Strong Nonlinear Coupling in a Si₃N₄ Ring Resonator. *Phys. Rev. Lett.* **2019**, *122*, 153906.
152. Cao, Q. T.; Wang, H.; Dong, C. H.; Jing, H.; Liu, R. S.; Chen, X.; Ge, L.; Gong, Q.; Xiao, Y. F., Experimental Demonstration of Spontaneous Chirality in a Nonlinear Microresonator. *Phys. Rev. Lett.* **2017**, *118*, 033901.
153. Mazzei, A.; Gotzinger, S.; Menezes Lde, S.; Zumofen, G.; Benson, O.; Sandoghdar, V., Controlled Coupling of Counterpropagating Whispering-Gallery Modes by a Single Rayleigh Scatterer: a Classical Problem in a Quantum Optical Light. *Phys. Rev. Lett.* **2007**, *99*, 173603.
154. Kippenberg, T. J.; Spillane, S. M.; Vahala, K. J., Modal Coupling in Traveling-Wave Resonators. *Opt. Lett.* **2002**, *27*, 1669.
155. Xie, R.; Li, G.; Chen, F.; Long, G., Microresonators in Lithium Niobate Thin Films. *Adv. Opt. Mater.* **2021**, *9*, 2100539.
156. Zhang, M.; Wang, C.; Hu, Y.; Shams-Ansari, A.; Ren, T.; Fan, S.; Lončar, M., Electronically Programmable Photonic Molecule. *Nature Photon.* **2018**, *13*, 36.
157. Wang, X.; Yin, Y.; Dong, H.; Saggau, C. N.; Tang, M.; Liu, L.; Tang, H.; Duan, S.; Ma, L.; Schmidt, O. G., Nanogap Enabled Trajectory Splitting and 3D Optical Coupling in Self-Assembled Microtubular Cavities. *ACS Nano* **2021**, *15*, 18411.
158. Englund, D.; Fattal, D.; Waks, E.; Solomon, G.; Zhang, B.; Nakaoka, T.; Arakawa, Y.; Yamamoto, Y.; Vuckovic, J., Controlling the Spontaneous Emission Rate of Single Quantum Dots in a Two-Dimensional Photonic Crystal. *Phys. Rev. Lett.* **2005**, *95*, 013904.
159. Dousse, A.; Lanco, L.; Suffczynski, J.; Semenova, E.; Miard, A.; Lemaitre, A.; Sagnes, I.; Roblin, C.; Bloch, J.; Senellart, P., Controlled Light-Matter Coupling for a Single Quantum Dot Embedded in a Pillar Microcavity Using Far-Field Optical Lithography. *Phys. Rev. Lett.* **2008**, *101*, 267404.

160. Cao, H.; Wiersig, J., Dielectric Microcavities: Model Systems for Wave Chaos and Non-Hermitian Physics. *Rev. Modern Phys.* **2015**, *87*, 61.
161. Song, Q. H.; Cao, H., Improving Optical Confinement in Nanostructures *via* External Mode Coupling. *Phys. Rev. Lett.* **2010**, *105*, 053902.
162. Yang, C.; Hu, Y.; Jiang, X.; Xiao, M., Analysis of a Triple-Cavity Photonic Molecule based on Coupled-Mode Theory. *Phys. Rev. A* **2017**, *95*, 033847.
163. Kapfinger, S.; Reichert, T.; Lichtmanecker, S.; Muller, K.; Finley, J. J.; Wixforth, A.; Kaniber, M.; Krenner, H. J., Dynamic Acousto-Optic Control of a Strongly Coupled Photonic Molecule. *Nat. Commun.* **2015**, *6*, 8540.
164. M. Bayer, T. G., J. P. Reithmaier, A. Forchel, Optical Modes in Photonic Molecules. *Phys. Rev. Lett.* **1998**, *81*, 4.
165. Helgason, Ó. B.; Arteaga-Sierra, F. R.; Ye, Z.; Twayana, K.; Andrekson, P. A.; Karlsson, M.; Schröder, J.; Victor, T. C., Dissipative Solitons in Photonic Molecules. *Nature Photon.* **2021**, *15*, 305.
166. Rodriguez, S. R.; Amo, A.; Sagnes, I.; Le Gratiet, L.; Galopin, E.; Lemaitre, A.; Bloch, J., Interaction-Induced Hopping Phase in Driven-Dissipative Coupled Photonic Microcavities. *Nat. Commun.* **2016**, *7*, 11887.
167. Cao, L.; Fan, P.; Brongersma, M. L., Optical Coupling of Deep-Subwavelength Semiconductor Nanowires. *Nano Lett.* **2011**, *11*, 1463.

Publications

1. **Xiaoyu Wang**, Yin Yin, * Haiyun Dong, Christian N. Saggau, Min Tang, Lixiang Liu, Hongmei Tang, Shengkai Duan, Libo Ma, * and Oliver G. Schmidt, * *Nanogap Enabled Trajectory Splitting and 3D Optical Coupling in Self-Assembled Microtubular Cavities*, *ACS Nano* 2021, 15, 18411.
2. **Xiaoyu Wang**, Zhen Wang, * Haiyun Dong, Christian N. Saggau, Hongmei Tang, Min Tang, Lixiang Liu, Stefan. Baunack, Ling Bai, Junlin Liu, Yin Yin, * Libo Ma, * and Oliver G. Schmidt, *Collective Coupling of 3D Confined Optical Modes in Monolithic Twin Microtube Cavities Formed by Nanomembrane Origami*, *Nano Letters*, accepted.
3. Haiyun Dong, Christian Niclaas Saggau, Minshen Zhu, Jie Liang, Shengkai Duan, **Xiaoyu Wang**, Hongmei Tang, Yin Yin, Xiaoxia Wang, Jiawei Wang, Chunhuan Zhang, Yong Sheng Zhao, * Libo Ma, * and Oliver G. Schmidt, * *Perovskite Origami for Programmable Microtube Lasing*, *Advanced Functional Materials* 2021, 2109080.
4. Jiang Qu, * Yang Li, Fei Li, Tianming Li, **Xiaoyu Wang**, Yin Yin, Libo Ma, Oliver G. Schmidt, and Feng Zhu, *Direct Thermal Enhancement of Hydrogen Evolution Reaction of On-Chip Monolayer MoS₂*, *ACS Nano* 2022, 16, 2921.
5. Christian N Saggau, * Sreeramulu Valligatla, **Xiaoyu Wang**, Haiyun Dong, Libo Ma, * and Oliver G Schmidt, * *Coaxial Micro Ring Arrays Fabricated on Self-Assembled Microtube Cavities for Resonant Light Modulation*, *Laser Photonics Reviews*, 2022, 2200085.

Presentations

1. Xiaoyu Wang, “Multiple resonant coupling in geometry-engineered optical microtubular cavities”, Talk, PhD Seminar, IFW Dresden, Germany, 08.02.2021
2. Xiaoyu Wang, “3D optical coupling in self-assembled microtubular cavities”, Talk, PhD Seminar, IFW Dresden, Germany, 07.04.2022
3. Xiaoyu Wang, “3D optical coupling in self-assembled microtube cavities”, Talk, PhD Seminar, TU Chemnitz, Germany, 12.05.2022
4. Xiaoyu Wang, “Strong optical coupling between 3D confined resonant modes in microtube cavities”, Talk, IIN retreat, Naturhotel Lindenhof Holzgau, Germany, 29.06.2022

Acknowledgements

Here I would like to acknowledge all the people who have given me a great deal of support and assistance during the completion of this dissertation.

First of all, I would like to express my sincere gratitude to my supervisor Prof. Dr. Oliver G. Schmidt for giving me the opportunity to pursue my doctoral degree in TUD. I truly appreciate his support, supervision and encouragement on my research studies.

Also, I would also like to thank the financial support from “Würzburg-Dresden Cluster of Excellence on Complexity and Topology in Quantum Matter”.

I greatly appreciate Prof. Dr. Vladimir Fomin for taking time to review my work.

Many thanks certainly should go to my group leader Dr. Libo Ma for his scientific guidance, fruitful discussion and careful revision of all my work. I deeply appreciated him for the kind help and support both at work and in life.

I'm very thankful to Prof. Dr. Yin Yin, who helped me a lot during my Ph.D. study. I appreciate his guidance on scientific research and how to be an independent researcher.

I would like to thank Dr. Haiyun Dong for his generous help with the experiments, many helpful scientific and nonscientific discussions, and constructive comments.

I would like to thank Dr. Min Tang for the great help with the understanding and calculation of strong coupling behavior in coupled microcavities.

I must thank Dr. Christian N. Saggau for his many efforts. He performed dry-etching method which is the basis for my sample preparation. He also did FDTD calculations related to my work. The cooperation with him promotes the work to be better.

I would like to thank people who helped along numerous experiments: Dr. Lixiang Liu and Hongmei Tang for SEM images, Dr. Weijie Nie for optical measurement.

I would like to thank to my colleagues: Dr. Jiawei Wang, Dr. Xiaoxia Wang, Dr. Minshen Zhu, Dr. Jin Ge, Dr. Bin Bao, Dr. Jiang Qu, Dr. Hua Zhang, Dr. Fei Li, Yang Li, Shengkai Duan, Zhe Qu, Dr. Sreeramulu Valligatla, for their nice discussion and support.

I would also appreciate much for the technical support from Dr Stefan Baunack, Ronny Engelhard, Liesa Raith, Martin Bauer, Sandra Nestler, and Carol Schmidt.

I am very grateful to our institute secretary Kristina Krummer-Meier, Julia Abram, Katrin Muenster for help solving the administrative issues.

I would like to thank my friends Dr. Yufang Xie, Xin Xu, Fei Jin, Wei Yang, Dr. Guoliang Shang, Yan Li *et al.* who are always ready to help and support me.

Last but not least, I would like to acknowledge my parents and sisters for their continuous support during my life. Especially I want to say thanks to my loving husband Dr. Zhen Wang for his constant love and support during my Ph.D. program in Germany.

Xiaoyu Wang, Dresden

10.05.2022

Erklärung

Hiermit versichere ich, dass ich die vorliegende Arbeit ohne unzulässige Hilfe Dritter und ohne Benutzung anderer als der angegebenen Hilfsmittel angefertigt habe; die aus fremden Quellen direkt oder indirekt übernommenen Gedanken sind als solche kenntlich gemacht.

Die Arbeit wurde bisher weder im Inland noch im Ausland in gleicher oder ähnlicher Form einer anderen Prüfungsbehörde vorgelegt.

Diese Dissertation wurde angefertigt im

Leibniz-Institut für Festkörper- und Werkstoffforschung Dresden

Institut für Integrative Nanowissenschaften

Helmholtzstraße 20, 01069 Dresden

Die wissenschaftliche Betreuung der Arbeit erfolgte durch Prof. Dr. Oliver G. Schmidt.

Ich versichere, an keiner Institution, auch nicht im Ausland, jemals den Antrag auf Eröffnung eines Promotionsverfahrens gestellt zu haben.

Ich erkenne die Promotionsordnung der Fakultät Mathematik und Naturwissenschaften der Technische Universität Dresden an.

Xiaoyu Wang, Dresden

10.05.2022

Curriculum Vitae

Personal Information

Name: Xiaoyu Wang

Date of birth: 03. 06. 1992

Place of birth: Henan, China

Nationality: Chinese

Education

Oct. 2019 – at present Ph.D. student, Physics

Leibniz-Institut für Festkörper- und Werkstoffforschung Dresden

Technische Universität Dresden, Germany

Sep. 2014 – Jun. 2017 Master of Engineering

University of Chinese Academy of Sciences, China

Sep. 2010 – Jun. 2014 Bachelor of Science

Jiangxi University of Science and Technology, China

Teaching

Apr. 2022 - Jul. 2022 Teaching assistant

Technische Universität Dresden, Germany

Lecture: Laboratory of Fundamental Physics

